Dependency of African precipitation on Sea Surface Temperature bias and variability patterns in the South Atlantic

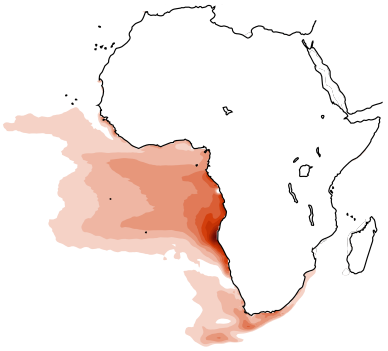

Dissertation
with the aim of achieving a doctoral degree
at the Faculty of Mathematics, Informatics and Natural Sciences
Department of Earth Sciences
at Universität Hamburg

submitted by

Franziska Leverenz

Hamburg, 2022

Department of Earth Sciences

Date of Oral Defense:	28.08.2023
Reviewers:	Prof. Dr. Detlef Stammer Dr. Armin Köhl
Members of the examination commission:	Chair Prof. Dr. Detlef Stammer Dr. Armin Köhl Prof Dr. Jin-Song von Storch Prof Dr. Matthias Hort Dr. Ann Kristin Naumann
Chair of the Subject Doctoral Committee Earth System Science:	Prof. Dr. Hermann Held
Dean of Faculty MIN:	Prof. Dr.-Ing. Norbert Ritter

ABSTRACT

The lack of predictive skill of interannual African precipitation variability in coupled climate models has been associated with the mean state eastern boundary SST warm bias in the South Atlantic. Despite increased accuracy and computational power over the last decade, the bias could not be eliminated and precipitation variability of the African Sahel region remains erroneous. This study analyzes the ability of the coupled model MPI-ESM-HR to reproduce precipitation anomalies in dependency of the represented SST field in the South Atlantic. The study aims to clarify to what extent the SST bias deteriorates the teleconnection between South Atlantic SST and African precipitation, using additional model runs with increased resolution of oceanic or atmospheric model components. The analysis of upwelling dynamics along the eastern boundary of the South Atlantic shows, that the higher resolved spatial details of equatorward near shore winds stress prevent an erroneous southward intrusion of warm tropical water into the Benguela upwelling region, leading to a large reduction of the mean state SST bias and an improved interannual SST variability. The reduced SST bias in the Benguela upwelling region reduces the equatorial westerly wind bias and improves tropical moisture flux dynamics. However, interannual SST variability, which drives variations of precipitation over Africa, still produces opposing precipitation anomalies over West Africa. For this study, the performance of precipitation over Africa is analyzed with realistic temperature and salinity anomalies assimilated into the coupled climate model to study how the representation of precipitation variability is affected in the presence of the mean state SST bias. The analysis shows that the deteriorated teleconnection between SST and precipitation is related to an intensification of the southward shifted Intertropical Convergence Zone (ITCZ) representation due to the SST bias via a severe reduction of zonal winds in the tropical South Atlantic, resulting in nonreproducible Sahel precipitation variability without any coherence to interannual SST modes. The result suggests, that the SST bias generally enhances local precipitation signals via an enhanced atmospheric surface flux sensitivity to SST variations and induces local southeastward shifts of tropical moisture convergence. The SST bias, however, only intensifies the defective representation of the ITCZ due to reduced momentum fluxes over eastern tropical ocean basins in the atmospheric component of the climate model which prevents a pronounced impact of SST variations on monsoon rainfall in the Sahel region independent of the SST pattern in the South Atlantic.

ZUSAMMENFASSUNG

Die mangelnde Vorhersagefähigkeit der interannualen afrikanischen Niederschlagsvariabilität in gekoppelten Klimamodellen wurde bisher mit der fehlerhaften Darstellung von mittleren Meeresoberflächentemperaturen (SST) entlang der östlichen Begrenzung des Südatlantiks in Verbindung gebracht. Trotz der enormen Verbesserungen von Genauigkeit und Rechenleistung im letzten Jahrzent konnte weder der SST-Fehler beseitigt noch die Niederschlagsvariabilität in der afrikanischen Sahelzone verbessert werden. In dieser Studie wird untersucht, inwieweit das gekoppelte Modell MPI-ESM-HR in der Lage ist, Niederschlagsanomalien in Abhängigkeit vom dargestellten SST-Feld im Südatlantik zu reproduzieren. Die Studie soll klären, inwieweit der SST-Fehler die Fernwirkung von SST im Südatlantik auf afrikanischem Niederschlag verschlechtert, indem zusätzliche Modellläufe mit höherer Auflösung der ozeanischen oder atmosphärischen Modellkomponenten durchgeführt werden. Die Analyse der Auftriebsdynamik entlang der östlichen Grenze des Südatlantiks zeigt, dass die höher aufgelösten räumlichen Details der äquatorwärtigen Winde ein fehlerhaftes Eindringen von warmem tropischem Wasser nach Süden in das Benguela-Auftriebsgebiet verhindern, was zu einer starken Verringerung des mittleren SST-Fehlers und einer verbesserten interannuellen SST-Variabilität führt. Der reduzierte SST-Fehler in dem Benguela-Auftriebsgebiet verbessert den westwärtigen Wind-Fehler am Äquator und verbessert die Dynamik der tropischen Feuchteflüsse. Die interannuelle SST-Variabilität, die für die Niederschlagsschwankungen über Afrika verantwortlich ist, führt jedoch immer noch zu gegensätzlichen Niederschlagsanomalien über Westafrika. In dieser Studie wird die Qualität reproduzierten Niederschlagsvariabilität über Afrika analysiert mittels eines gekoppelten Klimamodells in das realistischen Temperatur- und Salzgehaltsanomalien assimiliert wurden, um zu untersuchen, wie die Darstellung der Niederschlagsvariabilität durch den mittleren SST-Fehler beeinflusst wird. Die Analyse zeigt, dass der SST-Fehler die zonalen Winde im tropischen Atlantik stark veringert und dadurch den Verschub der innertropischen Konvergenzzone (ITCZ) nach Süden intensiviert und damit auch die Fernwirkung von SST auf den Niederschlag verschlechtert. Dies fürht zu einer nicht reproduzierbaren Niederschlagsvariabilität in der Sahelzone, die keinen Zusammenhang mit den interannuellen SST-Moden zeigt. Das Ergebnis deutet darauf hin, dass der SST-Fehler im Allgemeinen die lokalen Niederschlagssignale durch eine erhöhte Empfindlichkeit der atmosphärischen Oberflächenflüsse gegenüber SST-Schwankungen verstärkt und lokal die Konvergenz von tropischen Feuchteflüssen nach Südosten verschiebt. Der SST-Fehler verstärkt jedoch nur die mangelhafte Darstellung der ITCZ, die aufgrund reduzierter Impulsflüsse über den östlichen tropischen Ozeanbecken

in der atmosphärischen Komponente des Klimamodells entsteht. Wobei die mangelhafte Darstellung der ITCZ verhindert einen ausgeprägten Einfluss von SST-Variationen auf den Monsunregen in der Sahelzone unabhängig vom SST-Muster im Südatlantik.

Acknowledgement

I would like to express my gratitude to my supervisors Prof. Dr. Detlef Stammer and Dr. Armin Köhl, without whom this journey would not have been possible. I thank them for their invaluable patience and their highly qualified feedback. I am very thankful to Dr. Armin Köhl for his model assimilation support. Additionally, I would like to extend my sincere thanks to Meike Sena Martins for all her support and exchange of ideas. Furthermore, this work was only made possible by the support of the German Federal Ministry of Education and Research in the frame of the BANINO project. In addition, I want to thank ICDC, CEN, University of Hamburg and the German Climate Computing Center (DKRZ) for the data support.

I am also grateful to my office mates and fellow students, whom I had the pleasure to share my research time at the University of Hamburg with. Thanks for all the exchange of ideas and for keeping the motivation high. Sharing inspirational discussions, laughter and lunch, as well as helping each other out on random occasions made this time very valuable to me.

Special thanks to my family, friends and flatmates for their moral support and their belief in my research career. All of you beautiful people give me the courage and the support to be who I am and to achieve my personal goals. Many thanks to Reiner, who never stopped believing in me and provided me with an alternate workspace during the pandemic when home could not even come close to serving as an office. Many thanks also to Christiane and Marius for their irreplaceable emotional support and for being my steady anchor. I am also grateful to Florian for being a home to me during happy and stressful days. Special thanks to Jorina for keeping to push me when I need it and for helping to untangle my knotted thoughts from time to time. I am forever thankful for your unique friendship. Words cannot express my gratitude to Christian, who shared this wild ride with me and supported me with all his heart. Your contribution to this work is immense. Your positivity shines brighter than all the stars of the universe. Thanks for being you and thanks for sharing life with me.

Lastly, I would like to mention the lovely souls who left this world too soon, during the process of this thesis. Eric, Heike, Thomas, René and Timm, you will always be a part of all the hearts you touched with your inspirational fire, contagious euphoria and kindness.

Contents

List of Figures

List of Tables

List of Abbreviations

ABA	Angola Benguela Area
ABF	Angola Benguela Front
ACC	Anomaly Correlation Coefficient
AMO	Atlantic Multidecadal Oscillation
AMOC	Altantic Meridional Overturning Circulation
ANG	Angola area
AZM	Atlantic Zonal Mode
CC	Correlation Coefficient
CMIP	Coupled Model Intercompariosn Project
CT	Cold Tongue
CTW	Coastal Trapped Wave
EA	Equatorial Atlantic
EKW	Equatorial Kelvin Wave
ENSO	El Niño/Southern Oscillation
EOF	Empirical Orthogonal Function
FMA	February-March-April
GCM	General Circulation Model
GW	Global Warming
ITCZ	Intertropical Convergence Zone
JJA(S)	June-July-August(-September)
LHF	Latent Heat Flux
MAM	March-April-May
PC	Principal Component
PRC	Precipitation
RMSE	Root Mean Square Error
SST	Sea Surface Temperature
STD	Standard Deviation
TAS	Surface Air Temperature
Trop NA	Tropical North Atlantic
UI	Upwelling Index
WAM	West African Monsoon
WEA	Western Equatorial Atlantic
WSC	Wind Stress Curl

1 Introduction

Climate predictions provide useful information about future climate variability which is of major importance for decision-making and strategic planning by governments, societies and economics regarding adaptational and protective measures to encounter climate impacts and their risks. Climate predictions fill the gap between weather forecasts and long-term climate projections as they estimate probabilistic future climate conditions, covering time scales from seasons to decades and range spatially from local over regional to global scales (Li and Ding, 2015). The lack of predictive skill of African precipitation variability had been attributed to biased Sea Surface Temperature (SST) patterns in the South Atlantic. This study assesses the dependency of the quality of coupled climate model simulations on the representation of SST patterns along the eastern boundary of the South Atlantic Ocean, including the Benguela upwelling region. Coupled Earth System Model simulations are affected by enhanced SST exceeding observations by multiple degrees along the eastern boundaries of global oceans. The warm SST bias is particularly pronounced in the South Atlantic and South Pacific upwelling regions. It exists since the early development of coupled models and its source is still undetermined. Possible causes have been suggested, e.g. low atmospheric or orographic resolution related to deficient surface winds, insufficient offshore oceanic eddy transport, or the defective representation of stratocumulus clouds (Mechoso et al., 1995; Small et al., 2015; Ding et al., 2015; Richter and Xie, 2008; Richter et al., 2014b; Voldoire et al., 2019). Systematic biases in climate models are the alleged cause for diminished predictive skill (Manganello and Huang, 2009; Gaetani and Mohino, 2013; Ding et al., 2015; Scaife et al., 2019). This study aims to clarify to what extent climate simulations are affected by the South Atlantic SST bias with a focus on the performance of reproduced precipitation variability over Africa. In other words, the goal is to answer whether simulated precipitation variability is directly deteriorated by the defective representation of SST which would limit the potential of predictive skill.

Interannual climate predictions rely on a detailed understanding of climate variable interactions. Skillful predictions are still challenged by the complexity of interactions between ocean, atmosphere, and land interfaces via momentum, heat, and moisture fluxes on various spatial and temporal scales. Predictability describes the ability of represented physical processes to add to the quality of predictions (National Research Council, 2010). Predictability is dependent on chaotic internal processes and the variation of boundary conditions, e.g. SST which drives climate variability on interannual or longer time scales. Nonlinear interactions between high frequent processes reduce predictability, whereas

slow varying coupled ocean-atmosphere oscillations (e.g. climate modes like El Niño/-Southern Oscillation (ENSO)) add to climate predictability (Goswami and Ajaya Mohan, 2001). Understanding the local and remote effects of climate modes via teleconnections can provide better predictive model skill. Though, the availability of observational climate records drastically limits the identification of relevant modes. According to the National Research Council (2010), predictive skill is limited by the existence of natural predictive climate modes and its true magnitude can not be assessed. Yet, the minimum skill can be defined by the ability of models to reproduce observed climate variability. The defective representation of physical processes can lead to a lack of predictive skill in a model. As the identification of the source of the reduced predictability in models can lead to the possibility to improve the model skill, the aim of this study is to examine if elevated SST is the source of the low predictability of African precipitation. Or whether the predictability is already limited by the absence of pronounced natural modes, that drive precipitation variability. Finding an answer to this question could contribute to evaluating the urgency to solve the SST bias problem in terms of future model prediction quality.

The impact of elevated SST on the representation of the African climate in coupled models is still uncertain (Richter et al., 2018). As the intensity of the West African Monsoon is linked to tropical Atlantic SST variations on interannual time scales, the lack of predictive skill of precipitation along the West African Sahel area has been assumed to be linked to the South Atlantic SST bias (Caniaux et al., 2011; Gaetani and Mohino, 2013; Diatta and Fink, 2014). Most studies inferred that solving the SST bias problem would lead to improved predictive skill. However, so far only a few studies actually focused on the dependency of predictive skill on the mean state bias. For instance, Manganello and Huang (2009) found, that reducing mean state and variability errors of Pacific SST by a heat flux correction scheme resulted in the improved predictive skill of ENSO. Ding et al. (2015) showed higher predictive skill is obtained by an SST bias reduction because of its influence on surface wind stress and subsurface temperature. In contrast, Richter et al. (2018) suggested SST mean state biases do not necessarily improve the predictive skill of precipitation or surface wind. The divergent and inconclusive results highlight the need to fully understand the climatic influence of the Atlantic SST bias to scale its actual impact on climate model simulations and help to outline the potential effectiveness of further attempts to improve the SST representation.

Interannual SST variability modes in the South Atlantic, which potentially contribute to African precipitation predictability, are dominated by the Atlantic Zonal Mode (AZM) and related but less frequent Benguela Niños/Niñas. The AZM describes SST anomalies in the eastern tropical South Atlantic which lead to the displacement of convective patterns during boreal summer (Zebiak, 1993). Several studies have already shown that the AZM affects the variability of the West African monsoon and Sahel rainfall (e.g. (Vizy and Cook,

2002; Paeth and Friederichs, 2004; Losada et al., 2010)). The representation of AZM-like SST anomalies has been a challenge for coupled climate models which was suspected to be partly due to the mean state SST bias with implications on the representation of the precipitation anomalies over the African continent (Lübbecke et al., 2018). Significant improvements have been achieved with the development of the recent CMIP6 (Coupled Model Intercomparison Project Phase 6) model generation, showing only a weak link between the mean state SST bias and the representation of interannual SST variability (Richter and Tokinaga, 2020). To determine the role of the mean state SST bias as a limiting factor for climate predictability a further investigation of precipitation responses to SST anomalies in climate models is inevitable. The cyclic character of interannual variability is more pronounced for variations of SST than for precipitation, which is more affected by stochastic processes. Via pronounced teleconnections potentially predictable SST variations can imply predictability of regional precipitation anomalies as well. However, predictability of AZM like anomalies has been shown to be rather low compared to its much more pronounced Pacific counterpart ENSO (Richter et al., 2018) due to their forcing mechanisms being linked to remote and local wind fluctuations of largely stochastic character in combination with local thermodynamic processes among others (Richter et al., 2014a; Lübbecke et al., 2018). Despite moderate improvements, it has been shown that predictive skill for interannual SST variability in the South Atlantic remains poor even if the SST bias is reduced (Dippe et al., 2019) with possible implications for predictive skill of related precipitation variability. As the SST bias appears not to be the main source of low predictive skill of the SST variations, it remains to be determined to what extent the defective SST pattern affects the teleconnection between interannual South Atlantic SST and African precipitation anomalies. To eliminate the impact of low predictability of SST anomalies on predictive skill of precipitation anomalies, the performance of precipitation anomalies as a direct response to prescribed SST anomalies in a coupled model is analyzed in this study which would define the upper limit of potential predictability of African precipitation that could be expected in dependency of the SST pattern. Reproduced precipitation anomalies rely on the understanding of how moisture is transported in the atmosphere. Analyzing the impact of the SST bias on moisture flux and precipitation anomalies in response to SST variations can give insight into how climate model simulations rely on the accurate SST representation of the affected area. The analysis of the atmospheric variables provides also insight into the limitations expected from the atmospheric state of the model simulation. For an effective adaptational ability of the West African population, skillful precipitation predictions and a better understanding of climatic feedback mechanisms linked to interannual SST variations like the AZM or Benguela Niños/Niñas is imperative.

The eastern boundary of the South Atlantic is defined by one of the most pronounced coastal upwelling systems of global oceans which is hardest to represent in climate model

simulations (Small et al., 2015). The local maximum of the mean state SST bias has been attributed to deficiencies in the representation of upwelling dynamics with substantial remote effects (Mechoso et al., 1995; Large and Danabasoglu, 2006; Small et al., 2015). As the simulated upwelling dynamics are sensitive to the structure of the wind stress curl (Capet et al., 2004; Song et al., 2011; Renault et al., 2012; Desbiolles et al., 2014), it has been shown that high atmospheric model resolution leads to improved upwelling dynamics combined with a reduction of the SST bias (Large and Danabasoglu, 2006; Small et al., 2015). However, it remains unclear whether the ability to reproduce African precipitation anomalies induced by SST variations relies on the representation of upwelling dynamics along the eastern boundary of the South Atlantic. This study aims to show how upwelling favorable wind stress conditions affect the magnitude of SST bias, the representation of SST variability, and possible impacts on African precipitation variability.

1.1 Goals

As the lack of performance of reproduced climate variability in coupled climate models has been attributed to systematic biases, it remains to discuss the actual impact of the biases on the model's ability to reproduce interannual variability of precipitation. This study focuses on the severe SST warm bias along the eastern boundary of the South Atlantic and its influence on the West African Monsoon and precipitation over land areas near the coast along the Atlantic eastern boundary. The aim is to contribute to the improvement of future coupled climate model simulations by determining the role of elevated South Atlantic SST patterns in the model's ability to reproduce interannual variability of African precipitation. Three major goals are formulated to serve this purpose:

1st goal: **Investigate how the simulation of African precipitation changes in dependency of the model resolution and the magnitude of the SST bias.**

2nd goal: **Determine the impact of the SST bias on the teleconnection between African precipitation and interannual South Atlantic SST variability.**

3rd goal: **Evaluate the dependency of reproduced African precipitation variability performance on the representation of the South Atlantic SST pattern.**

The first goal is formulated to investigate the changes of systematic biases arising with altered model resolution in order to understand the mechanisms behind the changing magnitude of the SST bias and its implications for the representation of atmospheric variables. The quality of the representation of simulated variables dependent on the model resolution can give insight into the origin of certain mean state biases, underlying processes and their interconnection.

The importance of the second goal arises from the dependency of climate predictability on the presence of quantifiable modes, induced by relevant climate drivers. As this study deals with the relevance of the defectively elevated SST patterns for precipitation variability, atmospheric anomalies induced by SST as the driving force are of major interest. A deeper understanding of the relevant processes involved in SST variations and characteristic behavior on spatial and temporal scales, along with the induced climatic response is imperative to understand the teleconnection to African precipitation anomalies.

The actual impact of the SST bias on climate and precipitation performance, as formulated in the third goal, is motivated by the aim to investigate the limits and potentials for reproducible precipitation variations. The limited skill of coupled climate models in reproducing precipitation variations has often been attributed to the biased mean state of SST and several attempts to solve the SST bias problem have led to moderate improvements at expensive computational costs. A more detailed and quantitative understanding of the link between biased SST and the quality of reproduced precipitation variability can help to increase the effectiveness of further attempts to improve climate predictions. For this reason, the impact of the SST bias on the direct climatic response to SST variability needs to be investigated and the extent, to which precipitation variability is corrupted by those climatic deviations, needs to be estimated. In other words, the aim is to answer whether the performance of precipitation can be improved by eliminating the SST bias problem.

1.2 Strategy

The following approach serves the purpose to achieve the goals defined in Section 1.1. The latest version of the coupled climate model, MPI-ESM (Max Planck Institute for Meteorology Earth System Model) in high resolution, is chosen to analyze the representation of SST characteristics under biased mean state conditions in comparison to observational products with high spatial coverage. Several historical model runs with different resolutions of the atmospheric and oceanic components are analyzed to examine how the represented SST characteristics and performance of climate variables change in relation to the model resolution and magnitude of the mean state SST bias. The intensity of annual and interannual SST variability in time and space are analyzed to identify the dominant SST modes and their representation in the model simulations with characteristic amplitudes, spatial extent, and periodicity. Since upwelling dynamics define SST characteristics along the equator and eastern boundary, where the mean state SST bias is most elevated, upwelling indices are calculated from SST and surface wind fields for a better understanding of SST variability and the dynamics of relevant modes and how they can be simulated by the climate models. In order to understand the linkage between SST variability and the corresponding precipitation response, atmospheric moisture flux is calculated to retrace

the anomalous climate response. The deviations between model simulations of different resolutions can provide information about the impacts of the SST bias due to its changing magnitude. The coupled model simulation is additionally compared to an atmosphere-only simulation driven with realistic SST fields to estimate intrinsic atmospheric biases not related to elevated SST.

In addition, a sensitivity experiment is executed, where realistic ocean temperature and salinity anomalies are assimilated into the coupled climate model. It serves as a base to analyze the climatic response to realistic interannual SST events like Benguela Niños or AZM in the coupled model framework under biased mean state conditions, in order to quantify the SST bias impact in comparison to the atmosphere-only run.

Furthermore, the bias impact on the performance of climate variables and especially African precipitation is estimated by comparing skill measures of the sensitivity experiment and the atmosphere-only simulation, which both serve as a zero-lead forecast that simulates the direct response to realistic SST events. The performance of common modes between SST and precipitation is analyzed with the Empirical Orthogonal Function method. The analysis of both model simulations serves the purpose to examine the extent to which the performance of reproduced precipitation anomalies dependent on SST variations is deteriorated by elevated SST in the South Atlantic and to what extent the teleconnection between both variables can be captured by the model simulations with and without a biased SST mean state. The result can provide information about the dependency of precipitation variability on the SST pattern representation and how likely predictive skill could be increased by reducing the mean state SST bias. For an effective adaptational ability by the population of West Africa and coastal population of Southwest Africa a better understanding of the atmospheric teleconnections to SST variability is imperative.

The scientific background for this study is described in Chapter 2. The coupled climate model MPI-ESM and the here used reference data sets are introduced in Chapter 3, along with the outline of the sensitivity experiment containing realistic interannual variability. Chapter 4 is a presentation of the representation of South Atlantic SST and impacts on climate variables in MPI-ESM, along with alterations dependent on model resolution. It contains an analysis of the model's ability to represent upwelling dynamics along the eastern boundary and the annual cycle of the African Monsoon. Chapter 5 serves as a description of dominant interannual SST variability in the South Atlantic and its associated atmospheric response with implications of the SST bias. The climate model performance of West African precipitation and its dependency on South Atlantic SST variations is examined in Chapter 6. Chapter 7 provides a discussion and conclusion regarding the results of the previous chapters.

2 Scientific background

The scientific background of this study is briefly introduced in the following, in order to establish the base on which this study is built. The unsolved SST bias problem of coupled model simulations, which is essential for this study, is explained in greater detail in Section 2.1 with possible origins and attempts to solve it. Since the biased area is characterized by upwelling dynamics, the major upwelling regions of the South Atlantic are introduced in Section 2.2 along with their possible contribution to the SST bias problem and representation in coupled models. The annual feedback mechanism along the equatorial Atlantic and how it is affected by the SST bias is presented in Section 2.3. This feedback mechanism plays an important role in the context of the climatic response to SST variations. The dominant modes of interannual SST variability of the South Atlantic are described in Section 2.4 as the foundation for climate predictability.

2.1 Eastern boundary Sea Surface Temperature warm bias

Coupled General Circulation Models (GCM) are the state-of-the-art tool for long-term climate predictions. Their accuracy has improved over the last decades since computational power has increased. However, most climate model simulations are still challenged by systematic errors supposedly affecting predictive skill. The warm SST bias along the eastern boundaries of global ocean basins and corresponding equatorial regions is a famous example. Especially striking is the intensity of the mean state SST bias along the eastern South Atlantic and the eastern equatorial region. Simulated SST is exceeding observational SST here by multiple degrees which goes along with weak winds, underestimated upwelling intensity, biased representation of the current system, and affected tropical precipitation (Mechoso et al., 1995; Richter and Xie, 2008; Richter et al., 2014b; Small et al., 2015; Ding et al., 2015; Voldoire et al., 2019).

Since the lack of predictive skill of West African precipitation has been attributed to the mean state SST bias in several studies (e.g. Gaetani and Mohino (2013)), most attention was given to the revelation of possible sources aiming to eliminate the SST bias for a more realistic and skillful climate prediction. Several attempts led to significant improvements, yet biased SST along the Atlantic eastern boundary still persists. Since climate models are limited to a rather coarse resolution small-scale processes, such as ocean eddies or vertical atmospheric fluxes and energy transport, are parametrized. In addition, the fine structures of other variables like coastal wind or oceanic thermocline are underestimated in the coarse

grid and are also limited by orographic resolution which gives rise to error propagation in the complex interconnected climate system. Several studies show, that increasing the vertical and horizontal resolution of the ocean or atmosphere domain improves dynamics and in turn reduces the bias (e.g. Gent et al. (2010); McClean et al. (2011); Delworth et al. (2012)) with significant but limited success. Roberts et al. (2020) recently showed that increasing atmospheric resolution in CMIP6 models to 0.5° would reduce the Atlantic SST biases to a large extent but generates other circulation problems like a slowdown of the AMOC (Atlantic Meridional Overturning Circulation). To resolve processes like boundary layer turbulence or cloud microphysics very high model resolutions would be necessary and thus can not be expected to be resolved in the near future. The need to parameterize these processes will continue to cause systematic errors (Richter et al., 2018).

2.2 Upwelling dynamics along the South Atlantic eastern boundary

The Atlantic eastern boundary is characterized by the southward-flowing Angola Current which converges with the wind-driven and northward-flowing Benguela Current at the so-called Angola Benguela Front (ABF) between 15°S-20°S. The Angolan Current is supplied by the Equatorial Current and advects warm tropical water in poleward direction (Peterson and Stramma, 1991; Rouault et al., 2007). The location of the ABF is shifted southward in most climate models which could add to the SST warm bias (Exarchou et al., 2018). As the current structure off Angola is not well understood and observed the inaccurate representation of currents, advection, and heat transport in ocean models could be an additional source of the SST bias (Kopte et al., 2017).

South of the ABF, the Benguela Current is accompanied by the Benguela upwelling system which stretches along the narrow steep slope of the African shelf. It is one of the four most pronounced eastern boundary upwelling systems of the world's oceans (Chavez and Messié, 2009). The strong alongshore winds parallel to the coast induce offshore Ekman transport. The resulting divergent flow needs to be balanced by subsurface water flowing upwards towards the coastal surface. The fresh and salty upwelled water creates the typical temperature gradient between coastal waters and open ocean along with thriving ecosystems due to low oxygen and high nutrient contents (Rubio et al., 2009). The Benguela upwelling system stretches from 17°S to the southern tip of Africa. It is divided by a barrier of permanent upwelling, the so-called Lüderitz cell at 27°S. The northern part stretches from 17°-26°S including another maximum, the Cunene cell. Persistent alongshore winds here create almost permanent upwelling throughout the year. The southern upwelling system (28°-33°S) is characterized by a more pronounced seasonal cycle (Bachèlery et al., 2020).

North of the ABF along the Angolan coast winds are weak, yet upwelling is semi-seasonally taking place with a maximum during July/August. The semi-annual cycle of upwelling is suggested to be related to poleward traveling CTWs with an equatorial origin occurring as two pairs of down and upwelling CTWs traveling poleward along the coast. The second upwelling during November might be damped due to the stronger Angola Current (Philander and Yoon, 1982; Ostrowski et al., 2009).

Upwelling is taking place along the equator as well since the equator acts like a natural boundary due to the Coriolis force being zero directly at the equator. Equatorial upwelling is induced by Ekman pumping dynamics forced by local easterly and cross-equatorial southerly winds with a seasonal peak related to the onset of the West African monsoon (Li and Philander, 1997; Richter and Xie, 2008; Caniaux et al., 2011). The largest temperature gradient indicating equatorial upwelling is located between 0° and 20°W slightly south of the equator, and is named the equatorial cold tongue. The eastern equatorial upwelling dynamics are in addition partially driven by equatorial waves strongly dependent on the characteristics of the zonal thermocline (Wang et al., 2017). However, upwelling along the equator is much weaker compared to the eastern boundary upwelling due to weaker winds.

It remains a challenge in climate models to realistically represent upwelling dynamics and their variability together with the simulation of associated low stratocumulus clouds, thus ranking high on another potential contribution to the SST warm bias. Large and Danabasoglu (2006) found that restored southeastern boundary SST and salinity would remotely reduce SST and precipitation biases in the central Atlantic. The study by Small et al. (2015) shows that a combination of high resolution atmosphere (0.5°) and an eddy-resolving ocean model is necessary to obtain the most realistic representation of the Benguela upwelling system. Restoring SST along the upwelling zone (12°-30°S, coast to 8°E) does not result in a large remote equatorial response while restoring a broader region (Gulf of Guinea to 29°S, coast to 1°E) produces a substantial remote response. They suggest a realistic representation of coastal upwelling needs to be accompanied by a correction of coastal currents, shortwave radiation, and remote ocean temperature to have an impact on equatorial precipitation.

To obtain more realistic upwelling structures in addition to coastal currents a detailed simulation of wind stress is necessary (Capet et al., 2004; Song et al., 2011; Renault et al., 2012; Desbiolles et al., 2014). Regarding the theory of Fennel et al. (2012) and Junker (2014) upwelling can be divided into two categories of driving forces. The coastal wind stress-driven part is characterized by strong coastal wind stress which creates a response on the horizontal scale of the ocean's internal Rossby radius. The other part is driven by a consequent wind stress curl which generates a response on the scale of spatial wind stress

variations (Small et al., 2015). The spatial representation of the wind stress curl (WSC) then impacts the underlying currents. A zonally broad WSC located further offshore is related to a prevailing Sverdrup balance which creates a poleward current along the coast. More upwelling favorable conditions are a result of the wind stress curl being located further inshore. This in turn creates a jet in the upper ocean in the direction of the general surface wind flow along the coast and a counterflow in the direction of poleward propagating Coastal Trapped Waves (CTW) along the eastern boundary. The theory highlights the need for high resolution coastal wind simulations to produce a realistic upwelling representation along with the underlying current system (Oettli et al., 2021).

2.3 Equatorial Atlantic feedback mechanism

The atmosphere and oceans interact at their interfaces with each other via exchanges of heat, momentum, and water. Thus, coupling of these two volumes in a climate model involves SST, surface heat fluxes, surface wind stress, and water fluxes as driving forces. Biased mean states are a result of difficulties arising from coupling methods since coupling variables heavily interact with each other and biases can reinforce each other.

Since equatorial SST interacts with equatorial winds and the Intertropical Convergence Zone (ITCZ) along with monsoon rainfall (Large and Danabasoglu, 2006), the simulation of coupled feedback mechanisms is largely influenced by the SST bias and prone to further reinforcement. Richter and Tokinaga (2020) describe reinforcement through the Bjerknes feedback (Bjerkens, 1969; Keenlyside and Latif, 2007; Ding et al., 2015) as follows. Sea level pressure is low in the eastern equatorial Atlantic, while SST there is elevated, producing a westerly surface wind bias. Thus, the thermocline in the east deepens which reduces the upwelling intensity and reinforces the initial SST bias (Voldoire et al., 2019). Although they attributed the westerly wind bias to an atmospheric origin, because of its occurrence in boreal spring (March-April-May: MAM) which precedes elevated SST in boreal summer (June-July-August: JJA). Regarding observations, the ITCZ is located on the equator in MAM and moves north in JJA due to the seasonal temperature shifts. As a result, equatorial precipitation decreases, and equatorial trade winds increase. This leads to the formation of the cold tongue in JJA with an SST gradient from east to west. The cold tongue is linked to the West African monsoon since moist air from the equatorial Atlantic supplies the monsoon precipitation (Philander and Pacanowski, 1981). In coupled models, the ITCZ is generally located too far south and is also described as a double ITCZ in the Pacific area (Mechoso et al., 1995; Richter et al., 2014b; Li and Xie, 2014). Richter et al. (2014b) linked the shifted ITCZ in MAM to a delayed onset of equatorial trades and the West African monsoon season with further implications of a weak development of the cold tongue too far west. The resulting opposite equatorial SST gradient in JJA would affect equatorial winds and the thermocline. The location of the ITCZ is largely

affected by the SST bias (Large and Danabasoglu, 2006) since deep convection is triggered by SST gradients at shifted locations and reduces precipitation over West Africa (Richter and Tokinaga, 2020). However, Belmonte Rivas and Stoffelen (2019) found systematic errors in ERA-Interim and ERA-5 Reanalysis in terms of too weak mean meridional winds and variability regarding tropical trade winds and implications on the equatorial SST gradient and mesoscale convective airflow along the ITCZ. They associate low eddy wind divergence with unresolved airflows under moist convection conditions along the ITCZ linked to biased meridional transient winds.

Due to the complexity and coupled feedback mechanisms involved in the eastern boundary SST bias, the question remains if predictive skill and long-term climate change projections are seriously affected by the bias as suggested by Park and Latif (2020). Answering this question could refine where attention and efforts need to be directed to effectively improve prediction skill of coupled climate models. As tropical Atlantic SST is linked to West African precipitation (Mitchell and Wallace, 1992; Xie and Okumura, 2004; Caniaux et al., 2011) more light needs to be shed on to which extent the SST bias affects the predictive skill of precipitation.

2.4 Atlantic climate modes

Next to the erroneous representation of mean state SST and variations in amplitude and phasing of the annual cycle, diminished interannual variability accompanies the bias. Climate modes and their associated teleconnections can provide better predictive model skill and emphasize the importance of the realistic representation of Atlantic climate modes regarding the predictive skill of West African precipitation. This includes climate modes like the Atlantic Zonal Mode (AZM) and their associated climatic responses (Richter et al., 2014b; Ding et al., 2015). The AZM involves variations of the Atlantic cold tongue and the eastern tropical part of the South Atlantic, involving the area most affected by the mean state SST bias. The AZM is expected to depend on similar dynamics involved in ENSO (Zebiak, 1993; Keenlyside and Latif, 2007; Richter et al., 2014b). Compared to the tropical Pacific interannual SST variability in the Atlantic is small and the AZM is rather described as a modulation of the seasonal cycle, phase-locked to JJA (Richter et al., 2014b). A second mode on interannual to longer time scales is the Atlantic Meridional Mode (AMM), where an SST gradient between the northern and southern tropical Atlantic is involved. It is suggested to be linked to the Atlantic Multidecadal Oscillation (AMO) (Veiga et al., 2020).

As the local winds off the coast of Angola are rather weak this area is prone to be strongly affected by equatorial Kelvin Waves (EKW) remotely forced by weakened trade winds in the western equatorial Atlantic (Rouault, 2012). They transform into CTWs as they reach the eastern boundary and travel poleward along the coastline and generate SST

variability. Warm/cold events on interannual time scales, called Benguela Niños/Niñas, occur predominantly during boreal winter/spring (February-March-April: FMA) and are supposedly a result of such equatorial wind anomalies and high energetic CTWs (Bachèlery et al., 2016). During such events, warm tropical water intrudes into the Angola Benguela Area (ABA), 10-20°S and 8-15°E. Warm anomalies can reach into the northern Benguela upwelling region and locally affect upwelling intensity and the associated ecosystems. Those events are likely to affect climatic parameters such as precipitation over Africa and atmospheric circulation as well (Shannon and Nelson, 1996). The intensity of Benguela Niños is as well modulated by local conditions. Hormann and Brandt (2009) suggest a preconditioned thermocline by remotely forced EKWs might influence the cold tongue upwelling intensity in the following season. This might be as well the case for the CTWs along the coast.

The AZM and Benguela Niños dominate the interannual SST variability of the South Atlantic. Their spatial patterns and seasonal phase locking strongly resembles the characteristics of the SST bias. SST variability in the eastern equatorial Atlantic might be suppressed by the enhanced thermocline. Significant improvements have been achieved in terms of variability in recent versions of coupled models capturing the structure of the AZM. As a realistic representation of the interannual variability patterns is imperative for predictive skill, it is of major interest to what extent predictive skill exists in the presence of realistic SST variability. It might lead to further insights into how much the region could benefit from variability improvements. Richter et al. (2014b) found that some models show realistic variability patterns and capture the relevant climate modes in the presence of severe biases. They suggest the forecast skill is limited by general predictability in the tropical Atlantic region, however, could be increased for the African monsoon by extended ocean observations (Tompkins and Feudale, 2010).

3 Methods

For the purpose of analyzing the characteristics of the eastern boundary SST bias and its link to precipitation in a coupled model framework, the latest version of the Max-Planck-Institute Earth System Model (MPI-ESM1.2) is used. To examine how model skill and the representation of SST change with resolution, various model runs with different resolutions of ocean and atmosphere components are analyzed. All model runs used in this study and observational reference data is described in Section 3.1. The methods of analyzing general model performance and SST representation are explained in Section 3.2, including the computation of upwelling indices and estimation of interannual periodicity of SST. In Section 3.3 the analysis of atmospheric responses to SST variations is described to estimate the influence of the SST bias on the atmospheric model representation. The use of an atmosphere-only run to determine intrinsic atmospheric biases for an estimation of the SST bias impact on other climate variables is described in combination with an analysis of the atmospheric moisture flux. In addition, composites of interannual warm SST events are used to estimate the model's ability to reproduce realistic climatic responses to interannual SST variability. The sensitivity experiment of a historical model run, forced with realistic oceanic temperature and salinity anomalies, allows the examination of the biased representation of interannual precipitation anomalies induced by SST variations and is also used for the analysis of precipitation performance in the model simulation. Section 3.4 presents the methods used for the estimation of the model skill to reproduce interannual African precipitation anomalies and their dependency on the representation of South Atlantic SST pattern.

3.1 Models and data

3.1.1 Coupled climate model

MPI-ESM1.2 is a coupled GCM and is used in high resolution (MPI-ESM1.2-HR, here in the following: HR) as the reference model in this study. This state-of-the-art climate model is widely used for seasonal and decadal climate prediction. It is also the baseline for CMIP6 experiments. A detailed description of HR is available by Müller et al. (2018). HR comprises the ocean and sea ice submodel MPIOM with a quasi-uniform horizontal resolution of 0.4° with a tripolar grid TP04 which is isotropic in the Southern Hemisphere and has two poles in the Northern Hemisphere. The grid is regarded as eddy-permitting and has 40 unevenly spaced vertical levels (Jungclaus et al., 2013). The ocean submodel is

coupled to the latest version of the atmospheric submodel ECHAM6.3 with a horizontal resolution of 0.9° and 95 vertical levels truncated at T127 (Hertwig et al., 2015; Mauritsen et al., 2019), including the land-surface of JSBACH (Stevens et al., 2013; Reick et al., 2013). The Ocean-Atmosphere-Sea-Ice coupler version 3 (OASIS3-MCT) is applied for the coupling of both domains with a frequency of 1 h (Valcke, 2013). A horizontal discharge model is used to compute river runoff (Hagemann and Gates, 2003).

Due to increased computational power earth system models can be run with even higher resolution than HR. A higher resolution allows resolving processes which need to be parameterized in model simulations with lower resolution. Dynamical processes in the ocean and atmosphere are expected to improve and reduce systematic biases (Gutjahr et al., 2019). Hence, XR (MPI-ESM1.2-XR) and ER (MPI-ESM1.2-ER) with increased atmo-

Model Name & Abbreviation	Atmospheric Resolution	Oceanic Resolution	Reference
MPI-ESM-HR **HR**	0.9°x0.9° T127L95	0.4°x0.4° TP04L40	Müller et al. (2018)
MPI-ESM-XR **XR**	0.5°x0.5° T255L95	0.4°x0.4° TP04L40	Putrasahan et al. (2019)
MPI-ESM-ER **ER**	0.9°x0.9° T127L95	0.1°x0.1° TP6ML80	Von Storch et al. (2012) Stössel et al. (2015)
MPI-ESM-MR **MR**	1.9°x1.9° T63L95	0.4°x0.4° TP04L40	Guo et al. (2016)
Atmospheric GCM			
ECHAM6.3 **AMIP**	0.9°x0.9° T127L95		Mauritsen et al. (2019)
Sensitivity Experiment			
MPI-ESM-HR + GECCO3 T/S anomalies **HR GECCO3**	0.9°x0.9° T127L95	0.4°x0.4° TP04L40	Köhl (2020)

T: horizontal truncation, TP: tripolar grid, L: vertical levels

Table 3.1: Climate models used in this study and their corresponding atmosphere and ocean resolution. For the analysis, the time period of 01/1980-12/2014 is used, except for MR which is only available to 12/2005.

spheric and oceanic resolution respectively are analyzed next to HR to observe changes in the SST bias with resolution and the associated climatic impact.

XR is executed with the same MPIOM domain as in HR, but atmospheric horizontal resolution is increased to 0.5° with 95 vertical levels truncated at T255. In this version of the model coastal winds are represented with higher detail, whereas the SST bias along upwelling regions decreases and improves thermocline representation (Milinski et al., 2016). However, as surface winds generally decrease in this simulation, the AMOC weakens, stressing the sensitive balance between the ocean and atmosphere components (Putrasahan et al., 2019; Roberts et al., 2020).

ER is the eddy-resolving model configuration with an increased ocean resolution of 0.1° on a tripolar grid (TP6M). The northern hemisphere's grid is quasi-uniform, whereas the southern hemisphere's grid is scaled with latitude. This grid can resolve mesoscale eddies with exceptions along continental shelves, the Arctic Ocean, Nordic Seas, and North Atlantic marginal seas (Von Storch et al., 2012; von Storch et al., 2016; Gutjahr et al., 2019). While the ocean resolution is increased in comparison to HR, the atmospheric component remains unchanged with the same horizontal resolution of 0.9° and 95 vertical levels as for HR. Regarding Gutjahr et al. (2019), ER reduces biases in the ocean, near-surface atmosphere, and higher atmosphere. They conclude that large-scale atmospheric temperature distribution is affected by ocean resolution.

HR is also compared to the previous version of MPI-ESM in medium resolution (MR) which participated in CMIP5. Ocean resolution in MR is the same as in HR, albeit model physics are improved in HR. However atmospheric resolution is lower in MR, with 1.9° and 95 vertical level truncated at T63. An overview of all model simulations that are compared in this study is given in Table 3.1 together with the available time periods. In this study, the historical model runs are used.

3.1.2 Atmospheric General Circulation Model

Systematic biases of climate variables in a coupled model can originate from the oceanic or atmospheric component. In order to display how the SST bias interacts with climate variables, the atmospheric contribution to systematic biases can be removed or can be used as a reference. For this purpose, a historical AMIP-type simulation (here in the following: AMIP), containing the time period of 1979 to 2015, is included in this study. For the AMIP simulation, the atmospheric GCM used as the atmospheric component in HR is run in an atmosphere-only setting forced by observed SST. This allows insight into the model's ability to simulate precipitation and other atmospheric anomalies with respect to realistic SST fields. Systematic biases present in this simulation are of atmospheric origin and thus, are not a result of biased SST. A comparison of the AMIP and coupled model

simulation provides further insight into how intrinsic atmospheric biases are further reinforced in the coupled simulation and allows scaling the impact of the SST bias on other climate variables. In addition, considering the AMIP simulation as a zero-lead forecast, it can give an idea of reproducible precipitation variability in the presence of realistic SST variations, defined by (Richter et al., 2018) as an upper limit of achievable predictive skill of precipitation (Richter et al., 2018). Coupled models can, however, achieve higher predictive skill of precipitation, since surface heat fluxes may be biased in AMIP-style experiments (Wang et al., 2005; Wu and Kirtman, 2005).

3.1.3 Sensitivity experiment

A historical model run of MPI-ESM1.2-HR assimilated with ocean temperature and salinity anomalies from GECCO3 (German contribution to the Estimating the Circulation and Climate of the Ocean project, version 3) ocean synthesis was performed in the context of the study of Köhl (2020) and is here used as a sensitivity experiment to investigate the climatic response to realistic SST events under the influence of the mean state SST bias. Ocean temperature and salinity anomalies are assimilated into the historical CMIP6 run, instead of full field variables. Thus, the experiment features realistic interannual SST anomalies while retaining the biased mean state. This experiment is meant to shed light on the influence of the mean state SST bias on precipitation and other climate variables and how the performance of reproduced precipitation anomalies over Africa is affected by defectively elevated SST. The representation of realistic SST variability under biased conditions allows for analyzing actual SST events and their climatic response. In combination with the AMIP simulation, a comparison of biased and unbiased climatic responses to those events is possible. Furthermore, precipitation patterns and variability linked to interannual SST variability within the biased area are examined.

The experiment is executed with the HR setting of MPI-ESM1.2 which is initialized with estimates of oceanic temperature and salinity fields generated by an improved third version of GECCO ocean synthesis. A detailed description of the GECCO synthesis is provided by Köhl and Stammer (2008) and Köhl (2015). Observational data is assimilated into an ocean model to generate the synthesis product. The use of such products as initial conditions for seasonal and decadal predictions is a common method further described by Pohlmann et al. (2013). The recent version, GECCO3, uses the adjoint method and the same grid and bathymetry as MPI-ESM-HR with a 0.4° quasi-uniform horizontal resolution. The configuration is chosen to provide an appropriate and eddy-permitting product for the initialization of coupled climate models, such as MPI-ESM-HR, without the need to interpolate the data from a different grid which could affect prediction skill. Compared to its prior version the GECCO3 synthesis is improved and shows good agreement with the assimilated reference data (Köhl, 2020).

The climatology of GECCO3 temperature and salinity is removed from the data to create anomaly estimates which are then assimilated into MPI-ESM-HR for the historical nudging run to study the atmospheric response within the coupled model domain of HR to realistic SST anomalies as described by Smith et al. (2013). The realistic anomalies are added to the climatology of the model, such as the model keeping its own seasonality and can retain its preferred state. Thus, the mean state SST bias is still present in the model output. In contrast, forcing a coupled model with realistic full field temperature and salinity can trigger artificial heat adjustments of the model to compensate for deviations in the forcing fields and thus affects prediction skill (Kröger et al., 2018; Polkova et al., 2019). Hence, the anomaly method is a useful tool to examine climate dependencies on SST representation in a coupled model. The nudging is performed for the period 1948 to 2018, with a relaxation time of 11 days in the ocean. The historical run was chosen over the piControl simulation as radiative forcing and greenhouse gas forcing diverges from the reference data and would thus interfere with the evaluation of the model performance. Using the historical run instead of decadal projections enables the analysis of direct climatic responses to actual SST variations to analyze the impact of the SST bias on the teleconnection between SST and African precipitation. It can help to scale the upper limit of predictability that can be expected from climate predictions. The hereafter mentioned HR GECCO3 (abbreviated to G3) output refers to the MPI-ESM-HR run forced with GECCO3 temperature and salinity anomalies.

Climate predictions based on model runs initialized with realistic data are a powerful tool in climate science. The here described sensitivity experiment serves as a base to observe the impact of elevated SST in the South Atlantic on the response of other climate variables. The goal is to examine to what extent a skillful representation of climate variables depends on a realistic representation of SST in the South Atlantic.

3.1.4 Observations and reanalysis

To estimate the deviations of model simulations from realistic values observational data products and reanalysis products serve as a reference. Table 3.2 provides a list of the reference data used in this study which is described in the following. As a reference for SST, the Daily Reynolds - OISST sea surface temperature data obtained from NOAAs' National Center for Environmental Information (NCEI) is used. The OISST analysis product uses optimal interpolation (OI) with a horizontal resolution of 0.25° and daily temporal resolution, available from 1982 to the present. It combines infrared satellite SST data from an Advance Very High Resolution Radiometer (AVHRR) and in-situ data. The infrared SST data is large-scale bias adjusted by observations from ships and buoys. A further description is provided by Reynolds et al. (2007) and Banzon et al. (2016).

Precipitation data is used from The Global Precipitation Climatology Project (GPCP).

It contains a combination of several precipitation measurements from ground stations and satellites, weighted by the strength of each data type. Further information is given by Adler et al. (2016, 2017). Global fields of monthly data of version 2.3 are used here from 1979 to present on a 2.5° cartesian grid, as well as daily data from version 1.3 with a higher horizontal resolution of 1° available from 1997 to 2018.

High resolution near surface wind data over the ocean is obtained from QuickSCAT (Quick Scatterometer) data measured by microwave radars, available for a rather short time period from June/1999 to November/2009. Wind speed and direction at 10 meters height with a resolution of 0.25° is measured by the scatterometer's backscattered power. A 3-day composite is used excluding rainflagged grid points. SeaWinds data are produced by Remote Sensing Systems and sponsored by the NASA Ocean Vector Winds Science Team. Data are available at www.remss.com, distributed in netCDF format by the Integrated Climate Data Center (ICDC) University of Hamburg, Hamburg, Germany.

In addition, ERA-5 reanalysis data is used due to the availability of longer time periods from 1979 to the present and global coverage on high resolution of 0.28°. ERA-5 is the latest version of reanalysis data developed by the Copernicus Climate Change Service (C3S) and produced at the European Centre for Medium-Range Weather Forecasts (ECMWF). The data is processed by the ECMWF earth system model also used for weather forecasting. The computation includes routine measurements and assimilated observations from weather stations, radiosonde ascents, ship measurements, and satellite measurements. Further information is provided by Hersbach et al. (2020). Various variables of this data set are used in this study, including precipitation, wind vectors, air temperature, latent heat flux, specific humidity, and precipitable water vapor.

Data Name	Variable	Resolution	Period	Reference
OISST	SST	0.25°x0.25°	1982-2019	Banzon et al. (2016)
GPCP	Precipitation	1°x1°	1997-2018	Adler et al. (2017)
	Precipitation	2.5°x2.5°	1979-2018	Adler et al. (2016)
QuickSCAT	10 m Wind	0.25°x0.25	1999-2009	Risien and Chelton (2008)
ERA-5	various[1]	0.28°x0.28	1979-2019	Hersbach et al. (2020)
	Precipitation	0.25°x0.25	1979-2019	

[1] wind, air temperature, latent heat flux, specific humidity, and precipitable water vapor

Table 3.2: Observation and Reanalysis products used in this study to evaluate climate model simulations.

The analysis by Strub and James (2022) shows unrealistic increases of wind stress in near shore areas in ERA-5 wind stress fields. Thus, instead of using ERA-5 wind stress fields for further calculations of upwelling intensity, wind stress over the water was calculated from wind speed vectors available on an interpolated rectangular grid, as recommended by Strub and James (2022). The computed ERA-5 wind stress data was used next to QuickSCAT wind stress to cover longer temporal periods. As mentioned in Strub and James (2022); Belmonte Rivas and Stoffelen (2019), ERA-5 wind data shows various weaknesses, however, can sufficiently reproduce anomalies apart from higher frequencies. Thus, the data set serves here as a sufficient reference to model simulations.

3.2 Sea Surface Temperature analysis

South Atlantic SST was analyzed along with several dependent climate variables to gain insight into the model's ability to represent the mean state, the annual cycle, and interannual variability. In this study monthly mean data sets are used. For comparison purposes, the data sets are regridded to the lowest involved resolution and cut to the shortest available time period. Mean state biases of SST and other climate variables refer to the difference between observational time averaged variable fields and time averaged model variable fields. Interannual anomalies are computed by removing temporal trends and mean annual cycles from the time series. The general performance of SST and climate variables dependent on model resolution is analyzed by Taylor metrics described in Section 3.2.1. The approach to analyze the model resolution dependent upwelling representation in the coupled climate model is described in Section 3.2.2. The wavelet analysis method to define characteristic interannual SST periods and their intensity is presented in Section 3.2.3.

3.2.1 Taylor performance analysis

An overview of the model's performances associated with different resolutions is given via a Taylor Diagram as in Taylor (2001), containing standard deviation, pattern correlation coefficient, and centered root mean square error (RMSE) for SST and other atmospheric variables. Both standard deviation and RMSE are normalized here by dividing them by the standard deviation of the reference field to make the statistics of different variables comparable. The standard deviation of the reference σ_r is defined as:

$$\sigma_r = \frac{1}{N}\sum_{i=1}^{N}(r_i - \bar{r})^2. \tag{3.1}$$

The normalized standard deviation of the modeled data σ_x is then:

$$\sigma_x = \frac{\frac{1}{N}\sum_{i=1}^{N}(x_i - \bar{x})^2}{\sigma_r}. \tag{3.2}$$

The correlation coefficient R is defined as:

$$R = \frac{\frac{1}{N}\sum_{i=1}^{N}(x_i - x)(r_i - \bar{r})}{\sigma_x \sigma_r}. \tag{3.3}$$

The normalized centered root mean square error $RMSE$ is defined as:

$$RMSE = \frac{\sqrt{\frac{1}{N}\sum_{i=1}^{N}\left[(x_i - \bar{x}) - (r_i - \bar{r})\right]^2}}{\sigma^r}. \tag{3.4}$$

The performance metrics are computed for time varying fields over all grid cells and all time steps, whereas the sum is a double sum. For the computation the means of the values are subtracted, so the metrics do not include information about mean state biases. For comparison, the weighted means of global absolute biases are given along with the Taylor diagram.

3.2.2 Upwelling indices

The eastern boundary of the South Atlantic is characterized by its wind driven coastal upwelling system which brings cold and nutrient rich water to the surface via Ekman dynamics, affecting SST and its variability along the coast. As the SST bias is most elevated along the coastal upwelling area off Angola and the northern Benguela Upwelling area, the representation of upwelling processes in the model is of major interest. Three different upwelling indices (UI) are calculated here from SST and wind stress vectors to estimate the model's ability to represent upwelling with respect to different model resolutions in comparison to the observational reference data. Upwelling events occur at high frequencies such as days to weeks and vary on seasonal scales (García-Reyes et al., 2014). Since monthly mean values are used here to quantify upwelling processes, estimates only serve as a rough and simplified measure of potential upwelling intensity. The influence of highly variable bottom topography along the shelf is neglected here. The here computed indices do not compute the upwelling process itself, but rather upwelling favorable conditions like the presence of coastal alongshore winds and the potential result of upwelling processes by the coastal SST gradients. Nonetheless, the computed indices are sufficient to compare the coupled model's ability to capture those small scale features in time and space. The study of Small et al. (2015) showed an improved representation of Benguela upwelling processes only lead to a modest reduction of the SST bias, pointing out that correct SST representation does not solely depend on the representation of Benguela upwelling dynamics. However, their restoring SST experiments along the eastern boundary showed the importance of including the SST off the coast of Angola to achieve a good equatorial response. In addition, the study of Illig et al. (2020) shows the importance of alongshore winds along Angola to correctly model the dynamics of interannual SST variability. The studies highlight the importance of realistic SST and surface wind representation in the Angola area to correctly model equatorial dynamics and feedback mechanisms. Both

variables are crucial in the coupling process of climate models and directly involved in upwelling processes, hence, simulated upwelling dynamics along the equatorial cold tongue and the eastern boundary are examined in this study along with their seasonal variation.

As a simplified indication for upwelling a coastal SST gradient is used like in the study of Santos et al. (2005), who used this index to study the variability of the Canary upwelling system. Coastal and equatorial SST gradients are here computed by the difference between coastal/equatorial SST and SST 500 km further offshore/north, such as upwelling is indicated by negative gradients:

$$UI^{SST} = T_{coast} - T_{offshore}. \tag{3.5}$$

With respect to surface winds, two other upwelling indices are computed. As described before, the structure of near shore wind stress plays an important role in upwelling dynamics. Thus, two different wind dependent upwelling processes are taken into account. First, wind stress induced coastal upwelling can be theoretically computed by offshore Ekman transport using alongshore winds. Equatorward winds along the eastern boundary induce Ekman transport, creating a mass flux divergence across the shelf which needs to be balanced by vertical converging mass fluxes (assuming no alongshore variations) (Jacox et al., 2018). Since Ekman offshore transport is compensated by water upwelled from below and is thereby equal to the vertical transport, it can serve here as an indication for theoretical upwelling and is calculated as follows.

In the Ekman theory the equation of motion reduces to a balance between Coriolis force and frictional forces, under the assumption of a linear homogeneous ocean in a steady state, with no horizontal gradients with no lateral limitations:

$$fu = -\frac{1}{\rho_w}\frac{\partial \tau}{\partial z}, \tag{3.6}$$

with the Coriolis parameter f, the velocity vector u, a reference sea water density ρ_w taken here as $\rho_w = 125 kgm^{-3}$, viscous stresses τ varying with depth z (Jacox et al., 2018). An Ekman surface layer defines the surface thickness to depth, where internal stress drops to zero. The integration of τ over the Ekman surface layer yields the volume transport per unit length with respect to surface wind stress. It describes the integrated near surface transport perpendicular to the surface wind stress vector, directed to the right/left in the northern/southern hemisphere. The alongshore wind induced Ekman transport serves here as an index UI^w for coastal upwelling favorable conditions, computed as:

$$UI^{w} = -\frac{\tau_c}{\rho_w f} \tag{3.7}$$

with the wind stress component τ_c parallel to the coast. The alongshore wind stress component is calculated from zonal and meridional surface wind stress vectors by taking into account the orientation of the shoreline. Wang et al. (2015) used this method to compare upwelling intensity and duration of the main global upwelling systems and long term trends.

The second index regarding near shore surface winds is computed by considering Ekman Pumping. This process describes vertical transport driven by the wind stress curl (WSC). It is described by Risien and Chelton (2008) who analyzed QuickSCAT surface wind fields to highlight the importance of small scale wind features for ocean and atmosphere dynamics. Small et al. (2015) computed Ekman pumping to investigate the oceanic response to wind forcing. In the presence of Ekman pumping an Ekman transport divergence is initiated by spatial wind stress variability. Spatial wind stress variability is a result of drag induced by orographic boundaries which reduces wind stress magnitude towards the coast (Renault et al., 2016). To quantify the vertical transport to compensate for the divergence, the vertical velocities at the base of the Ekman surface layer can be computed from the WSC as in Risien and Chelton (2008):

$$UI^{wE} = \frac{\nabla \times \tau}{\rho_w f} + \frac{\tau_x \beta}{\rho_w f^2}, \tag{3.8}$$

with

$$WSC = \nabla \times \tau = \frac{\partial \tau^y}{x} - \frac{\partial \tau^x}{\partial y}, \tag{3.9}$$

computed using the central difference method. τ_x is the eastward component of the wind stress vector and $\tau - y$ is the northward component. $\beta = \frac{2\Omega cos(\phi)}{R_E}$ accounts for variations of Coriolis force with latitude, with earth rotation Ω, earth radius R_E and latitude ϕ. For Coriolis parameters close to zero Ekman theory fails, thus, results for alongshore Ekman transport and Ekman pumping in near equatorial regions (approximately between 5°N and 5°S) are not valid.

In reality, the assumed perfect conditions for these computations are not met. Thus, this index should not be considered as an absolute magnitude of upwelling, but rather indicates relative variability and upwelling favorable conditions.

As the observational reference ERA-5/QuickSCAT data daily-mean/3day-mean wind vectors are used to compute wind stress vectors which are then averaged to monthly mean wind stress vectors to make them comparable to monthly mean values generated by the model. Wind stress is calculated from wind vectors using the bulk aerodynamic formula

along with the Large and Pond neutral stability drag coefficient with modified specifications of the drag coefficient c_{10}, suitable for scatterometer wind data from QuickSCAT described by Large et al. (1994); Risien and Chelton (2008):

$$\tau = \rho_{air} C_{10} \overrightarrow{V_{10}} |\overrightarrow{V_{10}}|, \tag{3.10}$$

with air density $\rho_{air} = 1.223\ kgm^{-3}$.

3.2.3 Wavelet analysis

A wavelet analysis generates information about periodical power in variations of a time series by decomposing it into time-frequency space. It is used here to observe periodic behavior of SST and precipitation time series. A detailed description is provided by Torrence and Compo (1998). For example, wavelet analysis has been applied in studies of Gu and Philander (1995), who used this technique to analyze characteristics of ENSO, Szolgayová et al. (2013) examined the dependency between discharges, precipitation, and air temperature on the Danube river, while Sleziak et al. (2015) highlights the advantages of using Wavelet Transforms over Fourier Transforms. This method allows the identification of dominant modes in nonstationary time series and can even extract low signal-to-noise ratio features of a time series. It enables the detection of temporal variations of significant periodicity. Regions of high power in time frequency space can be compared between variables. Thus, coherent temporal variations between variables indicate a consistent phase relationship and highlight periodical dependency, since it is defined as a localized correlation coefficient in time frequency space.

Here SST periodicity is analyzed along the equator and eastern boundary of the South Atlantic to identify interannual modes and their representation in the coupled climate model under biased conditions. In addition coherence between SST and precipitation periodicity is examined in order to detect on which scales precipitation is linked to SST variations and to which extent this dependency is affected by biased SST.

According to Torrence and Compo (1998); Grinsted et al. (2004), a discrete time series x_n, with $n = 1, ..., N$, and consistent time steps t can be analyzed using a zero mean Morlet wavelet function, defined as

$$\psi_0(\eta) = \pi^{-0.25} e^{i\omega_0\eta} e^{-0.5\eta^2}, \tag{3.11}$$

with the dimensionless frequency ω_0 and dimensionless time η, where frequency and location in time can be altered. The wavelet function is applied as a bandpass filter to the time series. The continuous wavelet transform of a discrete time series x_n is the

convolution of x_n with a scaled and normalized wavelet. It can be written as follows,

$$W_n^X(s) = \sqrt{\frac{\delta t}{s}} \sum_{n'=1}^{N} x_{n'} \psi_0 \left[(n' - n) \frac{\delta t}{s} \right]. \tag{3.12}$$

The scale of the wavelet, s, can be varied and shifted along the time index n, whereas the power is obtained by $|W_n^X(s)|^2$.

To examine coherence of periodic power between two time series the cross wavelet power $|W^{XY}|$ is computed, where the cross wavelet spectrum is defined by Torrence and Compo (1998) as $W_n^{XY}(s) = W_n^X(s) W_n^{Y*}(s)$, using the complex conjugate $W_n^{Y*}(s)$ of $W_n^Y(s)$. The coherence of two time series is then defined by Torrence and Webster (1998) similar to the correlation coefficient as

$$R_n^2(s) = \frac{|S\left(s^{-1} W_n^{XY}(s)\right)|^2}{S\left(s^{-1}|W_n^X(s)|^2\right) \cdot S\left(s^{-1}|W_n^Y(s)|^2\right)}, \tag{3.13}$$

where S denotes the smoothing operator $S(W) = S_s(S_t(W_n(s)))$, with scaling along the wavelet scale axis with S_s and smoothing in time with S_t (Grinsted et al., 2004). The Monte Carlo method is here used to compute statistical significance. Random artificial time series are generated with first order autoregressive (AR1) coefficients of the analyzed time series to test against the null hypothesis that the signal is generated by red noise on a 95% confidence level.

3.3 Climate response to Sea Surface Temperature variations

The variability of the climate system is largely dependent on SST variations which directly impact ocean-atmosphere exchanges of momentum, energy, and water. The atmosphere responds to SST variations on weather and climate time scales, while it drives local and remote precipitation via thermodynamic and dynamic interactions, and large scale atmospheric circulations as well. The South Atlantic SST bias is assumed to affect predictive skill of the climate system, especially precipitation patterns over the African continent. Warm tropical SST can trigger deep convection, which impacts the upper level troposphere, as well as water mass and energy transports via Walker and Hadley circulations and monsoonal rainfall via atmospheric teleconnections (Sun and Tan, 2022). Thus, the SST bias poses a very likely error source which needs to be analyzed with regard to the severity of its impact on the teleconnection between SST and precipitation. Aiming to outline the impact of the SST bias, this study analyzes how precipitation patterns, water exchange between ocean and atmosphere, as well as atmospheric water fluxes and surface wind vectors change in the presence of the SST bias.

For this purpose, SST data is analyzed along with surface air temperature (T_{air}), pre-

cipitation (PRC), surface wind vectors ($Wind_u/Wind_v$), and surface latent heat flux (LHF) as an indication for evaporation, as well as computed atmospheric moisture flux and convergence. Moisture flux and convergence are further specified with their contributing thermodynamic and dynamic part.

The AMIP run serves as a reference for intrinsic atmospheric biases as it is forced with realistic SST fields and the same boundary conditions as the other model runs. A comparison with the HR simulation can show how atmospheric biases are reinforced due to the coupling of oceanic and atmospheric model components along with the arising SST bias. The difference between AMIP and HR atmospheric data can highlight possible atmospheric responses to the SST bias. Though, biases can arise from other sources, such as the land surface model, but are considered small here. The differences between model runs are examined in their mean state and seasonality to account for annual feedback mechanisms. Along with the difference between AMIP and HR, the difference between HR and XR is analyzed, in order to show how the representation of climate variables changes with resolution along with a changed magnitude of the mean state SST bias. The biased seasonal cycle along the equator and eastern boundary is investigated, as well as the biased seasonality of the African monsoon which is depicted as atmospheric variables averaged between 40°W and 40°E along latitudes between 30°N and 20°S. Only HR and XR runs are examined here (excluding MR and ER runs) since the SST bias reduction between both runs is large and could yield a significantly different atmospheric response.

In addition, the atmospheric response as a composite with reference to warm AZM events is analyzed in HR and XR runs, in comparison to the reference data, to show how atmospheric patterns are influenced by the SST bias on interannual scales. The sensitivity experiment and the AMIP run are used to examine atmospheric responses to actual Bengula Niño warm events to show how they are affected by the SST bias.

3.3.1 Atmospheric moistureflux

In order to gain a deeper understanding of changes in precipitation patterns due to the SST bias, components of the hydrological cycle of the atmosphere are calculated. According to Kleidon (2019), the hydrological cycle of the atmosphere is described by a balance between evaporation and precipitation which is subject to spatial variations due to moisture transport. Evaporation acts as a source of moisture in the atmosphere and is directly linked to surface latent heat flux, whereas precipitation is a moisture sink and releases latent heat into the atmosphere. Spatial variations result from zonal gradients of solar radiation which drive evaporation, and need to be balanced via moisture being transported by the atmospheric circulation. This results in convergence zones in the tropics and mid-latitudes. To follow the impact of the SST bias, atmospheric moisture fluxes and their convergence are calculated and their changes are assigned to thermodynamic

and dynamic contributions generated by the SST bias. Following Guo et al. (2018) the atmospheric moisture budget can be written as follows:

$$P = E - \frac{\partial W}{\partial t} - C \tag{3.14}$$

The supply of moisture for precipitation P is described by evaporation E, integrated water (in form of vapor, liquid, and ice) W, and convergence of vertically integrated moisture flux C.

The following described computation of the moisture budget terms follows Watterson et al. (2021); Ye et al. (2020). The vertically integrated water vapor is obtained by the integration of specific humidity q from surface pressure p_s up to the approximate upper end of the troposphere p_t (here chosen as 250 hPa), where most of the humidity is present:

$$W = g^{-1} \int_{p_t}^{p_s} q \, dp. \tag{3.15}$$

The horizontal moisture flux can be computed from specific humidity and the horizontal wind vector V_h:

$$\vec{Q} = q\vec{V_h}. \tag{3.16}$$

The horizontal moisture flux Q is then integrated through the troposphere to represent the horizontal water vapor transport within the troposphere:

$$\vec{F} = g^{-1} \int_{p_t}^{p_s} q\vec{V_h} \, dp, \tag{3.17}$$

From the vertically integrated horizontal moisture flux vector F the vertically integrated moisture flux convergence can be computed as follows:

$$C = -\nabla \cdot \vec{F} = -\frac{\partial \left(g^{-1} \int_{p_t}^{p_s} qu \, dp \right)}{\partial x} - \frac{\partial \left(g^{-1} \int_{p_t}^{p_s} qv \, dp \right)}{\partial y}, \tag{3.18}$$

For the computation of the horizontal moisture flux, daily data of specific humidity and wind vectors are used. The convergence is computed by using the finite difference method. Daily data are then averaged to monthly means. Since the data from the sensitivity experiment is only generated for monthly mean values, horizontal moisture flux and its convergence is also computed from monthly mean values to be comparable to the sensitivity experiment. Although accuracy is reduced by using monthly mean data for the computation, a comparison between anomalies from the daily and monthly data showed sufficient agreement. Thus, the computed data sufficiently serves the purpose to illustrate anomalies of horizontal moisture flux and its convergence during Benguela Niño events.

Thermodynamic and dynamic contribution

For a better understanding of the altered precipitation patterns under the influence of elevated SST of the South Atlantic, the horizontal moisture flux and its convergence are attributed to thermodynamic and dynamic contributions. The thermodynamic contribution refers to changes in atmospheric water vapor due to warming via changed evaporation rates. The dynamic response describes the altered moisture flux while evaporation rates stay unchanged but atmospheric circulation is affected by temperatures and advects moisture to altered locations.

Following Watterson et al. (2021) the thermodynamic part of changed convergence fields is simplistically evaluated by the fractional change of available water vapor (W) multiplied by the mean state of the reference convergence field C_r, assuming the change of water vapor is completely thermodynamic.

$$\Delta C_T = C_r \frac{\Delta W}{W_r} \tag{3.19}$$

The dynamic contribution is here assumed to be the remaining part of the changed field (omitting nonlinear and other terms):

$$\Delta C_D = \Delta C - \Delta C_T \tag{3.20}$$

Collins et al. (2013); Watterson et al. (2021) used this approach to attribute changes in precipitation due to global warming into thermodynamic and dynamic components and refer to the Clausius-Clapeyron scaling applied by Held and Soden (2006).

3.3.2 Atlantic Zonal Mode

Composites of South Atlantic SST anomalies associated with the AZM are analyzed with regard to their atmospheric response. SST anomalies along the coast of Angola (7°S-16°S) show highest interannual variability from May to July suggesting a seasonal phase locking. They are significantly correlated to wind anomalies during March/April, where significant Pearson correlation coefficients are determined by computing the 95% confidence level using the bootstrap method with 2000 repetitions (Tibshirani and Efron, 1993). The eight most extreme years during the period of 1982-2014, showing the eight largest positive and negative anomalies respectively, are chosen and seasonally averaged to depict the average seasonal development and atmospheric response to such events. Composites are generated for HR and XR runs, as well as for the reference data including OISST and ERA-5 data. The composites contain fields of SST, air temperature, precipitation, and surface wind vectors, along with latent heat flux, moisture flux, and convergence to account for the atmospheric moisture transport associated with these events.

3.3.3 Benguela Niños

Another composite analysis is applied in order to analyze the atmospheric response to Benguela Niño events with and without the influence of the SST bias. For this purpose, the sensitivity experiment run is used to present realistic Benguela Niño events in the coupled model domain and their impact on atmospheric dynamics in the presence of elevated mean state SST. In addition, the AMIP run is used to represent atmospheric responses to Benguela Niño events without biased SST. Both composites are compared to the reference data of OISST and ERA-5. Since the AMIP run is forced with observed SST and the sensitivity experiment is forced with realistic SST anomalies, actual observed Benguela Niño events can be analyzed. To define those extreme SST events the so called ABA index is computed from SST anomalies of the Angola Benguela Area (ABA) during the time period of 1982 to 2014, following Richter et al. (2010); Imbol Koungue et al. (2017, 2019). The ABA stretches from 10°S to 20°S and from 8° to 15°E, where SST is highly variable on interannual scales. SST anomalies of the ABA are derived from averaged SST over the ABA. The linear trend is removed from the ABA SST which is estimated by linear least square regression. Subsequently, the monthly climatology is removed yielding ABA SST anomalies. The ABA index is computed by normalizing the anomalies by their seasonally averaged standard deviation. Benguela Niños are then defined as anomalous warm events in the ABA, that exceed their seasonal standard deviation during at least three consecutive months during boreal winter/spring (January to May), such as the ABA index exceeding the value of one. The ABA index provides the opportunity to determine the years affected by Benguela Niño events and allows the creation of Benguela Niño composites by extracting associated SST anomalies and climate anomalies of those events and computing their average.

3.4 Precipitation performance analysis

In order to assess the impact of the SST bias on precipitation variability and other climate variables the performance of HR GECCO3 is analyzed in comparison to AMIP. As HR GECCO3 is forced with realistic SST anomalies by retaining the biased mean state and AMIP is forced with realistic SST full fields, both model simulations can be compared to observations to examine their ability to reproduce the climate response to SST variability. Performance of climate variables is quantified by anomaly correlation coefficients (ACC) and the RMSE normalized by the standard deviation of the reference time series. Yearly mean anomaly time series are used for the performance comparison in a Taylor diagram (as described in Section 3.2.1) and global maps of ACC and RMSE for precipitation. The RMSE is normalized since errors are proportional to the magnitude of variability which can locally and seasonally vary.

Climate variables are indexed over different regions to examine general performance. This means variables are averaged over a characteristic region for the time period 1982-2014. A three-month-running mean is applied to the averaged time series to account for seasonal shifts of the annual cycle between models. Anomalies are then generated by detrending and removing the seasonal cycle. The anomalies are seasonally stratified to receive inter-annual anomalies for every month of the year. A four year-running-mean is applied to the anomalies to remove the influence of quasi-biennial oscillations and concentrate on longer periods which are affected by the dominant SST variations of the South Atlantic. ACC and RMSE are then computed for the anomalies with respect to seasons. Significant correlations at the 95% confidence level are computed with the bootstrap method with 2000 repetitions.

Equatorial variables are indexed to evaluate if the biased annual feedback mechanism due to the SST bias, affects interannual performance of precipitation and zonal wind. In addition, precipitation indices are computed for regions affected by the West African monsoon rainfall, since those areas are directly affected by tropical Atlantic SST variations which modulate monsoon intensity. Lastly, the performance for precipitation indices along African land areas along the southwestern coast is computed, in order to evaluate the influence of SST variations induced by Benguela Niño events on coastal precipitation.

A coherent wavelet analysis, as described in Section 3.2.3, is applied to interannual precipitation anomalies and SST anomalies (1982-2014) in order to examine temporal scales and intensity on which precipitation during monsoon season is linked to Atlantic SST and affected by the SST bias. In addition, common variability patterns between SST and precipitation are analyzed on spatial scales using multi-variate EOF which is described in the following.

3.4.1 Multivariate EOF analysis

A multi-variate EOF analysis is used to derive dominant modes of coherent variability of African precipitation and South Atlantic SST. The method is used here to address the spatial phase relationship between both variables and how this dependency is affected by the SST bias. The method is suitable for this purpose since SST and precipitation patterns are well correlated. For the analysis, a normalized covariance matrix is defined from area weighted precipitation and SST anomalies for the time period between 1982 and 2014. Anomalies of GPCP and OISST are analyzed as a reference, along with anomalies generated by the AMIP run and the sensitivity experiment. The covariance matrix is decomposed into a set of EOFs and corresponding principal component (PC) time series. The EOFs are eigenvectors of the covariance matrix and describe coherent variability of the spatial patterns. The eigenvalues give the percentage of variability which is explained by each EOF mode. The method is described in detail by Wang (1992). The EOFs and

PCs are normalized by the corresponding PCs maximum value, for comparative purposes. Coherent variability between South Atlantic SST and African precipitation anomalies is examined in this study.

4 The Sea Surface Temperature bias and its climatic impacts

In a coupled climate model the eastern boundary SST warm bias affects the numerical simulation of atmospheric variables. The extent of the systematic biases is presented in this Chapter. An overview of global mean state biases in MPI-ESM coupled model simulations is given for SST and relevant atmospheric variables, along with their performance in relation to atmospheric and oceanic model resolution. A major feature of the South Atlantic eastern boundary is defined by the strong upwelling dynamics that affect coastal SST. As the mean state SST bias is especially pronounced in eastern boundary upwelling regions, the simulated upwelling conditions are investigated for different model resolutions. The South Atlantic SST variability is largest along regions characterized by upwelling dynamics. Thus, the relation between represented upwelling processes and physical dynamics, that contribute to the SST variability, is of major interest. Upwelling dynamics are highly dependent on spatial and temporal surface momentum flux variations which excite upwelling or precondition the ocean surface so that the effects of remotely forced up and downwelling waves are enhanced or weakened. In addition, the representation of upwelling dynamics in a coupled model is linked to the underlying current system which affects the simulation of general ocean dynamics. Upwelling favorable conditions could play an important role in the air-sea interaction with an effect on SST and climate variability. It is necessary to determine the effect of improved upwelling conditions with model increased model resolution on the representation of simulated SST and atmospheric variables to determine the contribution to the quality of simulated climate and precipitation variability.

As the magnitude of the SST bias changes with model resolution and the corresponding representation of upwelling conditions, the impacts of the different magnitudes of the South Atlantic SST bias on the atmospheric model component need to be examined. For this reason, intrinsic atmospheric biases in the AMIP simulation are compared to the coupled model simulations, in order to highlight the alteration of represented variables arising from the process of coupling oceanic and atmospheric submodels. As the AMIP simulation is forced with realistic SST fields, the atmospheric representation is not influenced by any ocean biases and shows only biases that are already present in the atmospheric component. The differences in mean states and seasonal cycles between the AMIP simulation and the coupled simulations show how atmospheric biases are reinforced under the influence

of the oceanic model simulation including the SST bias which arises from the coupling process. Additionally, the difference to a simulation with higher atmospheric resolution is shown to highlight the changes arising along with a decreased magnitude of the SST bias. The impact on the atmospheric moisture budget is investigated for a better understanding of simulated precipitation patterns affected by the coupling process and the SST bias. Furthermore, the simulation of the annual cycle of the tropical Atlantic region is examined in terms of altered feedback mechanisms linked to the SST bias which contributes to the biased mean state of the atmosphere. As this study focuses on the representation of African precipitation in the coupled model simulation, the impact of the coupling process and the SST bias on the annual cycle of the African monsoon is examined as well.

In the following the global mean state SST bias and its change with resolution is presented in Section 4.1 along with other atmospheric biases. In Section 4.2 the performance of SST and atmospheric variables within the coupled model domain dependent on model resolution is evaluated. An analysis of upwelling conditions follows in Section 4.3 with respect to the resolution of the atmospheric and oceanic model components. The impact of the South Atlantic SST bias on the atmospheric mean state moisture budget is estimated in Section 4.4. This Section shows how the atmospheric representation changes when coupled to the oceanic submodel with the arising influence of the SST bias which is shown in detail for the seasonal feedback mechanism of the tropical Atlantic and the seasonality of the African monsoon.

4.1 Global mean state biases

The SST bias in the South Atlantic is not a single phenomenon arising from the coupling of atmospheric and oceanic submodels but is part of a systematic bias problem affecting the eastern boundaries of global oceans. Atmospheric and oceanic biases contribute to the biased SST representation and the SST bias in turn generates additional deviations or reinforces already existing biases. To give an overview of the extent of the systematic bias problem, global SST deviations of MPI-ESM in high resolution (HR) are displayed in this Section along with biases of related atmospheric surface variables. The mean state bias of a variable is here obtained by subtracting the time averaged variable field of the reference data from the model data, such as positive/negative biases referring to the model values being too high/low. Subtraction of mean states of the reference model HR from MR, XR, and ER data yields the change of variable representation with model resolution. In a comparison of the observational OISST product and SST generated by the coupled climate simulation of HR, the regional deviations from realistic values become evident. The global mean state of OISST is displayed in Figure 4.1 A, and the difference between both mean state global SST fields is displayed in Figure 4.1 B. It shows the expected elevated SST values in the model simulation along eastern boundary regions, accompanied by a general

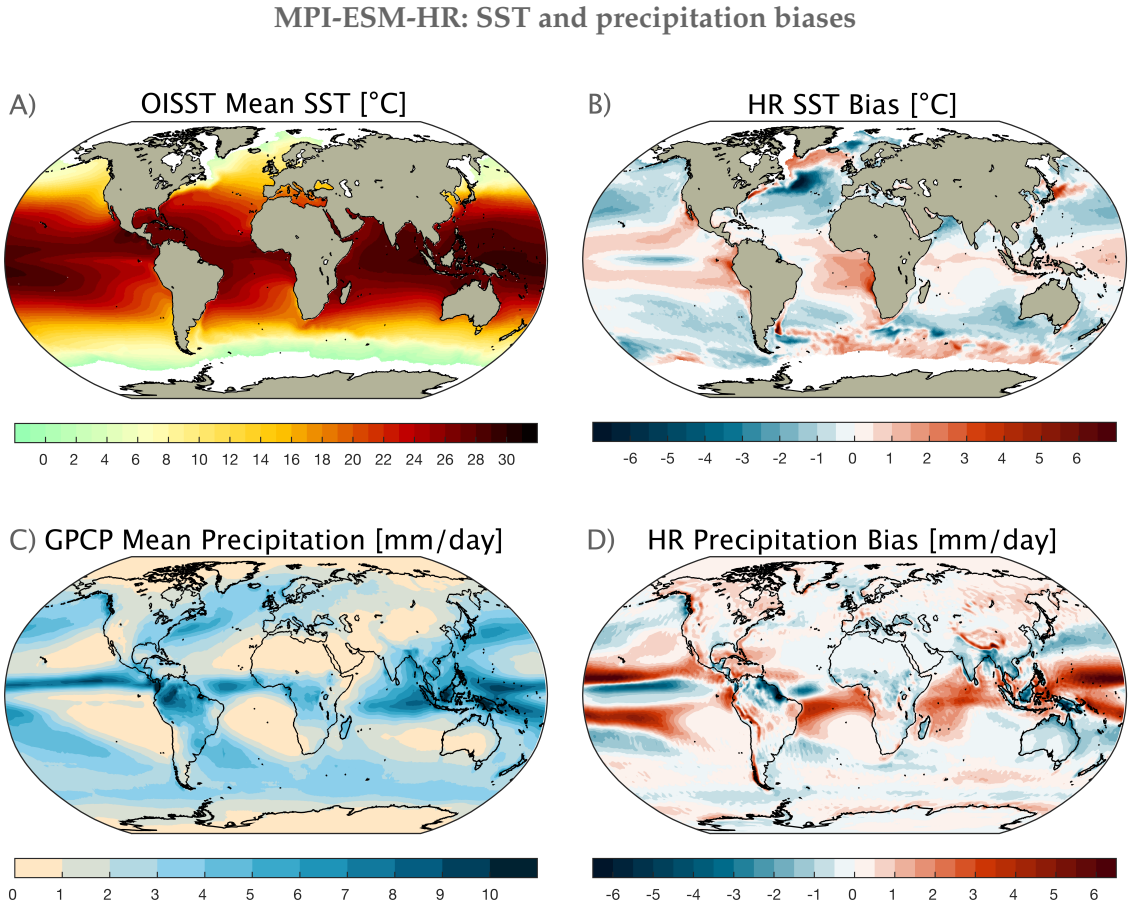

Figure 4.1: A) Mean state SST from OISST [1982-2005], and B) mean state SST bias in HR relative to OISST with shading in °C. C) Mean state precipitation from GPCP [1997-2005], and D) corresponding mean state precipitation bias in HR with shading in mm/day.

warming of tropical SST. The largest warm bias is located in the South Atlantic. It is most pronounced along the coast of Southwest Africa with its maximum in the ABA, between 10°S and 20°S. Mean SST exceeds reference SST by up to 5°C there. Biased SST stretches into the Northern Benguela upwelling region and along the eastern equatorial region with mean state SST being up to 2°C higher than the reference SST. The warm bias fades towards the South American continent. The linkage to the atmospheric representation becomes evident by comparing mean state precipitation biases to SST biases. The mean state of the observational precipitation product GPCP is depicted in Figure 4.1 C along with the corresponding HR bias in D. The strong mean state precipitation bias is largest in the tropics, where mean precipitation reaches its global maximum and is associated with the location of the ITCZ. Excess precipitation in the tropics follows elevated SST patterns. The result is a double ITCZ bias in the Pacific Ocean and a southward shifted ITCZ in the South Atlantic which is already described in many studies (e.g. Oueslati and Bellon (2015)).

The inter model simulation comparison of mean state SST and precipitation shows a

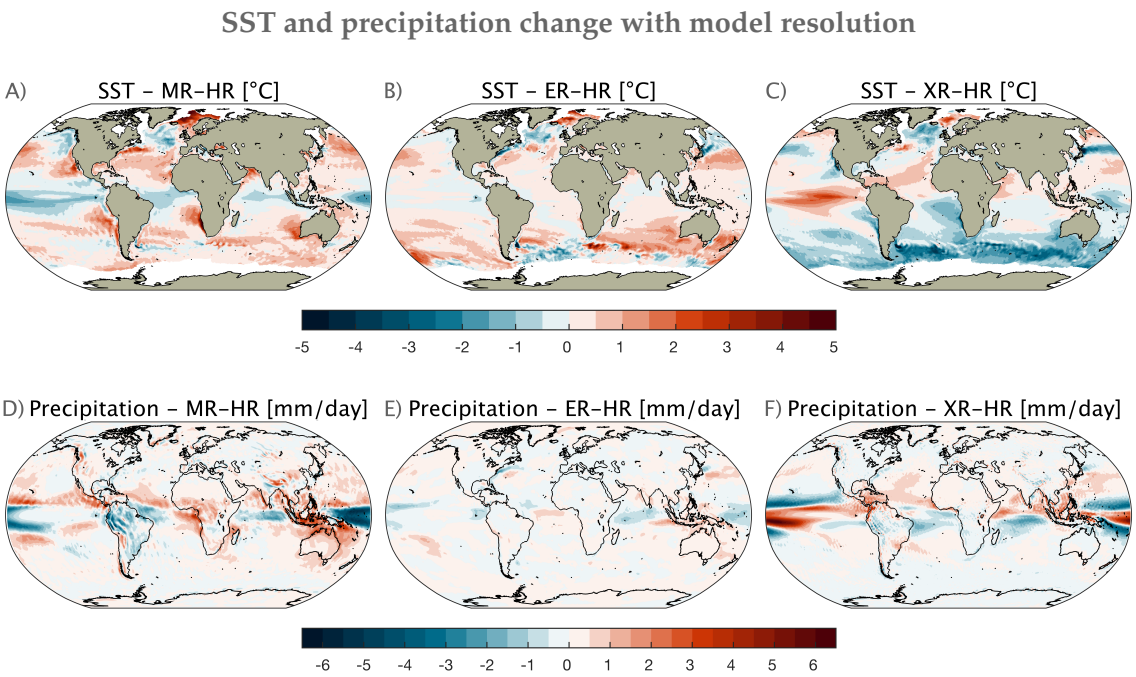

Figure 4.2: Changes of mean state SST (top) and precipitation (bottom) with model resolution relative to HR. A) Mean state SST of MR, B) ER, and C) XR subtracted by mean state SST of HR, with shadings in °C. Red/blue areas indicate increased/decreased values compared to HR respectively. The same accounts for mean state precipitation of D) MR, E) ER, and F) XR subtracted by mean state precipitation of HR, with shadings in mm/day.

significant improvement associated with increasing atmospheric resolution. Differences of global mean state SST between MPI-ESM simulations, with different resolutions of oceanic and atmospheric submodels, are displayed in Figure 4.2 A-C, where mean state SST of MR, ER, and XR is subtracted by mean state SST of HR. It shows how increased atmospheric resolution leads to a significant reduction of the South Atlantic SST bias by several degrees Celsius, especially along the northern Benguela upwelling region between 17°S and 27°S. Increasing the horizontal atmospheric resolution from 1.9° of MR to 0.9° of HR, the SST bias diminishes heavily along the eastern boundary but shows a general warming of tropical SST along the equator of around 1°C. With a further increase of horizontal atmospheric resolution to 0.5° in XR the South Atlantic SST bias is further reduced. Elevated SST in the ABA of the XR simulation reaches only 2.5°C at its maximum and 1.5°C along the equatorial cold tongue. While eastern boundary regions significantly benefit from increased atmospheric resolution, the general warming of tropical SST increases with higher atmospheric resolution. The tropical warming is most severe in the Pacific Ocean. In XR (Figure 4.2 C) the resulting meridional SST bias becomes most evident. Along high latitudes, SST values are too low but elevated in the tropics which enhances the meridional SST gradient already existing in HR. For ER in Figure 4.2 B the oceanic horizontal resolution is increased to 0.1°, while the atmospheric resolution remains unchanged in comparison to HR. The eastern boundary SST bias remains rather unchanged in this case.

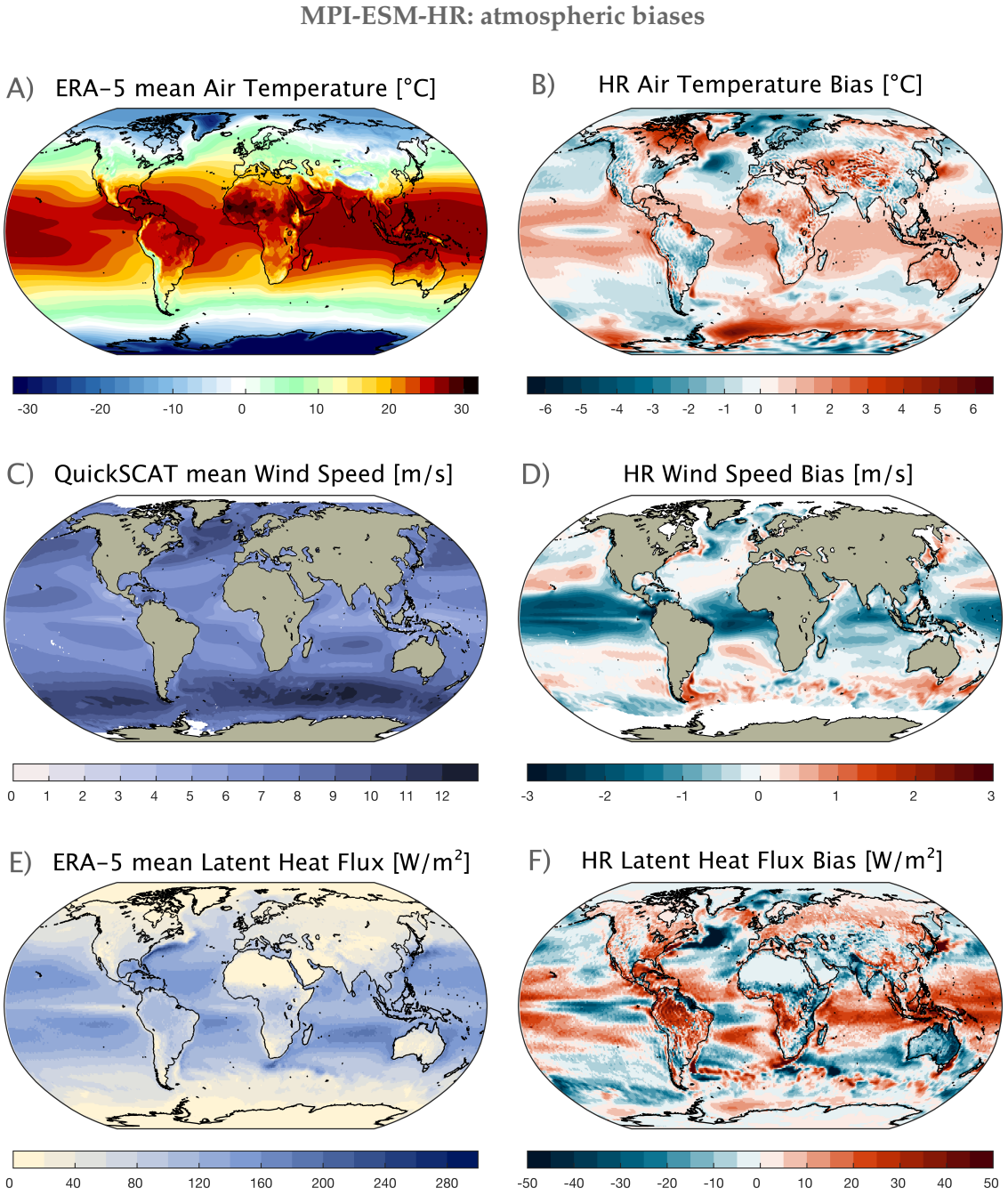

Figure 4.3: Global mean state maps (left): A) surface air temperature of ERA-5 [1980-2014], C) surface wind speed of QuickSCAT [1999-2009], and E) surface latent heat flux of ERA-5 [1980-2014]. Corresponding mean state biases (right) of HR in B), D) and F) respectively.

However, SST in high latitudes improves, especially in the Southern Ocean, where ocean eddies are now resolved. This suggests, resolving small scale oceanic and atmospheric processes does lead to a relevant improvement of mean state biases. Nevertheless, the remaining biases are still clearly apparent despite increased ocean or atmospheric resolution. The high computational costs of a further increase of resolution for both ocean

and atmospheric components might be out of proportion to the potential benefit at this point. According to the study of Richter and Tokinaga (2020), comparisons between model ensembles of CMIP generations show a direct link between resolution and SST improvements. However, some lower resolution models participating in CMIP6 show only small SST biases, indicating a bias reduction can be accomplished using other strategies as well. Figure 4.2 D-F shows how the change of the SST bias with atmospheric resolution is related to the simulation of tropical precipitation. Biased tropical precipitation patterns follow patterns of biased SST. This means excess precipitation occurs where SST is elevated and vice versa and suggests a strong linkage between the biases of both variables.

The mean state SST bias in HR affects the representation of atmospheric variables which is obvious for mean state precipitation. Precipitation patterns are influenced by SST via surface fluxes, that drive the atmospheric circulation. In order to evaluate the linkage between SST and precipitation biases other relevant atmospheric surface variables affected by the coupling process need to be examined as well. Hence, the mean state biases of surface air temperature, surface winds, and surface latent heat flux are depicted in Figure 4.3 for the historical HR simulation. These variables are important drivers of the atmospheric circulation under the influence of ocean dynamics and thus, SST patterns. As expected, surface air temperature biases follow the pattern of the SST bias with a general warming of the tropics and cooling of higher latitudes. Whereas air temperatures over the eastern tropical Atlantic are elevated, the bordering land surfaces of West Africa show negative biases and enhanced latent heat flux. In contrast, the African Sahel area is affected by elevated air temperatures and reduced latent heat flux, leaving it too warm and too dry. Surface winds over the oceans show a strong bias with reduced wind speeds up to 3 m/s along the tropical oceans and poleward shifted trade winds. The elevated biases along the tropics suggest a strongly biased feedback mechanism is arising from the coupling process.

4.2 Performance of Sea Surface Temperature and climate variables

The submodel resolution influences the performance of model variables which is summarized in a Taylor diagram for climate variables with global coverage in Figure 4.4 A and for a region covering the South Atlantic and tropical North Atlantic region (20°N-34°S, 50°W-40°E) in Figure 4.4 B. The diagrams show to what extent the simulated patterns of climate variables resemble those of the observational and reanalysis products in order to estimate relative skill of the model simulations dependent on the resolution of the ocean and atmosphere components. The pattern correlation, centered RMSE and amplitudes of spatial variations indicated by the standard deviation are graphically summarized in the diagrams for MR, HR, XR, and ER simulations. The RMSE and standard deviation are both normalized by dividing them by the standard deviation of the observation/reanalysis

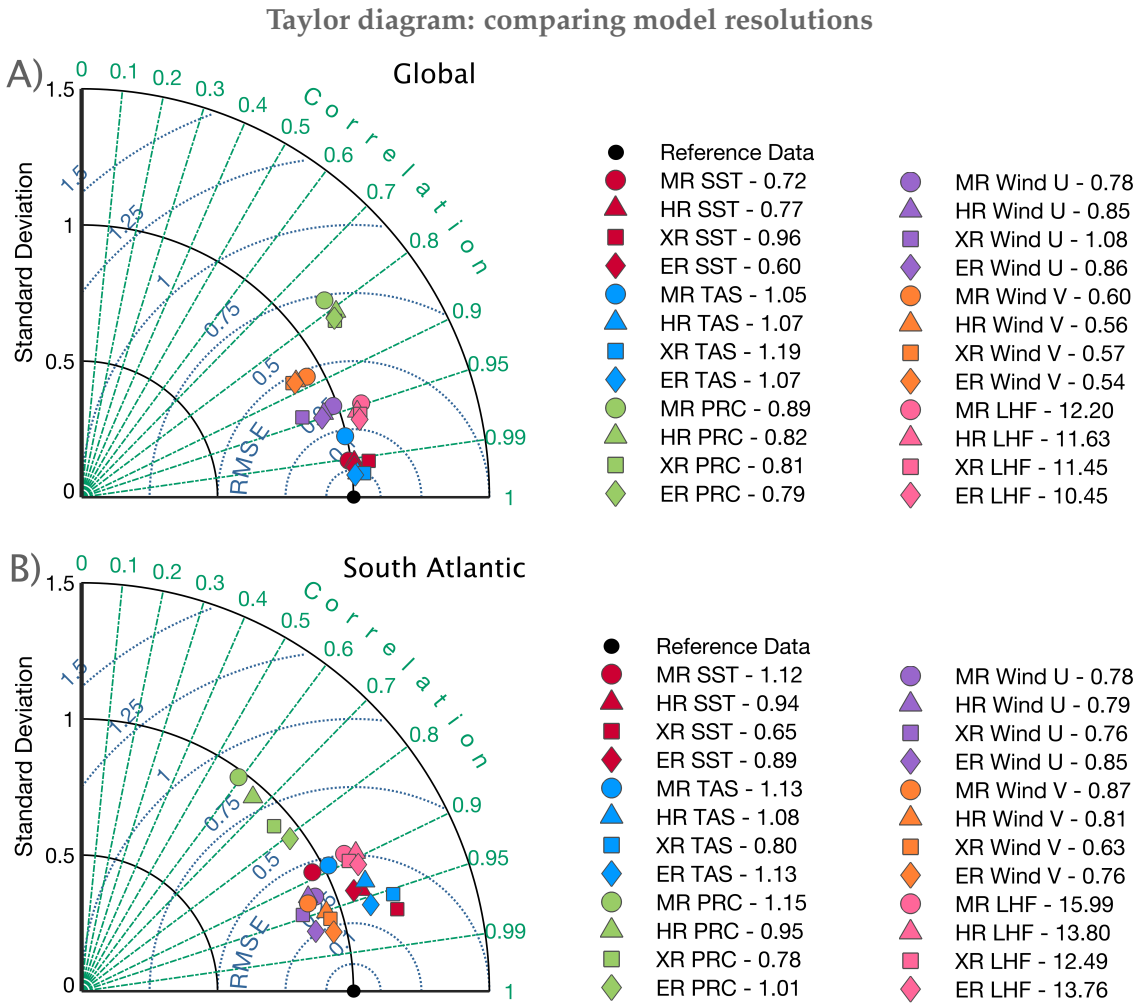

Figure 4.4: Taylor diagram showing relative performance of climate variables [1997-2014] with A) global coverage and B) for the South Atlantic plus tropical North Atlantic (20°N-34°S, 50°W-40°E). Climate variables (SST in red, surface air temperature in blue, precipitation in green, zonal surface wind in purple, meridional surface wind in orange, and surface latent heat flux in pink) are arranged in dependency of their pattern correlation, normalized standard deviation, and normalized RMSE with reference to observations/reanalysis shown for different model resolution (MR (circle), HR (triangle), XR (square), ER (diamond)). Here normalized means divided by the standard deviation of the observational reference. Values in the legend display corresponding averages of the absolute mean state bias (SST and surface air temperature in °C, precipitation in mm/day, zonal and meridional surface wind in m/s, and surface latent heat flux in W/m^2).

in order to make different variables comparable. The statistical relationship between simulated and observed patterns is largest for metrics nearest to the reference data point. OISST serves as a reference for SST, GPCP for precipitation, and ERA-5 for surface winds, surface air temperature and surface latent heat flux for the time period from 1997 to 2014. As simulated data of MR is only available until 2005, the measures are computed separately and are not perfectly comparable but serve to show the progress of the current

model generation. The statistics are computed for annually averaged fields for all grid points and all time steps. In order to provide a complete overview, the globally averaged absolute values of mean state biases are added to the legend of the diagram.

Significant improvements are achieved between different model generations which is indicated by the performance of MR compared to HR. MR shows significant performance deviations for most variables. For the global coverage, in Figure 4.4 A, the performance of ER is superior on average, even compared to XR despite the higher magnitude of the eastern boundary SST bias. According to Gutjahr et al. (2019) the large-scale atmospheric temperature distribution improves with increased ocean resolution as in ER which explains the improved performance of climate variables. In contrast, XR shows more elevated amplitudes of variation (standard deviation) than other model simulations regarding SST and surface air temperatures, whereas the standard deviation for zonal surface wind is significantly reduced. The globally averaged absolute SST bias is most elevated in XR despite the reduction of the eastern boundary warm bias. Performance metrics computed for the South Atlantic region including the tropical North Atlantic, displayed in Figure 4.4 B, show higher deviations between model simulations. The deviations between correlation values for precipitation are most obvious and emphasize the improvement of precipitation representation with increased resolution, showing best performance in ER which is also evident for zonal and meridional wind. Again it becomes clear that the temperature bias reduction of the South Atlantic in XR is accompanied by a strongly elevated standard deviation.

The diagrams show, that a large improvement in terms of model performance can be achieved with an increased resolution of the ocean component which also positively affects atmospheric variables. In contrast, the increased atmospheric resolution leads to smaller general performance improvements and introduces new problems as well. Despite the most solid performance of ER, the eastern boundary SST biases remain globally unchanged in ER in comparison to HR, whereas the increased atmospheric resolution in XR yields large improvements in the eastern boundary SST bias. The result suggests a high contribution of the atmospheric component to the SST bias problem which can not be compensated by higher resolved ocean processes. The contrasting results raise the question of which higher resolved atmospheric process the eastern boundary SST representation benefits from whereas the rest of the simulation does not. Putrasahan et al. (2019) shows, that surface wind speeds generally decrease with an increased atmospheric resolution, while Milinski et al. (2016) shows, that the SST bias improves along the South Atlantic eastern boundary with a detailed coastal wind representation due to higher atmospheric resolution. As the improvement of the SST representation is most pronounced along the Benguela upwelling region and apparently linked to a higher resolved alongshore wind representation, a closer look at the representation of upwelling processes in relation to

model resolution may lead to a better understanding of the SST bias problem, as the wind representation along the eastern boundary directly affects SST via upwelling dynamics.

4.3 The role of simulated upwelling dynamics

The representation of upwelling processes in coupled climate models is challenging due to the rather coarse model resolution which makes it difficult to properly simulate the coastal wind jets, that initiate coastal upwelling dynamics. To examine the ability of the coupled climate model to reproduce upwelling dynamics three computed upwelling indices from SST and surface winds are analyzed. The coastal SST gradient indicates potential upwelling processes along the eastern boundary and the equatorial Atlantic. Indices computed from coastal surface winds allow the estimation of the representation of upwelling favorable conditions, divided into coastal alongshore wind stress dependent upwelling and WSC dependent upwelling along the eastern boundary of the South Atlantic. The indices serve as a tool to shed light on the linkage between the representation of coastal surface winds and the eastern boundary SST bias. As the greatest improvement in terms of the eastern boundary SST bias was achieved by increasing the resolution of the atmospheric model component, the focus of this analysis is on the differences in reproduced upwelling conditions between HR and XR. The upwelling indices calculated for the coupled model simulations are compared to those of the observational reference product. Mean state estimates are analyzed as well as the seasonal variations for a better understanding of annual SST variations linked to upwelling dynamics and potential implications for feedback mechanisms and interannual variability.

4.3.1 South Atlantic upwelling representation

The SST gradient of the observational product OISST along the equator and the eastern boundary of the South Atlantic in Figure 4.5 A shows the temperature difference between ocean surfaces in upwelling regions and further offshore/north of the equator, such as a negative gradient implies colder SST in the upwelling region. Thus, the SST gradient is a rough estimate for locations potentially characterized by upwelling dynamics and indicates an averaged intensity of potential upwelling processes of the South Atlantic. The computed time averaged gradients of HR and XR in Figure 4.5 A suggest a general ability of the models to generate upwelling dynamics with best agreement with the OISST reference in the southern Benguela upwelling region. The OISST gradient is largest along the whole Benguela upwelling region between 17°S and 34°S, with coastal SST around 3°C colder than offshore SST. The gradient peaks at 25°S which is where the Lüderitz cell is located. Thus, the gradient is in good agreement with the observed upwelling intensity (Rubio et al., 2009; Small et al., 2015; Wang et al., 2015; Bachèlery et al., 2020). HR and XR can reproduce a similar gradient for the Benguela upwelling region with a tendency of a southward displacement which reduces with increased atmospheric resolution in XR.

The southward shift suggests weakened upwelling dynamics for the northern Benguela upwelling region in the model simulations which appear to be significantly improved in XR.

Along the coast of Angola, alongshore winds are weak and upwelling is not as strong as the Benguela upwelling dynamics. The Angola upwelling region is however defined by a thriving ecosystem (Binet et al., 2001; Jarre et al., 2015). Upwelling dynamics in these regions are induced by CTWs rather than surface winds and occur semiseasonally, with a maximum intensity during July when significant cross-shore SST gradients can

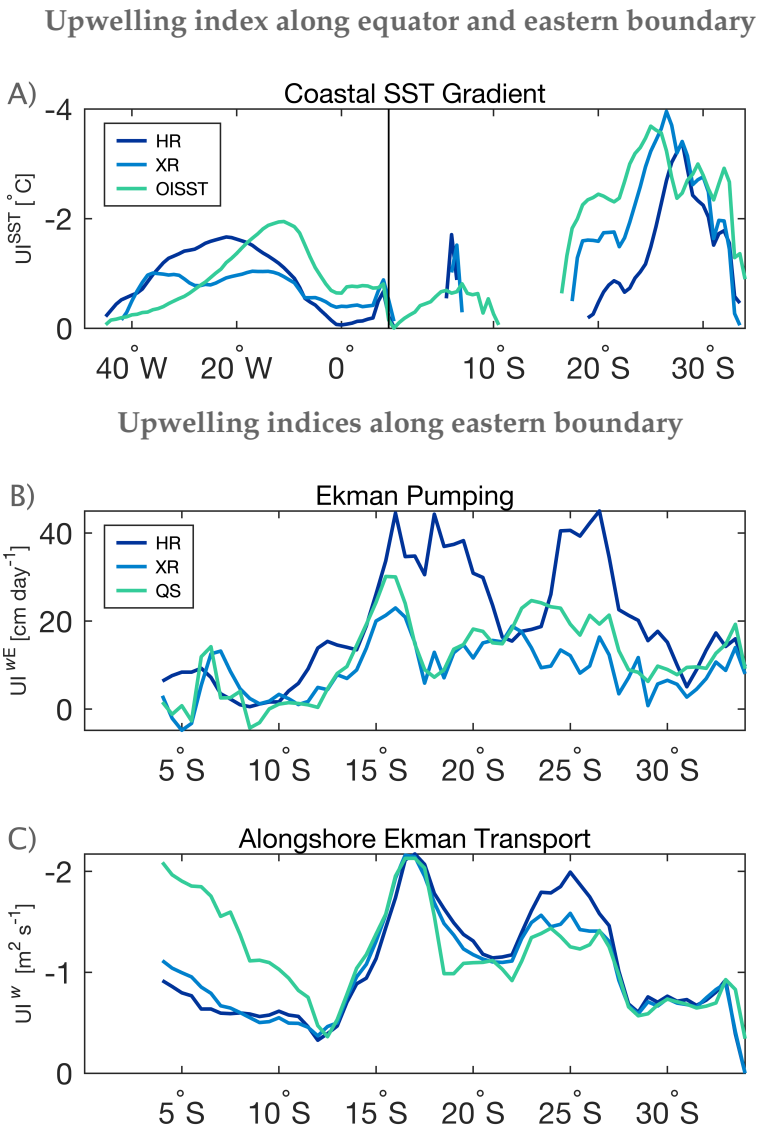

Figure 4.5: Mean upwelling indices for OISST and QuickSCAT (green), HR (dark blue) and XR (light blue) [1999-2009]: A) Coastal SST gradient along the equatorial Atlantic and South Atlantic eastern boundary in °C. B) Ekman Pumping (upwelling velocity) in cm/day, and C) Alongshore Ekman Transport in m^2/s along the South Atlantic eastern boundary.

be observed (Awo et al., 2022). The coastal SST gradient of OISST in Figure 4.5 A along Angola (between the equator and 12°S) indicates the presence of upwelling with the expected weak intensity. Both HR and XR can not reproduce this gradient. The peak at 5°S in HR and XR is instead associated with the Kongo river outflow. This suggests Angola upwelling dynamics are not resolved in the models or suppressed by the biased ocean and atmosphere variables.

The equatorial cold tongue region is characterized by seasonal upwelling dynamics related to accelerating easterly winds in boreal summer (Philander and Pacanowski, 1981). For this region the averaged SST gradient between the equator and tropical North Atlantic shows negative temperature differences up to 2°C colder along the equatorial ocean surface between 10°W and 20°. Similar patterns are observed in the models but shifted towards the West, indicating the ability to simulate similar dynamics. The gradient is largest between 20°W and 30°W for HR and is slightly smaller than the observed gradient but covers a broader area. The gradient in XR reaches only values half of the observed ones and stretches as well from 10°W to 40°W, but with two minor peaks. The shifted equatorial gradients and the absence of an indication for Angola upwelling dynamics highlight the link between suppressed upwelling dynamics in regions affected by the SST bias.

Upwelling favorable conditions are shown in Figure 4.5 B by offshore Ekman transport and in Figure 4.5 C by Ekman upwelling velocities along the South Atlantic eastern boundary which are related to coastal and near shore wind stress. The upwelling favorable winds are high along the Benguela upwelling region with local peaks, at 17°S, where the Cunene upwelling cell is located, and at around 25°S, where the Lüderitz upwelling cell is located (Boyer et al., 2000; Lett et al., 2007; Bachèlery et al., 2020). The average offshore Ekman transport computed from QuickSCAT alongshore winds is well reproduced by both model simulations between 12°S and 34°S. HR overestimates the offshore transport along the Lüderitz upwelling cell but yields otherwise similar results as XR. The result is in good agreement with the Benguela upwelling analysis by Wang et al. (2015). However, the index computed from QuickSCAT winds suggests strong enough alongshore winds exist along the coast of Angola as well and can provide upwelling favorable conditions, contrasting the statements of Awo et al. (2022). An Ekman response is expected for alongshore winds of a minimum of 5 m/s for at least 3 consecutive days (Li et al., 2019). With average wind speeds of 4-5 m/s along the coast of Angola and a seasonal amplitude of 1.2 m/s, seasonal wind induced upwelling processes are within the theoretically possible range. Since winds are too weak along the coast of Angola in the model simulations, upwelling favorable conditions are not met.

Average upwelling velocities computed from Ekman pumping dynamics shown in Fig-

ure 4.5 B suggest large deviations between model simulations of HR and XR, in contrast to the Ekman offshore transport dynamics in Figure 4.5 C. Whereas XR can reproduce the coarse pattern of WSC dependent upwelling velocities along the Benguela upwelling region with slight underestimations, HR largely overestimates the dynamics for the northern and southern Benguela upwelling region. The large difference between both model simulations requires further investigation of the consequences of the spatial representation of the WSC in the model simulations.

4.3.2 Wind stress curl dependent upwelling

Ekman pumping dynamics are induced by spatial offshore wind variations. In the South Atlantic, those dynamics are an important contribution to the coastal upwelling processes south of 15°S along the eastern boundary and add to the strength of the Benguela upwelling system. Ekman pumping dynamics are sensitive to the spatial representation of near shore wind stress with implications for the underlying current system. The spatial representation of meridional wind stress and related upwelling velocities computed from the WSC are shown in Figure 4.6 for the eastern South Atlantic, to further investigate the deficiency of simulating upwelling in HR in contrast to XR. The computed upwelling velocities in Figure 4.6 E from QuickSCAT surface winds are in good agreement with results by Risien and Chelton (2008) and Small et al. (2015). The general dynamics are resolved by HR, ER, and XR, but show different intensities and spatial extent. Whereas Ekman pumping dynamics are overestimated in HR and ER, XR can reproduce more realistic values due to higher resolved near shore surface winds which becomes evident in Figure 4.6 C. The improved representation of the near shore meridional wind stress pattern with high detail of spatial wind variations and narrower zonal extent leads to improved upwelling velocity computations. However, the representation of upwelling velocities in XR is limited by the horizontal resolution of the ocean which results in lower values for coastal time averages in Figure 4.5 B.

The meridional wind stress representation in HR and ER is very similar since the atmospheric resolution is equal. Thus, computed upwelling velocities yield a very similar pattern as well, indicating enhanced upwelling velocities compared to the QuickSCAT reference. The near shore meridional wind stress is rather broad in HR and ER in comparison to QuickSCAT and XR. As the core of the meridional wind stress is further away from the coast and higher in magnitude in HR and ER, the WSC structure is zonally broad which results in unrealistic intense Ekman pumping dynamics on a broad spatial scale. This in turn would be expected to increase the coastal SST gradient, as more cold water from below is expected to be upwelled along the coast. This is true for the region south of the Lüderitz cell at 27°S, where the coastal SST gradient of HR exceeds the OISST gradient. However, north of 27°S the indicated Ekman pumping dynamics do not lead to cooler temperatures at the coastal ocean surface in HR despite enhanced computed Ekman pumping

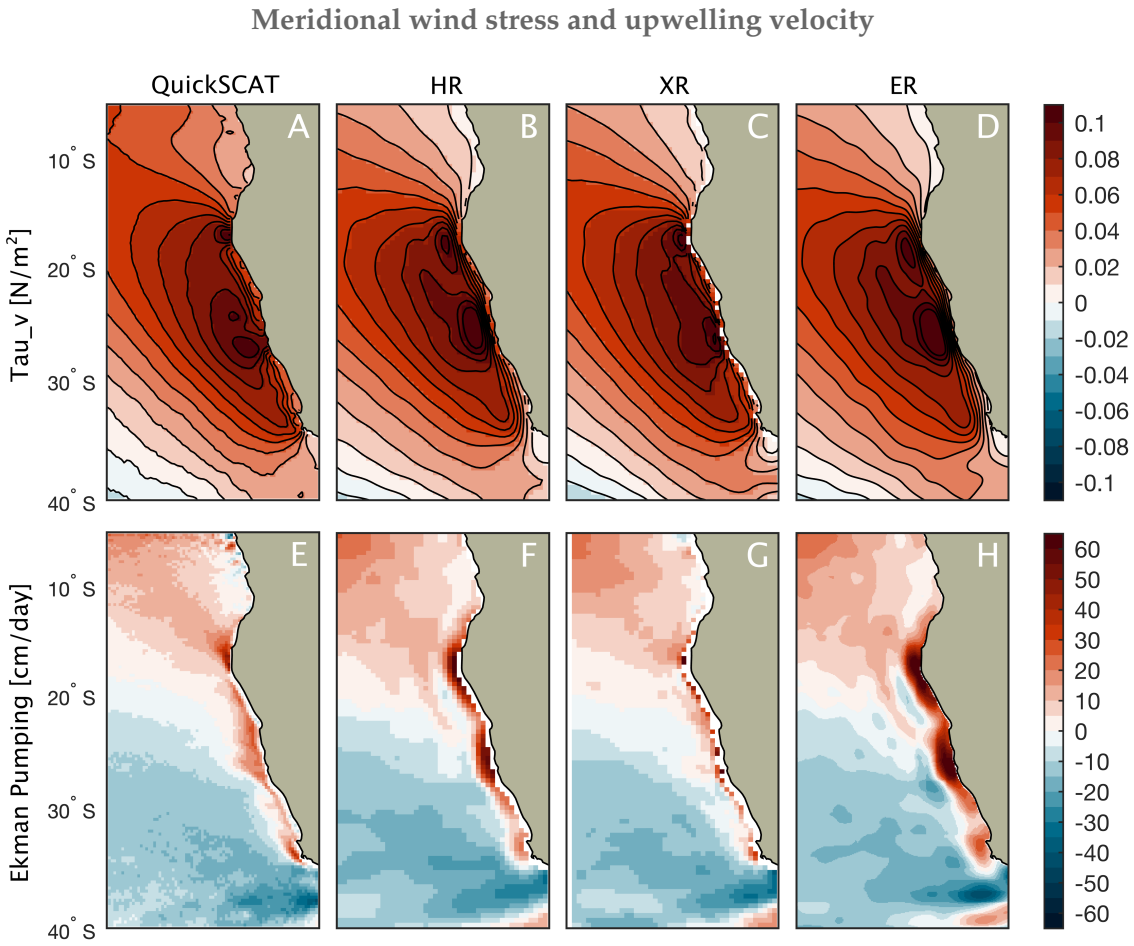

Figure 4.6: Top: Mean state of eastern South Atlantic meridional wind stress [1999-2009] of A) QuickSCAT, and MPI-ESM in resolutions of B) HR, C) XR, and D) ER with shading in N/m^2. Bottom: Corresponding Ekman upwelling velocity of E) QuickSCAT, F) HR, G) XR, and H) ER with shading in cm/day, such as positive (red) values indicate upward velocities towards the surface.

velocities. A possible explanation is enhanced southward intrusions of warm tropical water into the Benguela upwelling region which suppress the upwelling signal in coast SST. As described by Lübbecke et al. (2019) low wind anomalies along the coast of Angola lead to enhanced southward intrusions of warm water affecting the position of the ABF and SST in the northern Benguela upwelling region. The defective wind representation along the coast of Angola is suspected to enable an enhanced southward intrusion of warm water into the northern Benguela upwelling region which would lead to elevated SST and explain the southward shifted SST gradient of Figure 4.5, showing a reduced SST gradient between 17°S and 25°S despite the enhanced Ekman pumping dynamics in HR. However, the surface winds off the coast of Angola are almost equally low in HR and XR with only minor improvements in XR. However, the SST bias and upwelling dynamics of the Benguela upwelling region are largely improved in XR. A significant difference between XR and HR in the Benguela upwelling region is the spatial extent of

coastal Ekman pumping which is related to the zonal structure of the WSC. The zonally broad representation of the WSC in HR, linked to lower atmospheric resolution, creates a defective representation of Ekman pumping which is too broad in zonal direction and too intense. The differences in Ekman pumping intensities in combination with the SST bias magnitude could indicate that the subsurface water which is being upwelled is too warm. Additionally, the deficiencies in the representation of the WSC in HR may affect the underlying current system. Small et al. (2015) linked a defective broad representation of the WSC to a prevailing Sverdrup balance along the eastern boundary based on the theory of Fennel et al. (2012) and Junker (2014) which leads to an oceanic southward transport along the South Atlantic eastern boundary as far south as 30°S. This condition dominates the model simulation if the distance of the offshore wind jet core from the coast exceeds 300 km (Junker, 2014), which is the case for HR but not for XR. This crucial difference between model simulations would explain the large improvements in the representation of the northern Benguela upwelling region in XR with a significantly decreased SST bias. The mean state meridional wind stress in XR is still lower than observations but the spatial structure provides very likely an improved representation of the downwind near surface current towards the equator which diminishes the defective southward intrusion of warm tropical water.

4.3.3 Seasonality of upwelling indices

The seasonal cycle of the coastal and equatorial SST gradient is displayed in Figure 4.7 (left) along with the seasonal cycle of offshore Ekman transport along the eastern boundary of the South Atlantic (right). The seasonality of the Benguela upwelling system with peaks during boreal winter can be represented by HR and XR. Although, the displayed seasonal variation of the coastal SST gradient is dominated by positive gradients in the ABA which exceed observations. The southward shifted upwelling system in HR is associated with anomalous strong warm intrusions from the north during January, February and March associated with a shifted position of the ABF. A significant improvement can be seen for XR, where wind and SST indices indicate a well simulated seasonal cycle. The reduced southward shift of the Benguela upwelling system in XR is combined with less intense but still elevated positive SST gradients in the ABA. Upwelling dynamics dominate south of 18°S in XR but are still reduced in the northern Benguela upwelling region compared to observations.

In contrast, the semi-seasonal cycle of upwelling north of 15°S, along the coast of Angola, is not represented in both model simulations. As winds are not the only driver of upwelling, upwelling seasonality is strongly modulated by equatorial Kelvin waves which transform into CTWs traveling poleward along the eastern boundary. Ostrowski et al. (2009) shows poleward traveling CTWs generate semi-seasonal downwelling in March and October and upwelling in July and November which agrees with the OISST gradient seasonality.

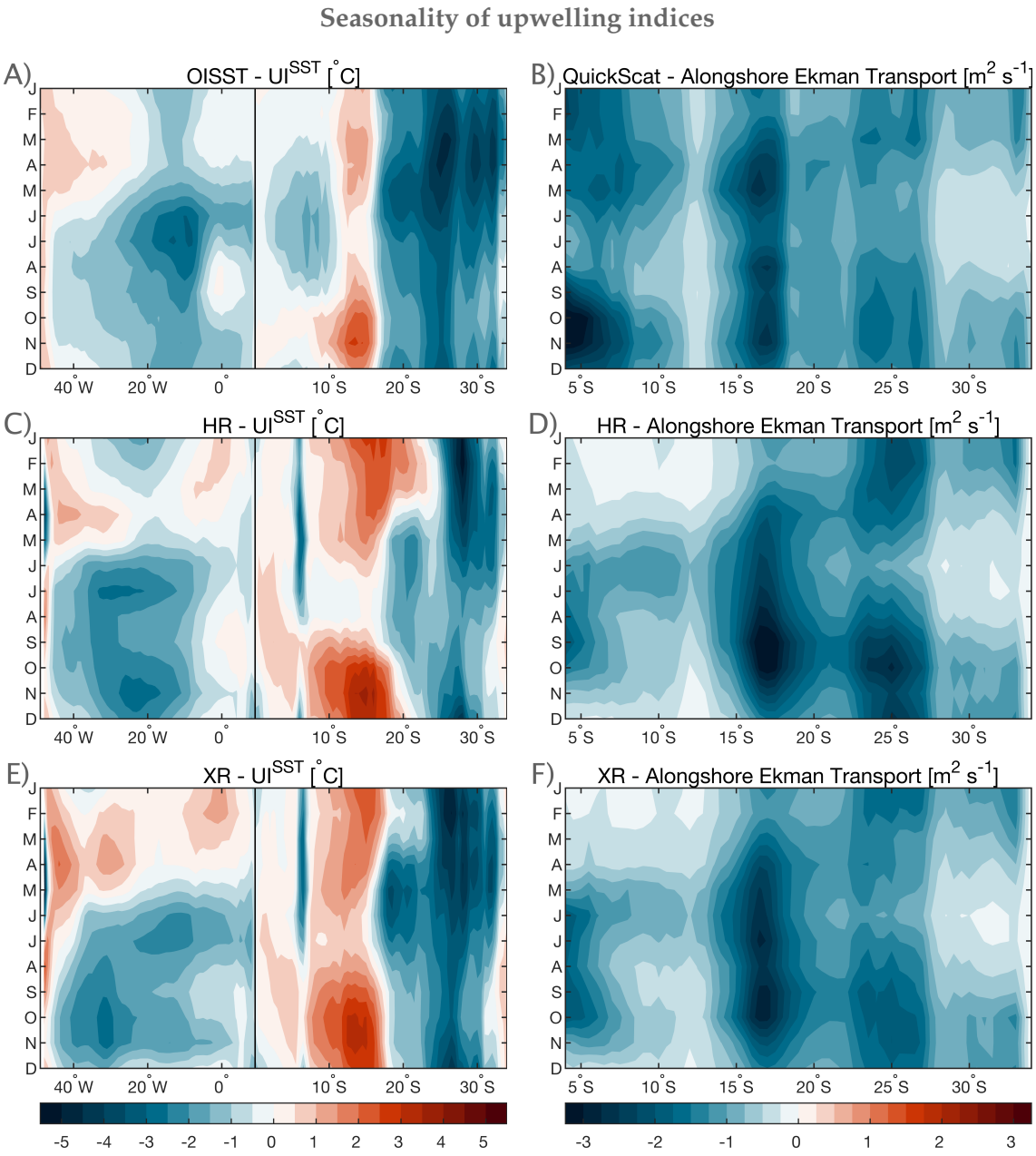

Figure 4.7: Seasonal cycle of upwelling indices [1999-2009]. Left: coastal SST gradient along equatorial Atlantic and South Atlantic eastern boundary with shading in °C for A) OISST, C) HR, and E) XR. Right: alongshore Ekman Transport along the South Atlantic eastern boundary with shading in m^2/s for B) QuickSCAT, D) HR, and F) XR.

In addition, the offshore Ekman transport along Angola indicates a biased seasonality of surface alongshore winds. Winds are much lower in the model simulations and also seasonally shifted. Alongshore winds would usually peak during April/May, after the downwelling season, and in November during upwelling season. The model simulations, however, show alongshore winds that peak in June/July in HR and June and October in XR. The biased seasonality is presumably a result of shifted SST gradients and wet

precipitation biases along the coast of Angola related to the southward shifted position of the ITCZ which is shown in Section 4.4.2. As explained by Lübbecke et al. (2019) reduced winds intensify warm interannual anomalies by anomalous poleward advection of warm surface water. Thus, the seasonally diminished winds in the Angola area and ABA very likely add to the stronger warm intrusions into the northern Benguela upwelling region. Local forcing mechanisms like alongshore winds act as a precondition for remotely forced up and downwelling CTWs. Thus, even if CTWs are the main driver for upwelling mechanisms along Angola, the lack of alongshore winds can increase seasonal downwelling or impede seasonal upwelling which also affects the northern Benguela upwelling region. With lower atmospheric resolution in HR, the southward intrusions are significantly enhanced and are the cause for the southward displacement of the ABF with implications for the associated SST bias in the northern Benguela upwelling region. The seasonal presentation of the SST gradient and alongshore wind induced offshore Ekman transport shows how the upwelling representation significantly improves for the northern Benguela upwelling region due to a detailed wind representation since less warm water is intruded from the north. However, the increased atmospheric resolution does not improve the relevant dynamics along the coast of Angola, as the seasonality and magnitude of alongshore winds north of 15°S is still impaired. Thus, the mean state SST bias can be largely reduced in XR but still affects the eastern equatorial Atlantic and the region off the coast of Angola, where coastal winds during boreal winter are reduced compared to the observational reference.

Upwelling along the equatorial cold tongue region peaks during JJA. Equatorial upwelling is a result of the amplification of trade winds due to the ITCZ shifting from the equator to the Northern Hemisphere in JJA. The equatorial cold gradient in HR is slightly delayed with a peak in July/August and shifted in space towards the west. The temporal shift is a result of the southward shifted ITCZ in HR which delays the onset of amplified trade winds. This is further discussed in Section 4.4. Due to the absence of wind in the eastern equatorial area where SST is elevated, the trade wind amplification affects equatorial areas further to the west and yields a shifted cold tongue during July/August in HR. Cold SSTs remain in the west until November generating a zonal SST gradient in the opposite direction as observed. In XR equatorial cooling of SST occurs in JJA between 10°W and 20°W as observed but with a less pronounced amplitude. The improvement can be related to the reduced SST bias and less biased precipitation patterns. However, as in HR, cooling in the west evolves from August to November, creating the second peak between 30°W and 40°W as seen in the averaged SST gradient graph in Figure 4.5 A. This is as well the result of amplified trade winds being shifted to the West.

The area affected by the SST bias shows general weak seasonal variability. In the model simulations, low winds are combined with enhanced SST and suppressed upwelling

dynamics. The importance of a detailed representation of momentum fluxes is highlighted by the improvements achieved for the Benguela upwelling region, where the coastal wind representation affects local upwelling dynamics and the eastern boundary current system. The representation of the underlying current system with tropical warm subsurface intrusions southward along the eastern boundary is most likely the important contribution to the SST bias problem and not the representation of upwelling dynamics by itself. The remaining contribution to the SST warm bias along the coast of Angola appears not to change with increased oceanic or atmospheric resolution since the spatial representation of the WSC is of minor importance in this region. The seasonality of the upwelling dynamics shows how the combination of remote and local processes leads to anomalous SST variations along the eastern boundary of the South Atlantic. It is of major interest to what extent the lack of simulated upwelling favorable conditions affects the seasonality of other atmospheric variables and the occurrence of interannual SST anomalies along with their climatic response.

4.4 Consequences of the South Atlantic Sea Surface Temperature bias

The atmospheric mean state biases shown in Section 4.1 can not be directly related to the SST bias since other model components contribute to the biased mean state patterns as well. Next to the climatic impact of the SST bias, the atmospheric model component exhibits internal systematic biases as well. In order to estimate the atmospheric consequences of the mean state SST bias, the AMIP simulation forced with realistic SST fields, which contains only intrinsic atmospheric biases, is compared to the coupled model simulations. The analysis shows the biases which already exist in the atmosphere-only simulation and also the difference between both model simulations. The difference shows which atmospheric biases are further increased or newly introduced along with the SST bias as a result of the coupling between atmospheric and oceanic model components via various feedback mechanisms. The difference between both model simulations can not show the sole impact of the SST bias on the atmospheric simulation but can highlight common features between biased patterns. To further outline the impact of elevated SST on the atmospheric simulation the difference between the HR and XR simulations is displayed as well. It shows the impact of the lower atmospheric resolution in HR along with the larger SST bias on the atmospheric simulations. The influence on the components of the atmospheric moisture budget is shown in this Section to investigate the underlying factors which control the changes of precipitation patterns in the simulations. In addition to the mean state biases, the annual feedback mechanisms of the tropical Atlantic and African monsoon are examined, as the seasonal variations allow for a better allocation of related biases between variables.

4.4.1 Mean state atmospheric moisture budget

The biased interaction between ocean and atmosphere interfaces in coupled climate models affects the atmospheric moisture flux. Elevated SST may lead to thermodynamic impacts as oceanic evaporation is expected to increase locally and result in increased precipitation. Since SST gradients affect surface momentum fluxes, dynamic changes in moisture flux transport are expected with altered SST patterns as well. Moisture fluxes and convergence are evaluated for the South Atlantic and African region. Their intrinsic atmospheric biases are displayed in Figure 4.8 A along with the difference between the atmosphere-only and coupled model simulation of HR in Figure 4.8 B and the difference between HR and XR in Figure 4.8 C, together with the changes in surface air temperature, precipitation and surface latent heat flux. The biased atmospheric moisture flux and moisture convergence are displayed to provide the connection between displayed surface variables and precipitation patterns. In addition, estimates of the thermodynamic and dynamic part of the biased moisture flux and convergence are displayed to facilitate the retracing of bias impacts on precipitation patterns.

Before evaluating the possible impact of elevated SST, the biases of the AMIP simulation are considered first. Surface winds in Figure 4.8 A.1 are accelerated in mid latitudes and very weak in the tropics. Especially the meridional component of the surface winds is severely reduced in the eastern tropical South and North Atlantic. The weakened winds spatially coincide with diminished surface latent heat flux, due to the dependency of oceanic evaporation on available heat and surface wind speed. The turbulent air movement induced by surface winds removes water vapor from the adjacent atmospheric boundary layer which in turn facilitates evaporation (Gimeno et al., 2013). The lack of surface winds and evaporation along eastern boundaries can in turn lead to a warming of surface oceans in a coupled model since less surface heat is removed from the ocean surface via latent energy fluxes. The reduced winds along the eastern tropical Atlantic are balanced by enhanced trade winds further south which indicates a general poleward shift of global trade wind patterns. The dislocated trade winds result in a dynamically induced poleward shift of tropical moisture convergence. The lack of equatorial winds creates a nearly symmetric increase of moisture convergence north and south of the equatorial Atlantic. This suggests, the double ITCZ problem in coupled models originates from a biased surface wind representation already present in the atmospheric model component which is supported by the findings of Xiang et al. (2017). In addition, a large part of the tropical moisture is advected by the shifted trade winds towards the western tropical Atlantic, leading to a wet precipitation bias along the tropical western boundary. Linked to the different distribution of landmasses in the Northern and Southern Hemisphere the wind bias over the eastern South Atlantic is more pronounced and results in a wet precipitation bias south of the equator and a dry precipitation bias along the tropical North Atlantic, affecting also the Guinea region of West Africa.

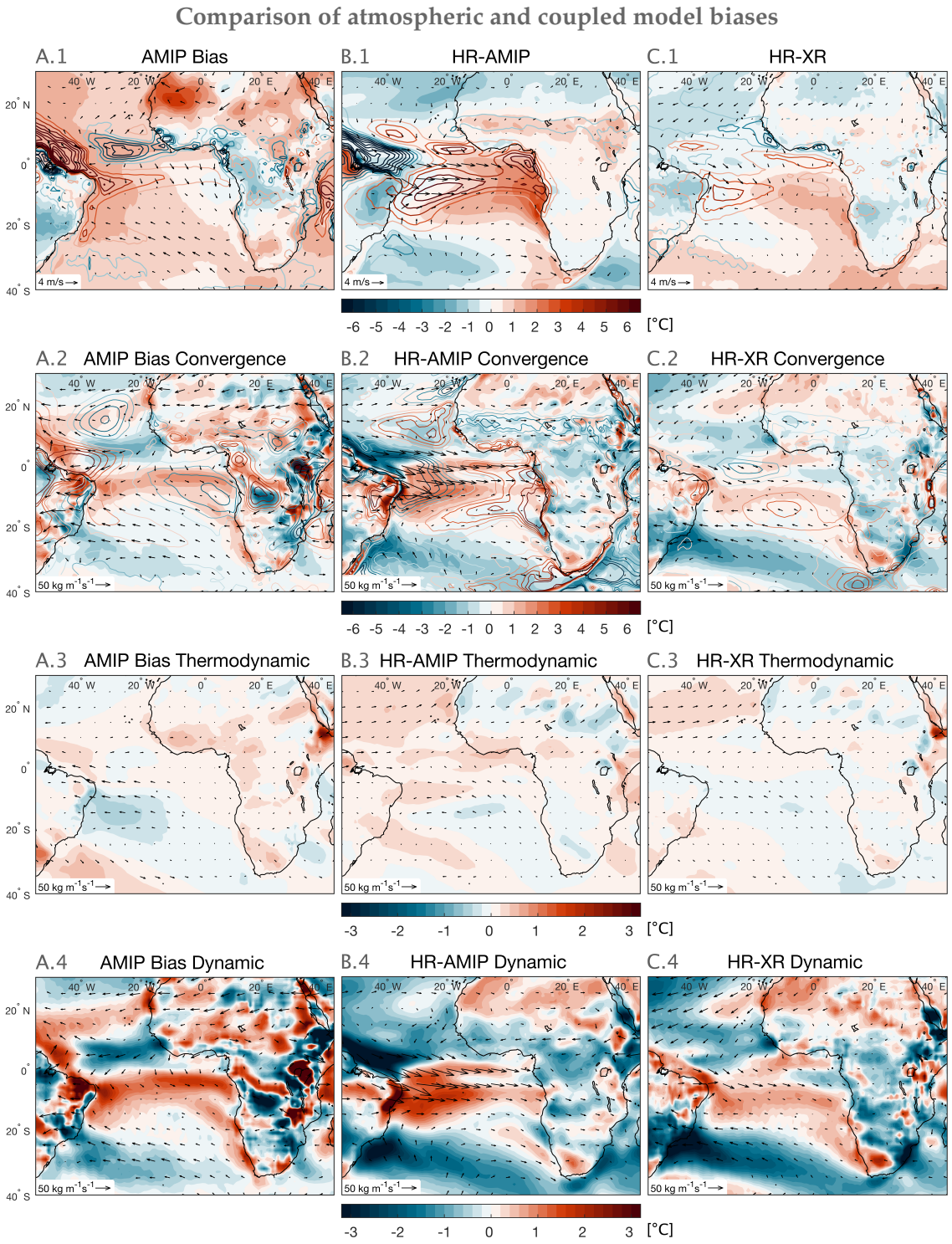

Figure 4.8: A) AMIP mean state biases (reference: GPCP/ERA-5), and AMIP subtracted from B) HR and C) XR [1997-2014]. First row: surface air temperature (shading in °C), precipitation (contour lines in 0.5 mm/day steps, omitting zero, +/- in red/blue), surface wind (arrows in m/s). Second row: moisture convergence (shading in mm/day), surface latent heat flux (contour lines in 5 W/m^2 steps, omitting zero, +/- in red/blue), horizontal moisture flux (arrows in kg/ms). Thermodynamic (third row) and dynamic (fourth row) components of moisture flux (arrows in kg/ms) and convergence (shading in mm/day).

The thermodynamic and dynamic parts of the changes in moisture flux and convergence, shown in Figure 4.8 A.3 and A.4, clearly emphasize the dynamical origin of the double convergence zone pattern. The reduced winds of the atmospheric simulation in the eastern tropical North and South Atlantic reduce the moisture transport towards the equator and lead to the early convergence of moisture south of the equator. The thermodynamic effect is comparatively very low and limited to a slightly increased amount of moisture being available over the western tropical Atlantic, where surface air temperature is slightly elevated. The excess moisture is transported by the trade winds toward South America. In addition, the cold and moist bias over land areas along the coast of Angola, which was already evident in the HR mean state biases, clearly originates from the atmospheric submodel and increased thermodynamic moisture convergence over African land areas north of the Gulf of Guinea.

Next to the intrinsic atmospheric biases, the difference between HR and AMIP is displayed in Figure 4.8 B.1 to B.4 along with the difference between HR and XR in C.1 to C.4. The latter serves as a reference to improvements of the atmospheric representation linked to a smaller mean state SST bias compared to HR. The SST bias in HR is accompanied by a strong westerly wind bias along the equator and western tropical Atlantic, evident in Figure 4.8 B.1. Wet precipitation biases follow the enhanced SST patterns resulting in high excess precipitation south of the equator. The enhanced SST pattern is additionally accompanied by enhanced latent heat flux, resulting in low oceanic evaporation in the western equatorial Atlantic and high evaporation in the east. The reduced trade winds along the equatorial South Atlantic are in all likelihood related to the zonally affected SST gradient and enhance in turn the poleward shifted moisture convergence in the South Atlantic. The altered SST gradients may be related to the dislocation of convective processes since convection occurs where temperature reaches a regional maximum. However, the thermodynamic impact of the SST bias is comparatively low. Evaporation is definitely enhanced over regions of elevated SST and Figure 4.8 B.3 shows an increase in moisture flux south of the equator. The moisture is advected by trade winds towards the equator and leads to a slight increase of moisture convergence just northeast and southwest of the equator and over the western Atlantic ocean. But this effect is very low in comparison to the dynamical contribution linked to the shifted SST gradients which becomes evident in Figure 4.8 B.4. The dynamical impact on moisture flux via elevated SST can explain a large part of the changed precipitation pattern since the shifted SST gradients slow down the zonal surface winds along the equator and the western tropical Atlantic. The reduced winds prevent the transport of moisture further to the north and result in an intensified convergence zone south of the equator. The African continent is affected by the divergent moisture flux north of the equator. Between 10°N and 15°N along the African Sahel region, the surface air is too hot and too dry, as evaporation and precipitation is decreased and less moisture converges in this area due to the dynamical change.

As the SST bias in XR is significantly reduced, the climatic impact is reduced as well. The patterns of changed atmospheric variables in XR are very similar to the patterns of HR but with a reduced magnitude. This supports the before described impacts of the SST bias. Figure 4.8 C.1. shows the part of the SST bias which is more elevated in HR, since mean states of XR are subtracted from mean states of HR. The improved upwelling representation of the northern Benguela upwelling region with a reduced southward advection of warm waters into the upwelling region leads to a large reduction of the SST bias in the ABA region, where the bias was most elevated, but also reduces a portion of the SST bias in the eastern tropical South Atlantic. In consequence with the southern part of the SST bias being largely reduced with higher atmospheric resolution, the biased precipitation response reduces as well. The southern extension of the precipitation bias decreases and the dipole characteristic of the precipitation difference along the Guinea region suggest that the southward shift of the precipitation pattern is less severe in XR. This is a result of the reduction of the zonal and meridional equatorial wind bias due to a less elevated SST gradient. In comparison to HR, a significant difference is present in XR. The trade winds in the higher tropical latitudes and mid latitudes are significantly reduced in comparison to HR, especially at the Northern Hemisphere, where surface temperatures are elevated in XR. Hence, moisture transport reduces as well yielding an increase of convergence in the mid latitudes and increased precipitation along the South Atlantic coast of South America. However, the ITCZ remains shifted to the south but with a reduced magnitude of excess precipitation. Precipitation increases in the XR simulation in the Guinea region, indicating a slight northward shift of the biased precipitation pattern. The comparison between the patterns of different model simulations allows for the assumption that the SST bias in HR and XR severely affects the surface momentum fluxes which in turn enhances the poleward shifted ITCZ in the Southern Atlantic in comparison to the AMIP simulation. The shifted convergence zone leads to changes in African precipitation patterns which will be further analyzed on seasonal scales in the following.

4.4.2 Seasonal Sea Surface Temperature bias implications

Next to the mean state climatic response to elevated SST in the South Atlantic, the seasonal interactions between SST and atmospheric variables can give further insight into biased feedback mechanisms and impacts on the representation of the African monsoon. Figure 4.9 A shows the standard deviation of the seasonal cycle of SST in the South Atlantic by observational OISST, indicating the average amplitudes of the seasonal variations. Seasonal amplitudes of SST in HR and XR relative to OISST are shown in Figure 4.9 B and C. The ratio between simulated and observed standard deviations displays smaller/larger seasonal amplitudes for values less/greater than one in blue/orange. The upwelling analysis already showed that seasonal variations are reduced in the eastern equatorial region and along the coast of Angola. Additionally, Figure 4.9 B and C confirms, that the seasonal amplitude of SST variations is reduced in the eastern South Atlantic, which is

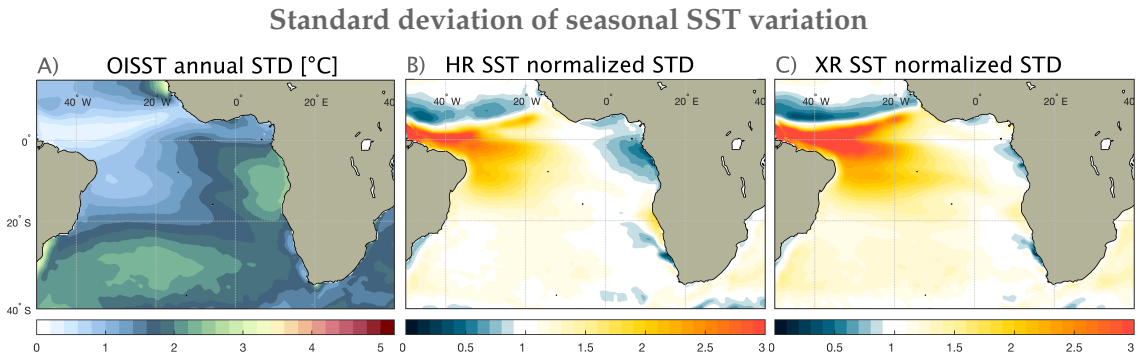

Figure 4.9: Standard deviation of SST [1982-2014] showing averaged amplitudes of the seasonal cycle for A) OISST with shading in °C. Corresponding standard deviations of B) HR and C) XR normalized by the standard deviation of OISST as a reference, such as dimensionless values larger/lower one indicate elevated/attenuated seasonal amplitudes respectively.

improved with a reduced SST bias in XR. The biased HR SST and less biased XR SST show similar patterns of defective seasonal amplitudes. In contrast to the reduced seasonal variation in the eastern tropical South Atlantic, coastal variability near 20°S is enhanced in the models. This is a result of the enhanced southward intrusions along the eastern boundary which affect seasonal SST variations in the northern Benguela upwelling region. The large meridional dipole in the western tropical South Atlantic indicates a general southward shifted pattern related to the displacement of the ITCZ. The relocated intensity of seasonal SST variations suggests a disturbance in the seasonality of the equatorial feedback mechanisms. The impacts of the shifted patterns on the atmospheric representation and possible reinforcing mechanisms are analyzed in the following.

Seasonal feedback mechanisms

The seasonal cycle of biased SST in combination with biased surface winds and precipitation along the equatorial Atlantic and the eastern boundary of the South Atlantic is displayed in Figure 4.10 and shows how those variables interact and reinforce each other on a seasonal average. SST, precipitation and surface winds, are seasonally averaged along the equator between 2°N and 2°S and along the eastern boundary of the South Atlantic between the coast and 3° zonally offshore. To explain the intrinsic atmospheric biases of the AMIP simulation in terms of seasonal variations in the South Atlantic (shown in Figure 4.10 A), global seasonal biases were evaluated as well but are not displayed here. The global seasonality of biased variables in AMIP suggests a strong linkage between seasonal deviations of surface air temperature and surface wind speed with peaks in boreal spring and fall. The global interhemispheric temperature gradient is meridionally shifted due to biased amplitudes of the seasonal cycle. Seasonal biases are especially severe for surface air temperature over land areas. Cooler temperatures over land in the Southern Hemisphere/Northern Hemisphere during boreal spring/fall lead to lower sea

level pressure over extratropical oceans and weakened trade winds. The seasonal biases of trade winds severely reduce winds over tropical eastern ocean basins, leading to a meridionally shifted trade wind pattern. This relation is supported by the study of Zhou and Xie (2017), who showed the linkage between biased land surface air temperatures and surface wind and precipitation shifts. As land areas are more extended in the Northern Hemisphere, the resulting biases are more severe over the ocean basins of the Southern Hemisphere. The AMIP biases displayed in Figure 4.10 A show reduced meridional winds along the equator and the eastern tropical South Atlantic during boreal fall and winter. The reduction of equatorial winds affects the moisture flux as already shown in Figure 4.8 A.2. The southward shifted moisture convergence zone south of the equator due to low meridional winds results in excess precipitation south of the equator. Since the wind is more reduced in the eastern tropical Atlantic moisture transport is enhanced toward the western tropical Atlantic, resulting in a wet precipitation bias. With the ITCZ moving north in MAM a severe westerly wind bias evolves along the equator with a wet precipitation bias along the equatorial cold tongue.

The seasonal presentation of intrinsic atmospheric biases allows the comprehension of the biased seasonality in the coupled model simulation. Elevated SST in HR is most pronounced in the ABA from boreal fall to spring, while meridional winds in AMIP are reduced along the coast of Angola. Just north of elevated SST precipitation is elevated as well. The seasonality of the SST bias is as well synchronized with the annual cycle of SST and likely related to seasonal southward intrusions of warm tropical water which is transported poleward along the eastern boundary. The remotely forced CTWs induce SST variations, that are locally affected by the low meridional winds along the coast of Angola. In combination with the defective undercurrent simulations related to the WSC, this yields an enhanced intrusion of warm tropical water further to the south and into

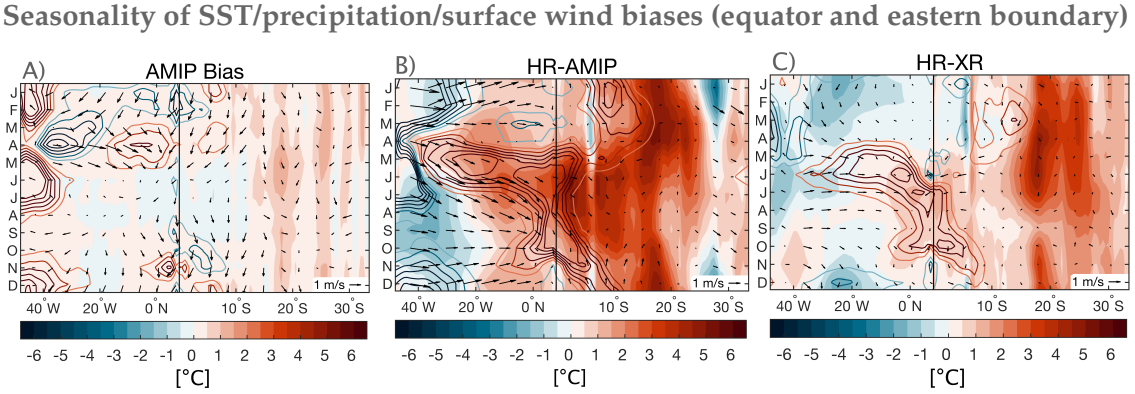

Figure 4.10: Biased seasonality along the equatorial Atlantic and South Atlantic eastern boundary [1999-2009]. A) AMIP biases (reference: OISST/G-PCP/QuickSCAT), and AMIP subtracted from B) HR, and C) XR, showing SST (shading, in °C), precipitation (contour lines in steps of 1 mm/day, omitting the zero line, +/- in red/blue) and surface wind vectors (arrows in m/s).

the Benguela upwelling region. The pronounced seasonality of the SST bias allows for drawing conclusions about affected wind and precipitation patterns. In HR the SST bias is strongest in the ABA during boreal spring when SST reaches its seasonal maximum. With seasonally decreasing SST during boreal summer and the vanishing meridional wind bias in AMIP, the SST bias moves north, and peaks during June/July along the eastern equatorial area. Excess precipitation follows strongly the SST bias maximum. The reduction during boreal summer along the coast of Angola allows meridional winds to pick up from June to October. Precipitation deficits are located in the western equatorial region, where SST is negatively biased.

As the SST bias in the coupled model simulation is characterized by elevated surface temperatures south of the Atlantic equator, this intensifies the poleward shifted tropical moisture convergence of the AMIP simulation, since convection occurs where SST reaches its regional maximum and warm SST slows down surface winds. Usually, the ITCZ moves north of the equator from June to August following the seasonality of surface temperatures linked to solar irradiation. As a result, trade winds pick up along the equator in the absence of the convergence zone and convective precipitation. Moisture is then transported to the Northern Hemisphere via deflected winds due to the sign shift of the Coriolis force across hemispheres and initiates the West African Monsoon rainfall. The accelerated trade winds then excite upwelling along the equatorial cold tongue. Due to the southward shifted ITCZ in the coupled model simulation, this process is delayed. Since the ITCZ is still located at the equator from May to July the onset of trade winds is delayed and results in a severe westerly wind bias during JJA along the equator. The wind bias delays the uptake of upwelling and reduces the intensity of this process which in turn causes SST to exceed observations in the eastern equatorial region. Warm temperatures in the east reduce zonal winds as the zonal temperature gradient is reduced and shifted to the west. Consequentially the cold tongue region is shifted to the west as well, resulting in a negative SST bias emerging in the west from June to November. The equatorial SST gradient which usually results from the cold tongue in the east is now reversed and further reduces zonal winds along the equator. In the east, the interaction between wind and SST enhances the SST bias. Warm SST reduces wind and low wind in turn reduces turbulent mixing. The consequence of the reduced winds is an increased thermocline thickness in the east. A thicker thermocline would hinder fresh water from being upwelled from below to reach the surface and would reinforce the SST bias. This relation is supported by the study of Richter and Tokinaga (2020).

The seasonality in XR shows the same biased interaction between SST, precipitation, and wind, but with less intensity due to a lower SST bias. Figure 4.10 C shows the difference between HR and XR simulations, highlighting the consequences of a more elevated SST bias in HR. It shows how a significant part of the equatorial wet precipitation bias from

May to July is removed with the reduction of the SST bias, as well as the most southern wet precipitation bias in FMA. Additionally, it shows how new equatorial precipitation and meridional wind biases are introduced with the warming of the tropics in XR during boreal winter. The westerly wind bias along the equator persists in the XR simulation but is moderately reduced as the zonal SST gradient is less elevated from May to October.

In general, further reinforcement of the SST bias can presumably result from diminished low stratocumulus formation. Naturally low clouds form above upwelling regions since cold surface water produces cold moist air being trapped below the warm and dry tropospheric air layer which excites cloud formation. Clouds reduce solar irradiance and thus, would reduce further heating (Richter, 2015). Furthermore, the seasonal maximum of the SST bias in the ABA coincides with the seasonality of downwelling EKWs/CTWs remotely excited at the equator. The study of Goubanova et al. (2019) shows, that approximately half of the elevated SST in the ABA from March to May is associated with downwelling CTWs advecting warm water too far south due to the biased mean state of the ocean. It becomes obvious that many different processes interact and reinforce each other within the seasonal cycle. This leads to temporal shifts in seasonality and altered spatial patterns of several quantities involved in the climate system. Identifying a single source of the bias problem appears unlikely, instead, a deeper understanding of the various underlying dynamics is imperative to adjust their representation in climate models.

West African monsoon

During the West African Monsoon season (June to September, JJAS) the ITCZ is located north of the equator, with moist southwesterly winds from the equatorial Atlantic region converging with dry northeasterly winds from the Sahara. The variability of the monsoon is majorly induced by the intensity of the Atlantic cold tongue and the Saharan Heat low. Variations of the monsoon substantially affect the regional population, especially in the Sahel area, since agriculture and food resources are highly dependent on the monsoon rainfall (Niang et al., 2020).

To depict the seasonality of the African monsoon the involved atmospheric variables are averaged along latitudes between 40°S and 20°E. The biases of seasonally stratified averages are shown in Figure 4.11. The deviations of monsoon dynamics of the atmospheric model component simulated by AMIP from the observational reference are shown in Figure 4.11 A.1 to A.4. In AMIP simulated Monsoon dynamics are affected by elevated surface air temperatures of African land areas in the Northern Hemisphere, coinciding with reduced equatorward winds in boreal spring. Along with the meridional wind bias of the Southern Hemisphere during boreal winter, this results in a double ITCZ like convergence intensification north and south of the observed position of the ITCZ

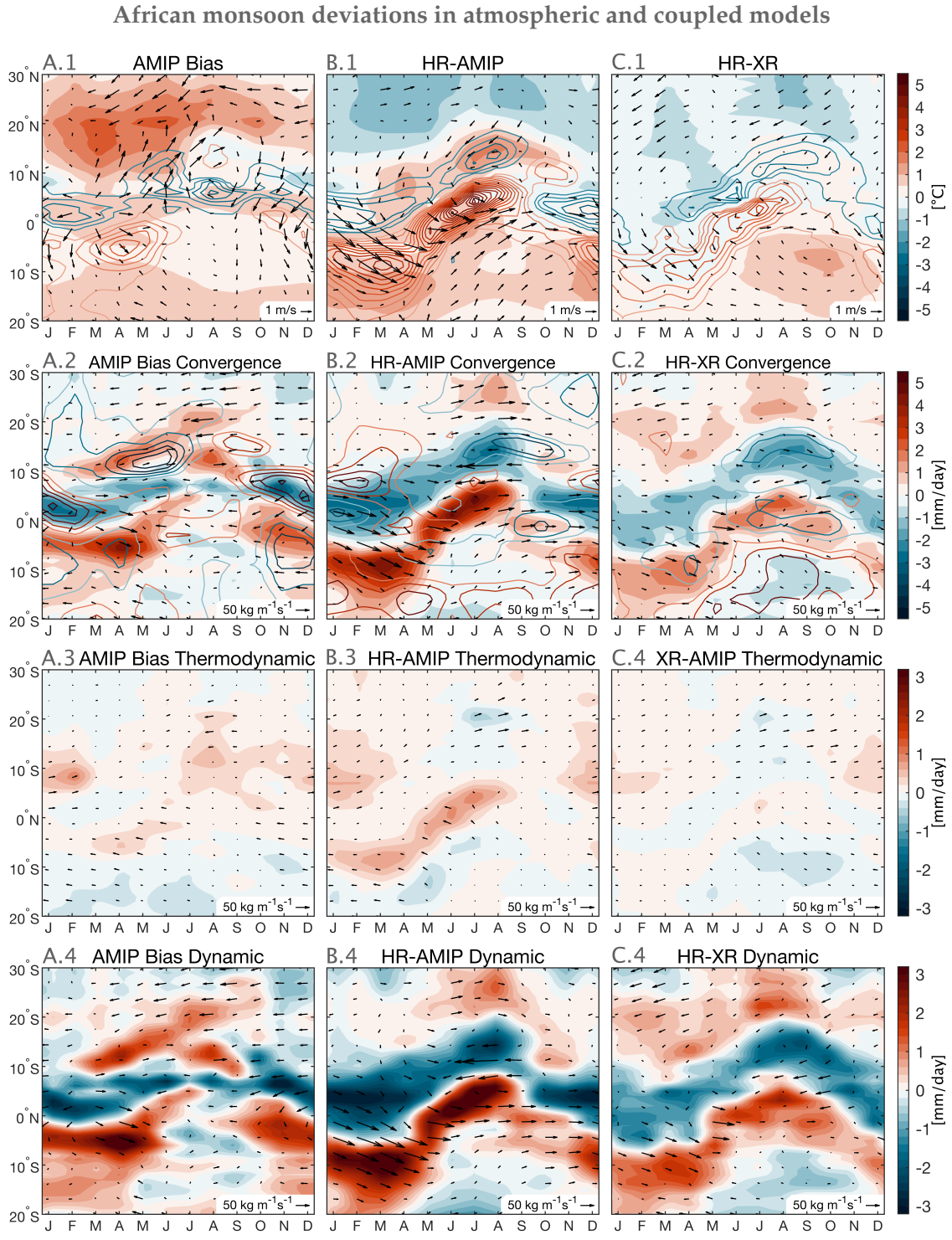

Figure 4.11: Biased African monsoon seasonality in averages between 40°W and 20°E along latitudes [1980-2014]. A) AMIP biases (reference: GPCP/ERA-5), and AMIP subtracted from B) HR and C) XR. First row: air temperature (shading in °C), precipitation (contour lines in 0.5 mm/day steps, omitting the zero line, +/- in red/blue), and wind (arrows in m/s). Second row: moisture convergence (shading in mm/day), latent heat flux (contour lines in 5 W/m^2 steps, omitting the zero line, +/- in red/blue), horizontal moisture flux (arrows in kg/ms). Thermodynamic (third row) and dynamic (fourth row) component of moisture flux and convergence.

dependent on the season. This creates excess precipitation further to the south from October to June and excess precipitation further to the north during monsoon season, mostly affecting the West African Sahel region. The biases are mainly caused by dynamic effects. Thermodynamic changes due to increased evaporation only slightly affect the Sahel region during monsoon season and the tropical North Atlantic during boreal winter. It becomes obvious that the westerly wind bias in MAM is linked to the maximum of excess precipitation along the tropical South Atlantic, suggesting that the reduced winds in the eastern tropical Atlantic cause the seasonally poleward shifted precipitation pattern which in turn causes a reduction of western equatorial zonal winds to decrease when the ITCZ reaches its climatological most southern position. The reduced equatorial precipitation along the equator in boreal winter is combined with increased easterly winds.

Figure 4.11 B.1-B.4 shows the monsoon dynamics in HR subtracted by the AMIP simulation. The difference results from the coupled feedback between oceanic and atmospheric submodels with biases in both components. It shows, that the representation of the West African monsoon in HR is biased by an intensification of the southward shifted part of the ITCZ but extended throughout the year, coinciding with elevated surface temperatures and westerly wind biases in the equatorial and South Atlantic. Surface temperatures are cooler on average in the Northern Hemisphere and elevated in the Southern Hemisphere than in AMIP which would theoretically lead to a northward energy transport that needs to be balanced by a southward shift of tropical precipitation Zhou and Xie (2017). As a consequence, monsoon rainfall along West Africa in JJAS is shifted southward and leaves the Guinea and Sahel area too hot and dry with reduced convergent moisture flux. The intensification is majorly related to dynamic changes since the magnitude of tropical South Atlantic trade winds is significantly reduced. Enhanced evaporation related to the increased surface temperature in the tropical South Atlantic thermodynamically increases the available moisture in the atmosphere which is then advected with the trade winds but slowed down by the wind bias in opposite direction. During JJAS the surface winds are elevated north and south of the usual position of the ITCZ but directed too far west and east on the Northern and Southern Hemisphere respectively. Thus, most of the moisture is not transported into the Sahel region, but past it, creating a strong negative convergence bias over the Sahel region.

The thermodynamic impact, shown Figure 4.11 B.3, due to elevated surface temperatures of the Southern Hemisphere is low but contributes to the strengthening of the southward shifted convergence zone. The Sahel region during monsoon season is thermodynamically affected due to the decrease in precipitation. It leads to decreased evaporation rates, combined with increased surface temperatures, creating a local thermodynamically induced reduction of moisture convergence. However, the dynamic changes linked to the SST bias dominate the atmospheric moisture pattern. Monsoon rainfall in the Sahel area is

significantly underestimated in the model simulation, due to the diminished transport of moisture toward this region. Negative surface wind biases over the South Atlantic and equatorial area coincide with the location of wet precipitation biases and positive convergence biases. With enhanced SST the location and intensity of the meridional surface temperature gradient changes which is naturally induced by seasonal variations of solar irradiation. Elevated SST south of the equator shifts the meridional gradient further to the south with implications for surface winds. Southeasterly surface winds of the Southern Hemisphere which approach the equator, slow down early and transport less moisture towards the north. The slowdown of winds generates a dislocation of moisture convergence further to the south, where the SST bias reaches its maximum. The result can be seen as a broader than usual convergence zone in meridional direction, where moisture is redistributed from the center, especially to the southern edge.

The difference between HR and XR is shown in Figure 4.11 C.1-C.4. With higher resolution of the atmospheric component, the bias of the interhemispheric surface temperature gradient can be reduced, as the tropical North Atlantic temperature rises and the SST bias in the tropical South Atlantic is reduced. The biased wind and precipitation patterns are still similar to the patterns in HR but the biases are significantly reduced in XR. The southward shift of the ITCZ is reduced with a reduced westerly wind bias. The relation between elevated SST and enhanced latent heat flux becomes evident for the South Atlantic which enhances divergent moisture flux towards the equator. The intensity of equatorward trade winds is however reduced in XR.

In summary, the SST bias arises together with large atmospheric biases and severely biased seasonal feedback mechanisms, affecting precipitation of the Sahel region. Intrinsic atmospheric biases are further intensified with the coupling of the oceanic submodel. The coupling also adds oceanic biases which in turn affect oceanic and atmospheric feedback mechanisms. The SST bias is related to a southward intensification of the ITCZ and divergent moisture flux further north. This results in the Sahel area being simulated as too hot and too dry with very little precipitation reaching this area on average. Zonal winds are largely reduced due to seasonal interaction with elevated SST. This dependency between both variables reinforces each other's deviations from observations. The atmospheric moisture budget is mostly affected by altered dynamics. The biased transport of moisture results in shifted precipitation patterns which reinforce the reduction of winds.

This Chapter shows how model resolution affects the performance of climate variables and the representation of the eastern boundary SST bias. An increased oceanic resolution can improve general performance metrics but the eastern boundary SST bias in the northern Benguela upwelling region results from the lack of a detailed surface wind representation along eastern boundaries which can only be provided by an increased atmospheric

resolution. The improved WSC representation with increased atmospheric resolution affects the underlying current system and prevents an enhanced southward intrusion of warm tropical water along the eastern boundary, which in turn reduces the SST bias. The remaining SST bias is related to the defective surface wind representation over eastern tropical ocean basins. The elevated SST in turn leads to an equatorial westerly wind bias and a severe intensification of the southward shifted ITCZ. The shifted pattern affects annual monsoon rainfall over West Africa, leaving the Sahel region too hot and dry. With a reduced SST bias in the Benguela upwelling region, the impact on African precipitation moderately decreases but the disturbed precipitation pattern remains affected.

5 Interannual Sea Surface Temperature variability

The characteristics of interannual SST anomalies in the South Atlantic are examined in this Chapter in order to determine their atmospheric response and their relation to the mean state SST bias. The dominant interannual SST modes and characteristic periods are investigated and compared to their representation in the model simulations in Section 5.1. The AZM and Benguela Niños/Niñas dominate the SST variability on interannual time scales in the South Atlantic. The evolution of these anomalies is analyzed in time and space together with their climatic response in Section 5.2 to understand the related dynamics and implications for climate variability. The influence of the biased SST pattern on the climatic response is thereby of major interest. Composites of warm AZM events are analyzed in the context of increased resolution of the atmospheric model component to determine whether the climatic response improves with a reduced SST bias in the Benguela upwelling area as in the XR simulation. In addition, a comparison of composites of realistic warm Benguela Niño events simulated by the AMIP model and the sensitivity experiment of HR GECCO3, which retains the biased SST mean state, shows how the SST bias influences precipitation patterns. In order to analyze the impact on precipitation variability, the corresponding anomalies within the atmospheric moisture budget provide information about the impact of SST variations on atmospheric momentum and moisture fluxes.

5.1 Dominant modes of South Atlantic Sea Surface Temperature

Along with the biased South Atlantic mean state SST the representation of SST variability is affected in model simulations. Amplitudes of SST variations are reduced where mean state SST values are erroneously elevated. This affects not only the amplitude of the annual cycle but interannual SST anomalies as well. Figure 5.1 A shows the standard deviation of observational interannual SST in the South Atlantic and a comparison to modeled SST variations in HR and XR in Figure 5.1 B and C respectively. Interannual SST variability of the South Atlantic is dominated by the AZM and Benguela Niños/Niñas which affect the tropical part of the eastern boundary. Amplitudes are highest along the coast of West Africa between the equator and 22°S. The maximum amplitude of the interannual variations is located in the ABA, where Benguela Niños create SST anomalies deviating from the seasonal mean of about 2°C on average. SST variability is high along the coast of Angola as well and affects the eastern equatorial region, including the cold

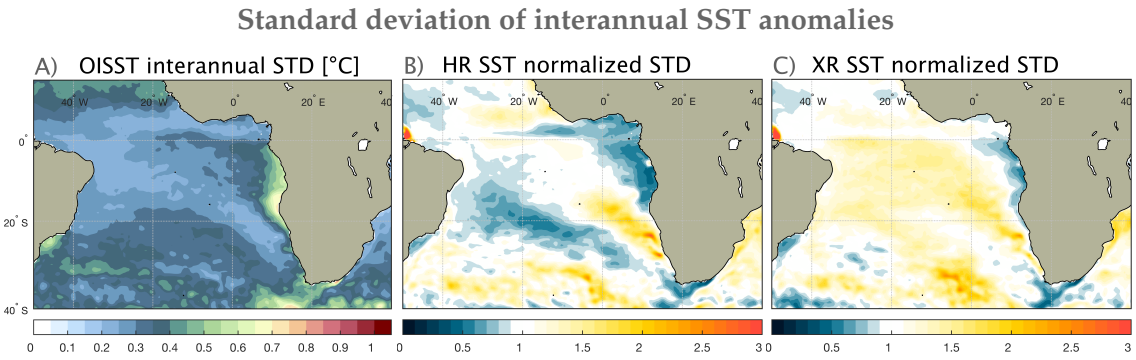

Figure 5.1: Standard deviation of interannual SST anomalies [1982-2014] for A) OISST with shading in °C. Corresponding standard deviation of interannual SST variations for B) HR and C) XR divided by the standard deviation of OISST as a reference, such as dimensionless values larger/lower one indicate elevated/attenuated amplitudes respectively.

tongue region. This region is affected by variations via the AZM which produces SST anomalies of approximately 1°C on average. The ratio between standard deviations of SST simulated by HR and of the OISST product in Figure 5.1 B shows diminished interannual SST variability, where it should be most pronounced. The enhanced amplitudes along the Benguela upwelling region show, that interannual SST anomalies reach into regions further to the south than usual. The amplitude is most reduced along the coast of Angola, where a thicker thermocline related to elevated SST may dampen interannual anomalies linked to the AZM. As the SST bias decreases in XR, amplitudes of interannual SST variability appear to be less affected but still show a similar pattern. The characteristic occurrence of SST anomalies in time and space is determined in the next step, in order to create expressive composites of the anomalies and investigate the atmospheric response.

Since interannual SST variability of the tropical South Atlantic dominates the equatorial and eastern part of the basin, SST variability along the equator and along the eastern boundary of the South Atlantic is displayed in more detail in Figure 5.2. The left column shows the seasonal stratified standard deviation of interannual SST anomalies (averaged between 2°N and 2°S along the equator and between the coast of the eastern boundary and 3° to the west) for OISST and model simulations of HR and XR. The right column shows the corresponding periodicity of those anomalies. The standard deviation shows a strong seasonal modulation of interannual anomalies, such as the SST anomalies increase or decrease the seasonal maximum of SST. Largest observational SST anomalies as shown in Figure 5.2 A occur between 13°S and 20°S during FMA. These anomalies are associated with Bengula Niños which modulate the seasonal maximum of SST in the ABA during FMA when the ABF reaches its climatological southernmost position (Lübbecke et al., 2019) and the thermocline outcrops to the surface in the ABA (Florenchie et al., 2004). The intensity of the event peak is modulated by local atmospheric forcing and by the timing of the passage of intraseasonal CTWs which cause a displacement of the thermocline

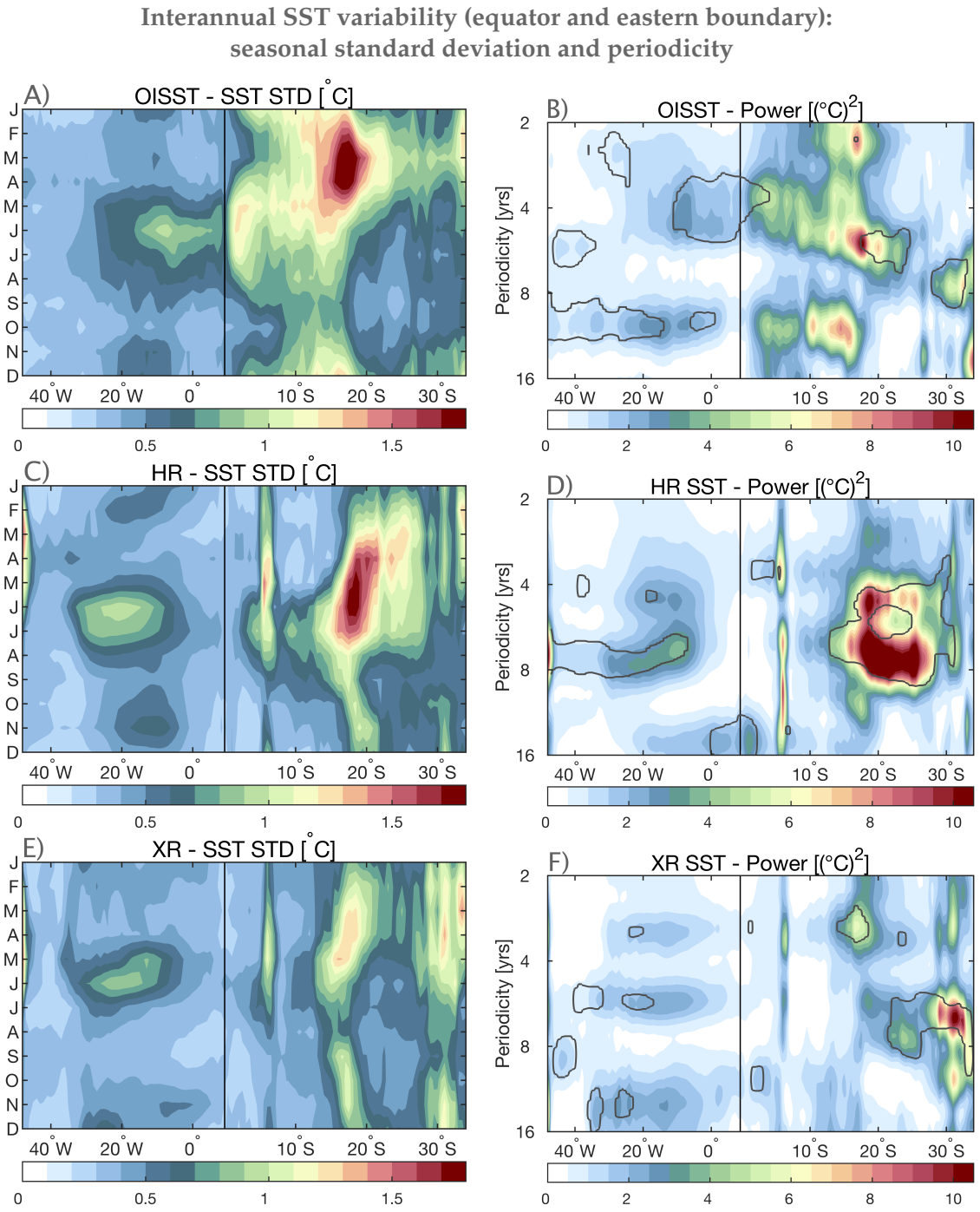

Figure 5.2: Left: Seasonally stratified standard deviation of interannual SST anomalies along the equatorial Atlantic and the South Atlantic eastern boundary with shading in °C, for A) OISST, C) HR, and E) XR. Right: Corresponding global wavelet spectrum showing dominant periods of SST variations (in years) indicated by power in $°C^2$ for B) OISST, D) HR, and F) XR. Significant periodic power on the 95% confidence level outlined by thick gray line.

(Imbol Koungue and Brandt, 2021). Along the Benguela upwelling region anomalies are comparatively low and peak around March which also coincides with the climatological maximum of upwelling intensity. SST along the coast of Angola is affected by anomalies

that modulate its semiseasonal cycle, highlighting the linkage between interannual SST anomalies and the intensity of downwelling and upwelling CTWs. Most pronounced anomalies along the coast of Angola also affect the equatorial cold tongue region. Those anomalies during May/June stretch along the eastern boundary from 18°S to the equator and eastern equatorial area (0°-20°W) with a peak during June/July. These anomalies are associated with the AZM which are mostly seasonally linked to boreal summer when the thermocline is shallowest along the coast of Angola (Keenlyside and Latif, 2007). Illig et al. (2020) showed that SST anomalies in the ABA precede AZM events in the eastern tropical Atlantic due to the influence of local wind forcing linked to the weakened South Atlantic Anticyclone which initiates local and remote forcing. They highlight the strong relationship between the AZM and Benguela Niños/Niñas as both phenomenons are forced by EKWs and subsequent CTWs in overlapping regions and seasons, stating it is debated whether they should be viewed as one mode of SST variability.

Figure 5.2 B shows the dominant periods of observational SST variations for the same regions as in Figure 5.2 A which allows the association of characteristic periods to the interannual SST variations. It highlights the strong variability of the ABA, between 10°S and 20°S, varying on various interannual periods. This suggests different types of dynamics that affect SST in this region on interannual scales. Periods along the coast of Angola coincide with periods along the equatorial Atlantic which allows linking the AZM to a periodicity of 3-4 years. The strongest signal is found in the ABA at periods of 5-6 years which reach into the northern Benguela upwelling region. Those periods substantially differ from those of the equator and thus can be linked to Benguela Niño/Niña events which predominantly affect the SST in the ABA and are characterized by southward intrusions into the Benguela upwelling region. The closely related periodic display of these two processes emphasizes the assumption that both types of anomalies could be variations of related dynamics dependent on the seasonal timing and intensity of initiation. Periods related to Benguela Niños/Niñas are associated with longer periods as these extreme events are sensitive to local forcing conditions (Lübbecke et al., 2019) and not all SST anomalies evolve into a full Benguela Niño/Niña extreme events. The extreme events which intrude far into the Benguela upwelling region are rarer and thus periods increase toward higher latitudes. The higher frequent variations with periods of 2 to 3 years affect the ABA and also the central equatorial region and may be associated with the quasi-biennial oscillation of the South Atlantic Anticyclone which induces local SST anomalies in the ABA and the equatorial region (Richter et al., 2010). Only in rare occasions these anomalies are intensified in combination with other forcing mechanisms and evolve into an extreme event. The lower frequent variations along the equator and the coast of Angola with periods around 11 years, could be linked to SST variations induced by the AMM since SST variations along the coast of Angola are involved but the 11 year periods are only significant along most of the equatorial Atlantic.

Figure 5.2 C shows, that dominant interannual SST anomalies in the HR simulation are displaced further to the south. The maximum variability between 15°S and 22°S is not only shifted towards the south but is also shifted in season with peaks around April at 20°S and around June/July further north. Thus, variability is seasonally delayed by 1-3 months in the model simulation. The semi seasonal occurrence of interannual anomalies along the coast of Angola is not present in the model with an obvious general lack of variability in the Angola area. Additionally, variability during June/July at the equator between 10°W and 30°W is enhanced and shifted to the west. SST varies with periods around 5 and 7 years along the equator and the eastern boundary between 10°S and 30°S. The seasonality and periodicity of these SST anomalies give the impression of being related to a mix of processes between AZM and Benguela Niños/Niñas. Most likely the process of AZM anomalies is disturbed by the defective representation of Benguela upwelling dynamics and the associated WSC which results in an unimpeded southward transport of anomalies and leaves the Angola region mostly unaffected due to an increased thermocline thickness associated with the elevated SST and low surface winds. In general, periods in the HR simulation are longer than observed.

Interannual SST variability in XR is less seasonally pronounced but occurs during similar seasons at similar locations as in HR. However, the periodicity is very different from the HR simulation. The equatorial region and the ABA are both majorly affected by SST anomalies with three different periods as in the observations but with shifted frequencies. AZM related processes occur with shorter periods of approximately 3 years which is somewhat higher frequent than the observations and is also less pronounced along the coast of Angola. Periods of 5-6 years are associated with SST anomalies along the Benguela upwelling region. The periods of the low frequent SST anomalies dominating the equatorial region are longer than the observational periods. The higher atmospheric resolution in XR significantly affects the representation of interannual SST variability. The improved WSC representation results in less defective southward intrusions associated with interannual SST variations. However, interannual variations in the Angola area remain largely biased. Since SST variations in the model simulations diverge from observations in terms of seasonal occurrence, length of periods, and also location wise, the climatic response to the SST modes is expected to be affected as well.

5.2 Atmospheric Response to interannual Sea Surface Temperature events

The AZM and Benguela Niño/Niña events dominant SST variability on interannual time scales in the South Atlantic and are examined in this Section. The spatial and temporal extent of the SST anomalies is analyzed along with the related atmospheric response, in terms of anomalous horizontal momentum and moisture fluxes which create precipitation

anomalies. AZM events have a severe impact on the variability of the West African monsoon and Benguela Niños/Niñas strongly affect Southwest African precipitation. Since African precipitation variability is controlled to a considerable extent by SST modes, the predictability of SST modes forced by wind fluctuations would add to the predictability of precipitation patterns. The analysis of the simulated teleconnection between the SST modes and African precipitation is meant to highlight the discrepancies of reproduced SST dependent precipitation variability arising with the SST bias. First, a composite of AZM anomalies dependent on trade wind relaxations is examined in Section 5.2.1 for HR and XR. It is followed by a composite analysis of realistic Benguela Niños events represented in AMIP and HR GECCO3 in Section 5.2.2 to highlight the influence of the mean state SST bias on the climatic response to SST anomalies.

5.2.1 Atlantic Zonal Mode

Interannual warm SST anomalies related to the AZM are associated with surface wind relaxations over the tropical South Atlantic ocean basin. The relation is shown in Figure 5.3, where interannual anomalies of the upwelling index computed from upwelling favorable alongshore winds along the coast of Angola (7°S-18°S) during FMA are correlated to seasonally stratified interannual SST anomalies. A 3-month-running mean was applied to the anomaly time series to account for small seasonal deviations. Positive correlation coefficients indicate a relation between low/enhanced alongshore wind dependent Ekman transport and warm/cold SST for locations along the equatorial Atlantic and the eastern boundary of the South Atlantic. The result shows that warm SST anomalies evolve in

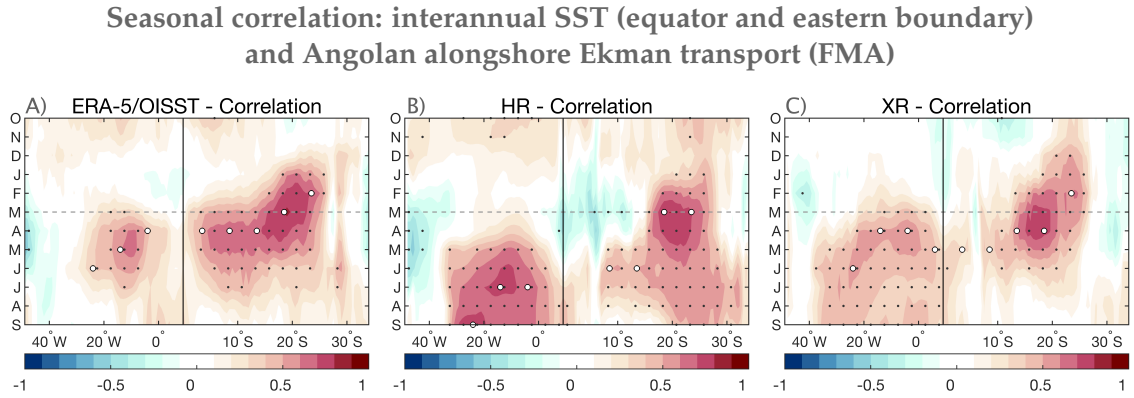

Figure 5.3: Correlation coefficients for interannual anomalies of alongshore Ekman transport during FMA averaged along the coast of Angola (7-18°S) and seasonally stratified interannual SST anomalies [1982-2014] along the equatorial Atlantic and South Atlantic eastern boundary for A) ERA-5/OISST, B) HR, and C) XR. Black dots indicate significant correlation on the 95% confidence level computed by the bootstrap method with 2000 repetitions. White circles mark the seasonal maximum correlation. Below the gray dashed line, positive coefficients indicate warm/cold SST anomalies lag low/enhanced alongshore wind induced upwelling conditions.

the ABA and northern Benguela upwelling region with decreasing alongshore winds in FMA when the thermal gradient in meridional direction along the coast is largest and the seasonal downwelling CTW reaches the ABA (Illig et al., 2020). Figure 5.3 A shows that the initial warming evolves simultaneously with decreasing alongshore winds in the ABA and is followed by increasing SST along the eastern equatorial Atlantic and along the coast of Angola in April/May. The warming is forced remotely by wind stress perturbations at the western equatorial Atlantic which creates high energetic downwelling EKWs and subsequent CTWs traveling poleward along the eastern boundary. The depth of the thermocline in the eastern equatorial Atlantic is much deeper than in the ABA and limits subsurface anomalies reaching the surface to May-June-July when the thermocline is seasonally shallow and ocean-atmosphere interaction is strong (Keenlyside and Latif, 2007; Illig et al., 2020). Illig et al. (2020) states, that the coastal warming is dependent on the month of the remote wind stress forcing but the timing and the amplitude of the actual event are controlled by local meridional wind stress variability. The following composite analysis shows that extreme SST events in the ABA like Benguela Niños occur with wind stress anomalies earlier during the year than AZM events and leave the eastern equatorial Atlantic less affected.

According to (Hughes et al., 2019) a typical Kelvin wave travels with a phase speed of 2.5 m/s across the equator and is thus expected to modulate SST along the eastern boundary 1-2 months after being excited at the western equatorial Atlantic. Kelvin waves that reach the eastern boundary can also be reflected as westward traveling Rossby waves and further amplify the warm SST anomaly along the eastern equatorial area. The combined forcing by local and remote wind anomalies results in the El Niño like SST anomaly in the eastern tropical Atlantic which is shown in Figure 5.4. The lagged correlation coefficients show a similar mechanism for the HR and XR simulations as shown in Figure 5.3 B and C. For HR the equatorial warm SST lags the ABA SST anomaly by 2-3 months instead of 1-2 months as shown for the reference. The correlation along the coast of Angola is rather low which indicates only a weak impact of the poleward propagating CTW in this region presumably linked to a deepened thermocline. In XR this relation appears to be weaker but the timing of the eastern equatorial SST anomaly is in better agreement with the reference. The equatorial SST anomaly lags the initial coastal wind forcing by only 1 month. The local SST response in the ABA is not located as far south as in HR and highlights the impact of the improved alongshore wind representation for the simulation of South Atlantic SST variability. However, in both model simulations, the SST anomaly in the ABA is seasonally delayed and related to longer lasting equatorial SST anomalies.

The composite analysis of warm AZM events supports the linkage between wind and SST anomalies as indicated by the correlation coefficients. The temporal evolution of the AZM composite is displayed in Figure 5.4 A.1-A.3 and Figure 5.5 A.1-A.3 for the observational

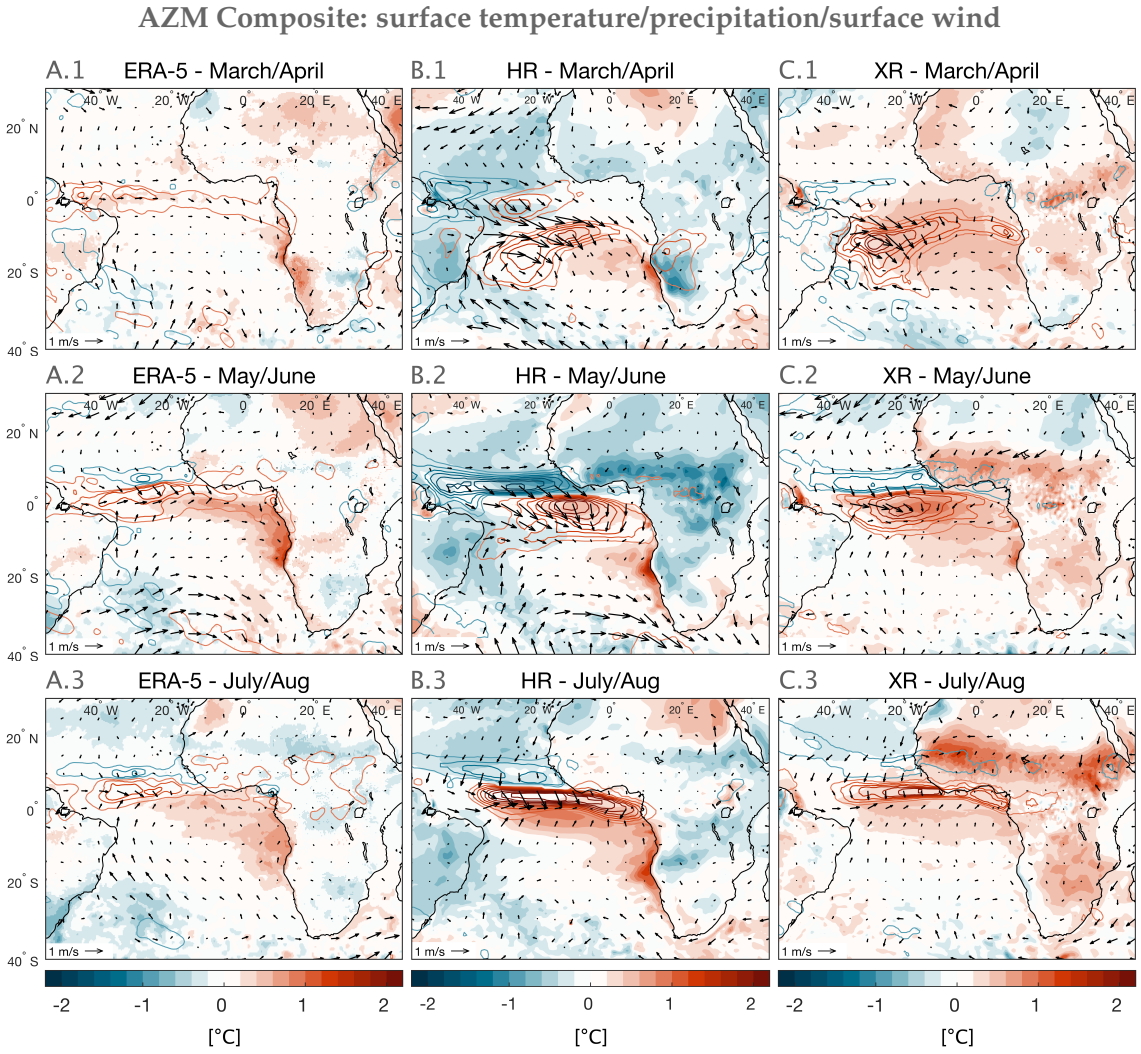

Figure 5.4: Seasonal evolution of warm AZM composites from AZM events between 1982 and 2014 for A) ERA-5/OISST, B) HR, and C) XR, showing SST and climate anomalies during March/April (first row), May/June (second row), and July/August (third row). Shadings show SST anomalies and surface air temperature anomalies over land areas in °C. Contour lines show wet/dry precipitation anomalies in red/blue in steps of 0.5 mm/day, omitting the zero line. Arrows indicate surface wind anomalies in m/s.

reference from March to August. The trade wind relaxation in March/April is accompanied by anomalous high moisture convergence and precipitation along the equator, as well as small warm SST anomalies. During March/April the position of the ITCZ is directly over the equator when equatorial SST reaches its seasonal maximum and zonal winds drop down to their seasonal minimum. The composite of the onset of the AZM events in Figure 5.4 A.1 and Figure 5.5 A.1 shows that precipitation is anomalously large along the equator related to increased evaporation and equatorward moisture flux over the tropical North Atlantic. The increased equatorial moisture convergence and precipitation likely affect surface winds. As a result, meridional winds along the coast of Angola are anomalously weak and SST is already increasing with anomalies of approximately 1°C

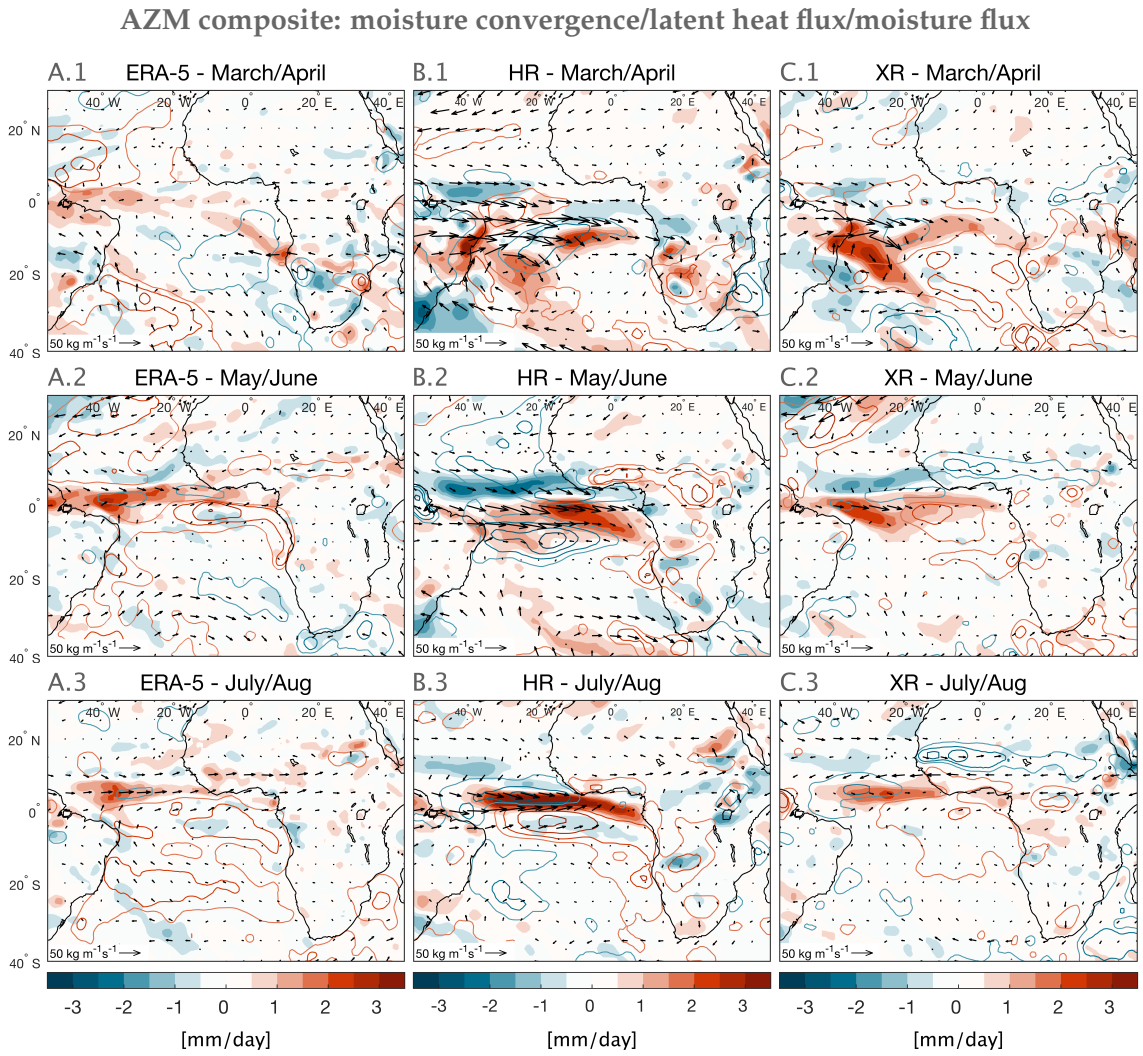

Figure 5.5: Seasonal evolution of warm AZM composites from AZM events between 1982 and 2014 as in Figure 5.4 but showing corresponding anomalies of moisture convergence (shading in mm/day), surface latent heat flux (contour lines show positive/negative anomalies in red/blue in steps of 4 W/m^2 and omitting the zero line) and horizontal moisture flux (arrows in kg/ms).

in the ABA. The SST anomaly may be locally induced by the weakened winds but may also be a result of an intensified climatological CTW due to zonal wind relaxations in the western equatorial Atlantic. The Benguela upwelling region remains mainly unaffected in terms of alongshore winds and SST anomalies. The upwelling region holds up as a barrier that prevents temperature anomalies travel further southward along the eastern boundary. SST anomalies intensify in May/June along the coast of Angola and the eastern equatorial area due to the arrival of the equatorial forced EKW and subsequent CTW. Oceanic evaporation then increases where SST is elevated, while moisture converges mainly in the western equatorial Atlantic and produces wet precipitation anomalies. The increasing SST anomalies may be fueled by the seasonality of the upwelling CTW around June which can bring warm equatorial subsurface anomalies to the surface. The eastern

equatorial warming may be linked to the reflected Rossby wave. With the eastern equatorial warming during May/June the zonally affected SST gradient further reduces zonal equatorial winds which further amplifies moisture convergence in the western equatorial area. With less zonal winds less moisture can be advected and enhances equatorial rainfall. The elevated SST along the coast of Angola increases the meridional SST gradient along the eastern boundary and results in the acceleration of meridional surface winds in the ABA in June/July and likely contributes to the fading SST anomalies in July/August. The seasonal upwelling CTW which can act as an enhancing contribution to the SST event may also be another possible factor for the early end of the expanding SST anomaly as it continues to disperse surface anomalies. During monsoon season in JJA more moisture converges into the ITCZ than usual while the position of the ITCZ and the related precipitation pattern is shifted to the south. The result is enhanced rainfall over West Africa as oceanic evaporation of the eastern tropical Atlantic is increased and moisture flux is directed further to the northeast, just north of the eastern tropical Atlantic SST anomalies. The Guinea and Sahel region are mostly affected by enhanced precipitation.

For the HR simulation the composite analysis in Figure 5.4 B.1-B.3 and Figure 5.5 B.1-B.3 shows an intensified pattern of anomalies. The initial warming related to reduced surface winds occurs in the tropical South Atlantic and more elevated along the northern Benguela upwelling region. Intensified trade winds and high evaporation rates over the tropical North Atlantic precede warm SST anomalies similar to the observational composite. The result is enhanced moisture convergence south of the equator accompanied by largely enhanced precipitation and reduced surface winds. Wind anomalies are very high and affect almost the entire tropical South Atlantic accompanied by a more spatially extended ocean surface warming than in the observational composite. Alongshore winds are weakened along the coast of Angola and the ABA during March/April but seem not to affect local SST. Instead, the northern Benguela upwelling region experiences a strong warm SST anomaly more of the character of a Benguela Niño event. This suggests, the anomaly is most likely generated by a climatological downwelling CTW of high energetic character which is not dissipated by the Benguela upwelling dynamics and related undercurrent and thus can intrude further to the south due to the defective simulation of surface winds in HR. During May/June the equatorial cold tongue region and the ABA experience additional SST anomalies as well which supports the theory of the influence of remotely forced EKWs/CTWs, which are generated simultaneously with the initial warming of the ABA and bring subsequently warm subsurface to the ocean surface where the thermocline is shallow which amplifies the warm event. The initially southward shifted moisture convergence over the equatorial Atlantic intensifies in the east where SST is elevated in contrast to the observational reference. The SST anomaly further expands spatially during July/August and further intensifies the moisture convergence along the equator with a wet precipitation anomaly. The strong moisture convergence response to the equatorial

SST anomaly results in a locally condensed and intensified precipitation response with intensified divergent moisture flux north and south of the anomaly with a slight negative precipitation anomaly over the western part of the Sahel region instead of a positive anomaly. The initially southward shifted atmospheric pattern, together with increased atmospheric sensitivity to SST anomalies in terms of dynamic and thermodynamic feedback, generates an intensified precipitation response being located too far south with excess precipitation being mostly limited to the oceanic areas along the equatorial Atlantic including the Gulf of Guinea. Additionally, during July alongshore winds along the coast of Angola pick up again, potentially as a consequence of SST gradients and the intensified equatorial convergence zone.

In comparison, SST anomalies in XR are less intense in magnitude but extend on a broader spatial scale. The main difference to HR is, that SST anomalies are located further north, such as the anomalous warm water transported from the equatorial area does not intrude into the northern Benguela upwelling region as they due in HR. This is in better agreement with the reference, but the generated precipitation anomaly resembles mostly the spatial pattern seen in HR, albeit at a lower intensity. Additionally, XR generates a defined dry precipitation anomaly over West Africa, affecting mostly the Sahel region, resembling an opposing climatic response for this area than observed. The reduced latent heat flux in combination with elevated air temperatures along the Sahel area are even enhanced in XR compared to HR. The increased atmospheric resolution in XR and the reduced SST bias provide an improved wet precipitation response during AZM events over the tropical Atlantic Ocean and an improved representation of the moisture convergence anomaly along the tropical Atlantic. The intensified moisture convergence over the eastern equatorial Atlantic is not present in XR. However, the persistent tropical wind bias and poleward shift of tropical moisture convergence in combination with the remaining mean state SST bias in the Angola area still generates an anomalous low moisture convergence over African land areas.

In contrast to observations, the AZM like SST anomalies in the model simulations causes a negative precipitation anomaly along the West African land areas instead of a positive one during monsoon season. This is caused by the southward shift of the moisture convergence zone which creates a divergent moisture flux anomaly along the Sahel and Guinea region, whereas the wet precipitation response concentrates over oceanic regions. The magnitude of the SST bias is thereby not the critical factor. With higher atmospheric resolution and a reduced SST bias in XR, the precipitation anomalies linked to AZM events differ in intensity but not much in their location in comparison to HR, with only a slight northward shift of the atmospheric response in XR. The opposing precipitation response over West African land areas in the model simulations is an important characteristic with high potential implications for the representation of climate and especially

precipitation variability in coupled climate models. The increased atmospheric sensitivity to SST anomalies may contribute to further deterioration of the condition. The reduction of the SST bias leads to a generally improved climate response being less shifted toward the eastern equatorial Atlantic, but can not solve the biased precipitation representation over the African continent.

5.2.2 Benguela Niño warm events

Extreme SST events called Benguela Niños occur during FMA in the ABA. These warm events are associated with highly elevated amplitudes and occur less frequent than warm AZM events. On average Benguela Niños cause SST in the ABA to rise 2°C higher than usual. A Benguela Niño composite is generated to analyze the atmospheric response to this type of SST anomaly as described in Chapter 3.3.3. Warm SST events during FMA which agree with the Benguela Niño criteria are found in the years 1984, 1995, 2001, and 2011 for the ABA index computed from OISST. The ABA index is displayed along with its seasonality and periodicity in Figure 5.6 for OISST as an observational reference and for the AMIP and HR GECCO3 simulation. The climatic response to Benguela Niños in AMIP and HR GECCO3 is supposed to highlight the modification induced by the mean state SST

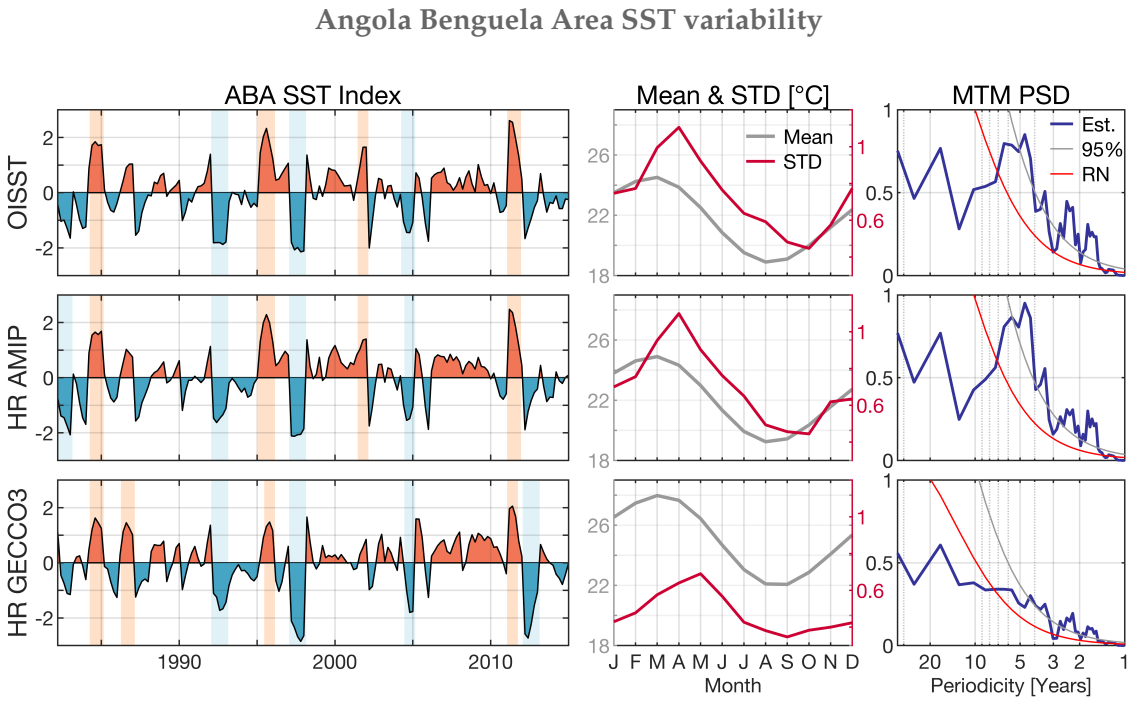

Figure 5.6: ABA index for the identification of Benguela Niño/Niña events (left) for OISST (top), AMIP (middle) and HR GECCO3 (bottom). Orange/blue bars mark years with warm/cold Benguela Niño/Niña events. Middle column shows the corresponding seasonal mean SST in the ABA and seasonal standard deviation of interannual SST anomalies. Right column shows power spectral density of ABA SST by MTM (blue line), with corresponding red noise (red line) and 95% confidence level (gray line).

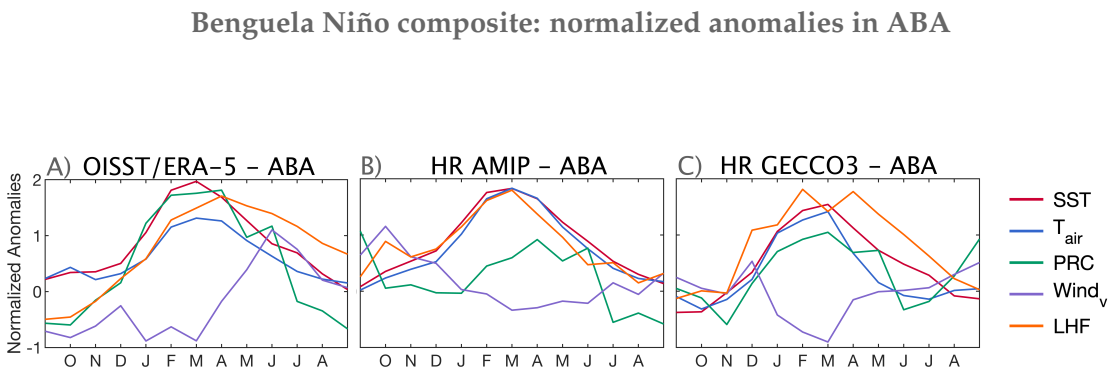

Figure 5.7: Composite of Benguela Niño events emerging in FMA between 1982 and 2014, showing mean anomalies (normalized by their seasonal standard deviation) in the Angola Benguela Area of SST (red), surface air temperature (blue), precipitation (green), surface meridional wind (purple) and surface latent heat flux (orange) from precedent September to subsequent September.

bias. The years affected by Benguela Niño events defined by the ABA index agree with findings of Imbol Koungue et al. (2019). The Benguela Niño SST anomalies are reproduced by AMIP and HR GECCO3. However, the less intense Benguela Niño event of 2001 is not identified in HR GECCO3 as the defined criteria are not sufficiently met. Nevertheless, all four events are included in the composite analysis. Figure 5.6 shows the elevated seasonal cycle of ABA SST in HR GECCO3, as only interannual anomalies are realistic in this simulation. Interannual variability peaks one month later during the year in HR GECCO3, which may indicate underrepresented Benguela Niño like SST anomalies in the coupled model, which are dependent on the right timing of initial equatorial forcing and the local climatological conditions. The power spectral density of realistic SST variations

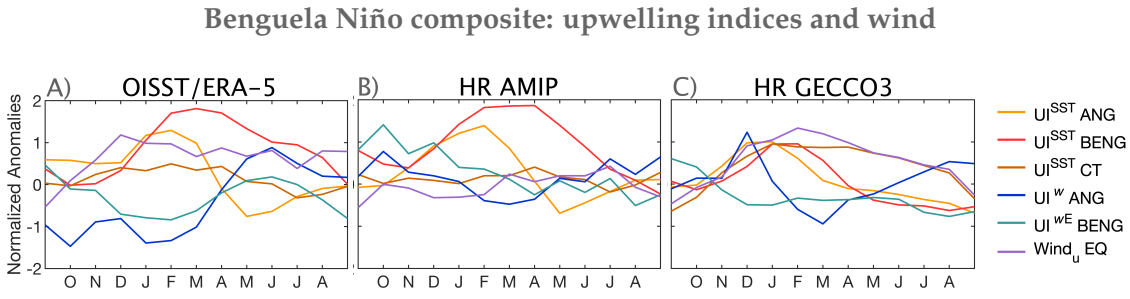

Figure 5.8: Composite of Benguela Niño events emerging in FMA between 1982 and 2014, showing mean anomalies (normalized by their seasonal standard deviation) of zonal wind averaged along the western equatorial Atlantic 40-20°W (purple) and regionally averaged upwelling indices: UI^{SST} along the coast of Angola 7-16°S (orange), UI^{SST} along the northern Benguela upwelling region 18-23°S (red), UI^{SST} along the equatorial cold tongue region 20-10°W (brown), UI^{w} along Angola (blue), UI^{wE} along the northern Benguela upwelling region (green) from precedent September to subsequent September.

in the ABA shows a general periodicity of 5-6 years which is less apparent for the HR GECCO3 simulation.

The Benguela Niño composite is derived from variable fields averaged over the 4 Benguela Niño years. To account for seasonal shifts in the onset of the individual events and deviations between data sets, the peak month of each event is taken as the reference time. Anomalies of the 4 years are then averaged monthly over the 6 months preceding the anomaly peak and the 6 subsequent months. The 13 consecutive months averaged over 4 events form the composite. Composited anomaly fields are generated for SST and atmospheric variables to show the spatial evolution of Benguela Niños for different seasons. The result is shown in Figure 5.9. The restricted time period of available data allows drawing conclusions only from four events which are not sufficient to account for statistical significance. However, results serve as a general overview of potential atmospheric responses to those events and allow the comparison of atmospheric anomalies generated by SST variations with and without the presence of the mean state eastern boundary SST bias. A more detailed and defined atmospheric response to real time Benguela Niño events can only be derived from longer time series.

The local atmospheric response to Benguela Niño events is shown in Figure 5.7 by anomalies for each month six months before and after the event. As Benguela Niños peak during March on average, the peak month of the SST anomaly in the graphic is marked as March as well, to allow for an easier association of anomaly evolution with seasons. The anomalies are normalized by the standard deviation associated with each month to identify extraordinarily high anomalies. The local response is very similar in AMIP and HR GECCO3 in comparison to the reference. The observational reference in Figure 5.7 A shows, with the rise of SST, surface air temperature and precipitation rise as well, and meridional winds drop down. An increase in evaporation is lagged by one month. Meridional winds increase to anomalous high equatorward winds as SST decreases again. The surface air temperature increase is somewhat greater in proportion in AMIP and HR GECCO3. The local precipitation response is however smaller due to shifted locations of wet precipitation anomalies in AMIP and HR GECCO3. The reduction of meridional winds associated with elevated SST is small in AMIP. Both AMIP and HR GECCO3 do not show a significant increase of meridional winds after SST approaches usual magnitudes again. This may be due to local wind dynamics being affected by the much more pronounced local convergence zone in the eastern tropical South Atlantic which is shown in Figure 5.10.

Normalized upwelling indices composited for Benguela Niño events in Figure 5.8 show, that upwelling indicated by the SST gradient and alongshore winds is low along the coast of Angola during boreal fall and winter before Benguela Niño event and decrease even more from January onward. Angolan upwelling picks up again in May as alongshore

winds increase which increases anomalous high upwelling favorable conditions. The upwelling index associated with the WSC in the northern Benguela upwelling region starts to decrease already in December before the warm event and gets back to normal levels in May. Coastal temperatures there stay elevated throughout boreal summer. The remote forcing of Benguela Niño events by the relaxation of surface momentum fluxes along the western equatorial Atlantic can be traced through zonal winds. The easterly winds drop down during the preceding boreal winter, shown by a positive anomaly of the usual negative wind vector. The lag between wind relaxations and SST events is approximately 2 months. Hence, zonal wind anomalies at the western equatorial Atlantic combined with rising SST in the ABA during boreal winter can already indicate a following extreme SST event and can thus predict local precipitation anomalies as well. However, the atmospheric simulation of AMIP which is forced with realistic SST can not reproduce this relation. Equatorial wind anomalies only evolve later as a consequence of elevated SST in combination with anomalous moisture convergence which is shown in Figure 5.9. In contrast, the coupled HR GECCO3 simulation can reproduce the relation of western equatorial wind anomalies preceding SST extreme events in the ABA.

The spatial evolution of Benguela Niño events from March to August along with the respective climatic response is displayed for the observational reference and the AMIP and HR GECCO3 simulation in Figure 5.9. The composites show the nonnormalized SST anomaly evolution with associated wind patterns and precipitation response. Additionally, Figure 5.10 shows the associated latent heat flux and atmospheric moisture flux, and convergence patterns. In contrast to warm AZM events, easterly winds along the equator already drop down in boreal winter. The equatorial surface wind anomaly is combined with anomalously large amounts of equatorial precipitation and the ITCZ being located further south than usual as more moisture is transported southward due to elevated oceanic evaporation over the tropical North Atlantic. The wind anomaly of observational reference composite in Figure 5.9 A.1 suggests, that the wind relaxation over the South Atlantic is associated with a decrease of the extratropical atmospheric high pressure system over the South Atlantic which creates a cyclonic wind anomaly. With anomalously low winds the SST of the tropical South Atlantic slightly increases. The much more elevated SST anomaly in the ABA, associated with a highly energetic downwelling CTW excited by the equatorial wind anomaly, also affects the northern Benguela upwelling region. In the subsequent month, the SST anomaly prevails in the ABA and the easterly wind in the extratropical South Atlantic picks up again. Moisture convergence increases in the western equatorial Atlantic and the ITCZ remains shifted to the south. This leads to reduced moisture convergence over West African land areas and a lack of precipitation which intensifies during monsoon season in JJA and affects the Guinea and Sahel region. The enhanced western equatorial Atlantic moisture convergence is not a result of the SST anomaly in the ABA, as it evolves even before the strong rise of SST in the ABA. The

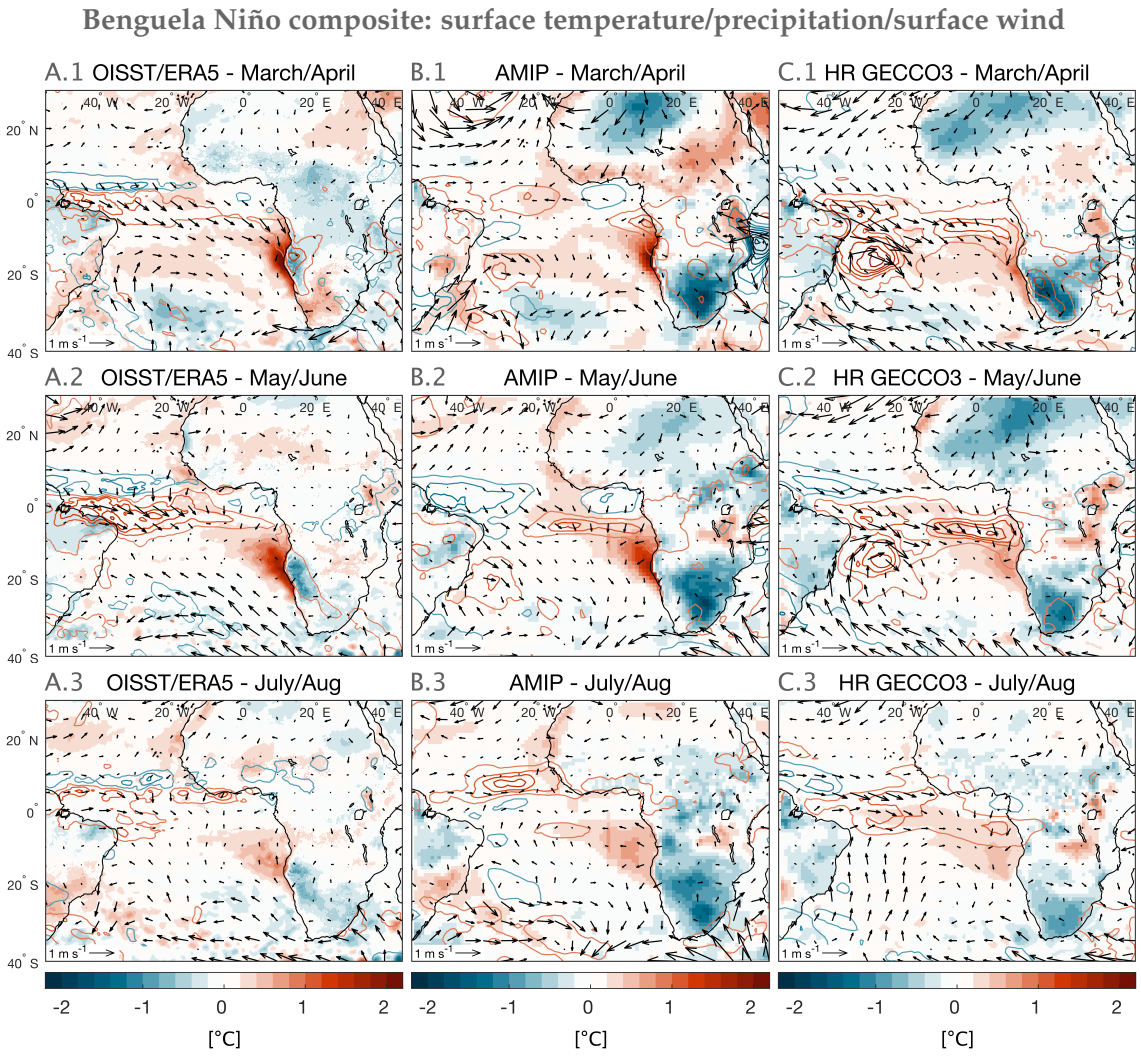

Figure 5.9: Seasonal evolution of Benguela Niño composite from events between 1982 and 2014, for A) OISST/ERA-5, B) AMIP, and C) HR GECCO3. Anomalies are shown during March/April (first row), May/June (second row) and July/August (third row), showing SST anomalies and surface air temperature anomalies over land areas with shading in °C, wet/dry precipitation anomalies with contour lines red/blue, in steps of 0.5 mm/day (omitting the zero line), and surface wind anomalies indicated by arrows in m/s.

SST event causes a local wet precipitation anomaly over southwestern African land areas which is most pronounced during March/April and spreads out during May/June.

AMIP and HR GECCO3 show a significant difference to the reference composite by simulating the convergence anomaly. Anomalous high moisture convergence over the western equatorial Atlantic is not realistically represented by the models. Wind anomalies of the models respond more intensely to SST variations and thus, result in different convergence anomalies which are intensified in the western tropical South Atlantic and in the eastern equatorial Atlantic. The local precipitation response to the extreme SST event in the eastern tropical South Atlantic is elevated in both model simulations. Both

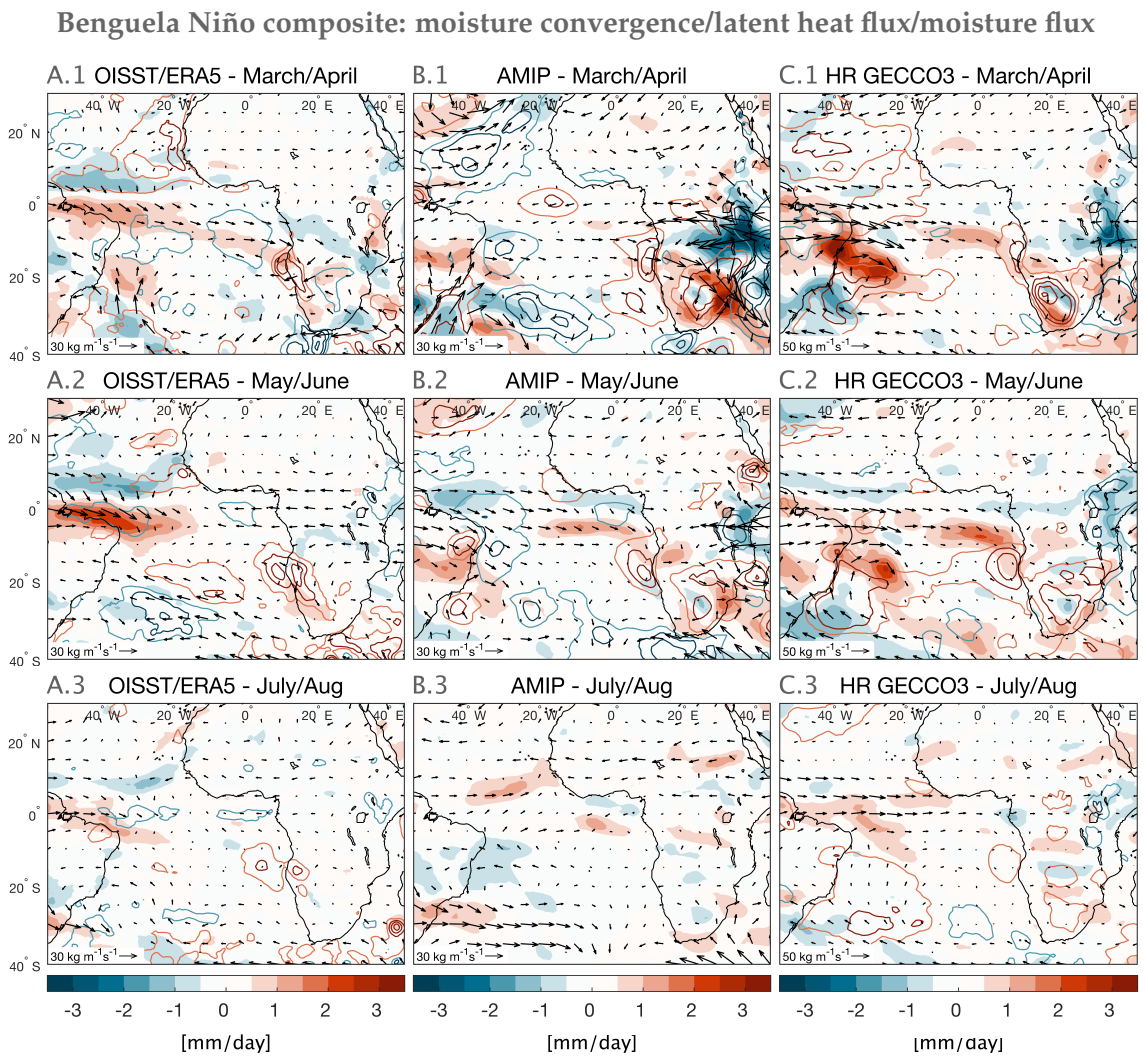

Figure 5.10: Seasonal evolution of Benguela Niño composite from events between 1982 and 2014 as in Figure 5.9 but showing anomalies of moisture convergence (shading in mm/day), surface latent heat flux (contour lines, in steps of 5 W/m^2, +/- in red/blue) and horizontal moisture flux (arrows in kg/ms). Note different scales for moisture flux reference arrows for HR GECCO3 (right column).

models simulate a widespread wet precipitation anomaly during March/April over the southern part of the African continent. A wet precipitation anomaly evolves from March to June over the eastern tropical Atlantic. The position of this precipitation anomaly is very similar in both model simulations and just differs in intensity, which is most evident during May/June. Thus, the mean state SST bias in HR GECCO3 has little impact on the location of the shifted moisture convergence pattern with only a slight shift to the east, but the intensity of precipitation anomalies induced by SST variations is highly increased in the coupled model simulation. During July/August the SST anomaly vanishes and precipitation anomalies simulated by AMIP and HR GECCO3 start to diverge more significantly from each other. However, both simulations fail to reproduce the dry precipitation

anomaly along the Guinea and Sahel regions.

In summary, the analysis of interannual SST anomalies leads to the conclusion, that West African precipitation related to SST variations of the South Atlantic is not well represented in the model simulations but opposing precipitation anomalies along the Guinea or Sahel region prevail even if the South Atlantic eastern boundary bias is reduced or not even present. The representation of the interannual SST variability improves with increased atmospheric resolution since the WSC along the Benguela upwelling region affects the simulation of SST anomalies along the eastern boundary. The improved WSC prevents SST anomalies to dominate the northern Benguela upwelling region. However, the SST anomalies associated with warm AZM and Benguela Niño events produce southward shifted tropical precipitation responses which generate an opposing response over West African land areas independent of the mean state bias. The composite analysis of Benguela Niños proves that the southward shifted precipitation response dominates the pattern also in the atmospheric model component and is very likely related to intrinsic atmospheric biases. The mean state SST bias additionally intensifies precipitation anomalies over oceanic areas. The atmospheric variables in the coupled model simulation of HR appear to be hypersensitive to SST anomalies, with unrealistically large impacts on local surface winds and evaporation. The defective climatic response over African land areas to interannual SST events is expected to affect the performance of precipitation variability with and without the presence of a mean state eastern boundary SST bias. It remains to be clarified to what extent the SST bias reinforces this deficiency.

6 Dependency of precipitation skill on Sea Surface Temperature

The previous Chapters investigate the extent of the South Atlantic eastern boundary SST bias and its impact on the atmospheric mean state simulation and interannual precipitation anomalies linked to SST variations. The analysis clearly shows the direct linkage between the eastern boundary SST bias and the displacement and spatial concentration of precipitation patterns mainly via highly sensitive surface momentum fluxes. The results additionally demonstrate very clearly the fundamental influence of intrinsic atmospheric biases on the simulated location of the ITCZ and related monsoon rainfall over the African continent on seasonal and interannual time scales. Based on these results the performance of the atmospheric and coupled model in reproducing precipitation variability linked to realistic SST variations will be analyzed in this Chapter, with the aim to investigate to what extent the precipitation signal is deteriorated by the SST bias.

Precipitation over the African continent is strongly linked to SST variations of the South Atlantic as it influences the position of the ITCZ and the magnitude of moisture convergence. SST variations can induce local precipitation anomalies but the SST impact on characteristics of the ITCZ dominates precipitation anomalies linked to seasonal monsoon rainfall over African land areas. In climate simulations, a poleward shifted mean state convergence pattern in the tropics is induced by intrinsic atmospheric biases which affect the dynamics of atmospheric moisture flux. The seasonal simulation of monsoon rainfall over West Africa is further deteriorated by the eastern boundary SST bias of the South Atlantic, as it induces additional dynamic biases reducing the transport of moisture towards the Sahel region. As a result, the monsoon rainfall in the Sahel region is significantly reduced and moisture convergence and precipitation are erroneously elevated south of the equator, intensifying the bias of the southern part of the poleward shifted ITCZ throughout the year. The dynamic impact of the SST bias clearly outnumbers thermodynamic effects. On interannual time scales, SST variations induce characteristic precipitation anomalies over the African continent. Hence, a significant part of the variability of the precipitation signal in this region is dependent on SST anomalies. Interannual SST variability is dominated by the AZM and Benguela Niño/Niña events which induce SST variations of 1 to 2 °C along the eastern boundary of the South Atlantic with pronounced periods between 3 and 5 years. The anomalies generate large precipitation anomalies over West Africa via the influence on the ITCZ and local anomalies along Southwest Africa. The strong linkage between SST

and precipitation anomalies increases the potential for reproducing interannual variations of African precipitation dependent on SST variations. The climatic response to these SST variations is however biased in the coupled climate model simulation, producing an opposing precipitation anomaly along West Africa. With increased model resolution the representation of the WSC along the Benguela upwelling region is improved and the mean state SST bias is significantly reduced, as thereby the erroneous southward transport of warm tropical water into the Benguela upwelling region is largely prevented. Additionally, the position and periodicity of interannual SST anomalies are improved along with the corresponding representation of precipitation anomalies. However, the opposing precipitation response over West Africa to SST anomalies remains even with a reduced eastern boundary SST bias and is even present in the atmosphere-only simulation which is forced with realistic SST. Thus, the erroneous simulation of the ITCZ is expected to reduce the potential to reproduce African precipitation anomalies, especially along the Guinea and Sahel regions. It remains to be clarified if the SST bias reinforces the atmospheric deficit and further deteriorates the African precipitation signal.

In this Chapter, the climatic performance is examined for the atmospheric simulation of AMIP, driven with realistic SST, and for the HR GECCO3 model which is forced with realistic SST anomalies while retaining the biased SST mean state. The comparison of both model simulations provides insight into the extent to which precipitation performance is influenced by the SST bias. An overview of the performance of both models is given in Section 6.1. In addition, periodic behavior of African precipitation related to SST variability is analyzed to quantify the potential contributions to the precipitation signal. Section 6.2 deals with the reproduced variability of the West African Monsoon and in Section 6.3 the performance of precipitation along the coast of Southwest Africa is examined.

6.1 Model performance

The AMIP and HR GECCO3 simulations are used to evaluate the performance of climate models forced with realistic SST fields and realistic interannual SST anomalies respectively in order to estimate their ability to reproduce interannual variations of precipitation dependent on the representation of SST. The general performance of simulated climate variables of AMIP and HR GECCO3 is examined and summarized in a Taylor diagram in Figure 6.1 for the time period from 1982 to 2014 with OISST as a reference for SST, GPCP for precipitation, and ERA-5 for surface winds, air temperature, and latent heat flux. The global analysis in Figure 6.1 A shows a similar level of performance for AMIP and HR GECCO3 in representing climate variables like surface air temperature, precipitation, zonal and meridional surface wind, and surface latent heat flux. Correlation coefficients are slightly better for AMIP simulations with a slightly smaller RMSE as well. Largest difficulties appear to be encountered in simulating meridional wind and especially precipitation in

both models. Both variables largely deviate from the observational reference in time and space. Since the performance of climate variables over the South Atlantic and surrounding regions is of major interest for this study, the performance metrics are computed for this region (20°N-34°S, 50°W-40°E) as well and show large deviations from the global mean performance, as shown in Figure 6.1 B. The mean state eastern boundary SST bias is still present in HR GECCO3, and thus, correlation coefficients resembling the pattern of the variable and the RMSE are deteriorated for SST and surface air temperature as expected. In addition, the representation of variability indicated by the standard deviation is affected as well, since deviations from the reference are larger in HR GECCO3 than in AMIP. It is obvious that surface latent heat flux and precipitation are strongly affected by the SST bias. The performance of both variables in HR GECCO3 shows large deviations for this region. Correlations coefficients are severely reduced and the RMSE is increased. Variability of SST is enhanced in HR GECCO3 while it is diminished for zonal surface wind. In contrast, the meridional wind simulation in HR GECCO3 restricted to the South Atlantic shows better performance and is also in better agreement with the reference than in AMIP, despite the larger mean state bias in HR GECCO3. This is a result of larger deviations at mid latitudes in AMIP and can be related to the resolution of the SST forcing field. These general performance metrics suggest to expect less performance due to the mean state SST bias, as a result of shifted precipitation patterns.

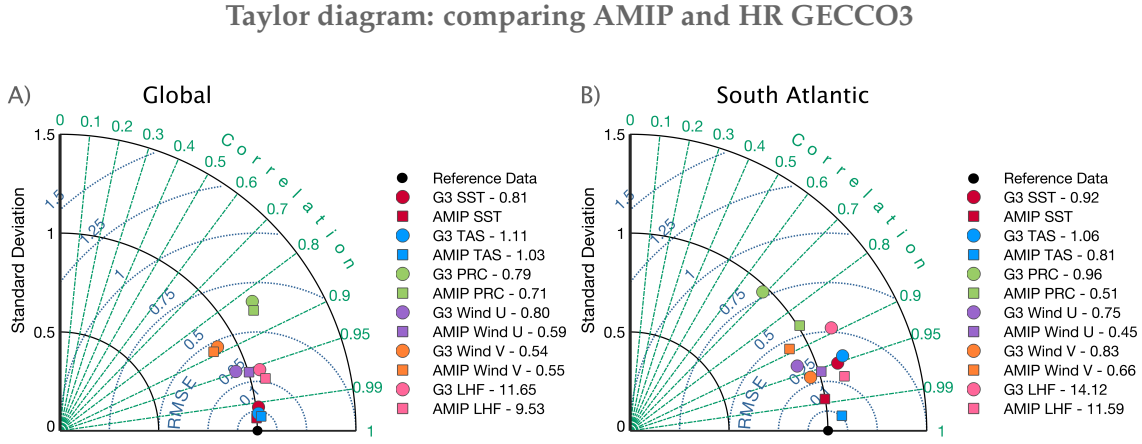

Figure 6.1: Taylor diagram showing performance of model variables [1982-2014] from AMIP (square) and HR GECCO3 (circle) with global coverage (left) and covering the South Atlantic area plus tropical North Atlantic (20°N-34°S, 50°W-40°E) (right). Climate variables (SST in red, surface air temperature in blue, precipitation in green, zonal surface wind in purple, meridional surface wind in orange and surface latent heat flux in pink) are arranged in dependency of their normalized standard deviation, normalized RMSE and pattern correlation with reference to observations/reanalysis (OISST/GPCP/ERA-5). Here normalized means divided by the standard deviation of the observational reference. Values in the legend display corresponding averages of the absolute mean state bias (SST and surface air temperature in °C, precipitation in mm/day, zonal and meridional surface wind in m/s, and surface latent heat flux in W/m^2).

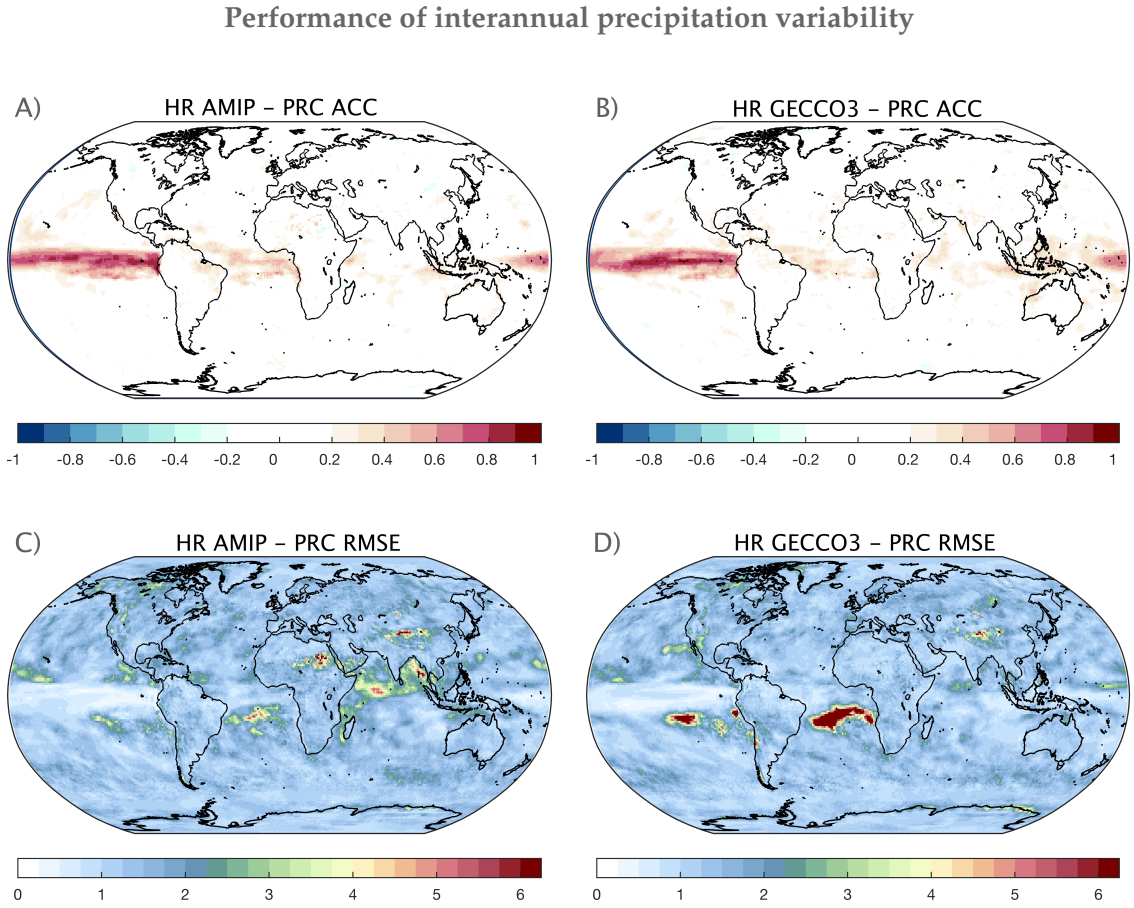

Figure 6.2: Global performance of interannual precipitation variability in AMIP (left) and HR GECCO3 (right) with reference to GPCP [1997-2014], indicated by ACC (top) and normalized RMSE (bottom), where normalized means divided by the standard deviation of the reference.

ACC and RMSE maps for annual precipitation anomalies in AMIP and HR GECCO3 with GPCP (1997-2014) as a reference in Figure 6.2 show, that the representation of interannual precipitation variability in the model simulations is mostly limited to equatorial regions, where precipitation is most elevated and highly variable. Precipitation anomalies along the equatorial Pacific Ocean are in good agreement with the reference for both models. This is a result of the pronounced ENSO dynamics (Philander, 1989) which produce a strongly coupled ocean and atmosphere interaction, where climate variations highly depend on very characteristic SST variations. This adds significantly to precipitation performance in model simulations (Barnston et al., 2012). The performance of precipitation over the tropical Atlantic is moderate for both models in comparison to the tropical Pacific but still more pronounced compared to the Indian Ocean. The same decrease in performance regarding the tropical ocean basins is observed for many other climate models by Scaife et al. (2019). Along the equatorial Atlantic, the AZM induces a similar air-sea coupling phenomenon like in the Pacific which drives tropical precipitation

with impacts for tropical Atlantic Ocean rim countries and increases the model skill to reproduce precipitation patterns (Doi et al., 2016). Even if weather forecast systems show high predictive skill for tropical Atlantic precipitation on time scales of days to weeks, the interannual predictability is reduced in the tropical Atlantic compared to the tropical Pacific in a large range of coupled climate models which has been linked to the biased mean state SST (Gaetani and Mohino, 2013; Ding et al., 2015; Scaife et al., 2019). In contrast, Richter et al. (2018) do not expect any improvements with a reduced SST bias, as predictive skill may be limited by itself in the tropical Atlantic region. As the ACC is slightly reduced in the eastern equatorial Atlantic for HR GECCO3 compared to AMIP, the SST bias may affect the reproduced precipitation signal. The RMSE maps show the poleward shifted tropical precipitation patterns in both models with greater impact for HR GECCO3, where the RMSE is especially high in the tropical South Atlantic, where interannual SST variations produce a large precipitation response. For the Indian Ocean, where precipitation variability is linked to South Atlantic SST variations, the ACC slightly increases and the RMSE decreases in comparison to the AMIP simulation.

6.1.1 Equatorial rainfall

Equatorial variables are indexed to evaluate if the biased annual feedback mechanism due to the SST bias, affects interannual performance of precipitation and zonal wind. SST is averaged over the cold tongue region (CT, 2°N-4°S, 0°-20°W), precipitation is averaged over equatorial Atlantic (EA, 5°N-5°S and 40°W-10°E) and zonal wind is averaged over the western equatorial Atlantic (WEA, 5°N-5°S, 40°W- 20°W), where the biased SST affects it the most. This area is also important for interannual SST anomalies excited by wind relaxation. The averaged time series are detrended and the seasonal cycle is removed to calculate the ACC and the RMSE for seasonally stratified interannual variations with reference to OISST for SST, GPCP for precipitation, and ERA-5 for zonal surface wind for the time period of 1982 to 2014. The result is shown in Figure 6.3 and gives a deeper insight into the seasonal performance of the tropical Atlantic variables involved in the characteristic air-sea coupling which is suspected to be the main source of predictability for this region. Cold tongue SST performance in Figure 6.3 A and D serves the purpose to verify the ability of AMIP and HR GECCO3 to realistically represent SST variations which are important drivers of precipitation anomalies. Both models show high and significant correlations with the reference anomalies. SST performance of AMIP is nearly perfect with correlation coefficients higher 0.9 since the model is forced with realistic SST fields. Performance for HR GECCO3 is slightly reduced but with correlations higher than 0.8 still in good agreement with the reference, while the RMSE is within the range of the standard deviation of the reference SST. Interannual precipitation anomalies are significantly correlated to the reference precipitation throughout all seasons, as shown in Figure 6.3 B. However, AMIP shows less skill in reproducing anomalies during boreal spring which is the peak season for interannual precipitation anomalies. Amplitudes

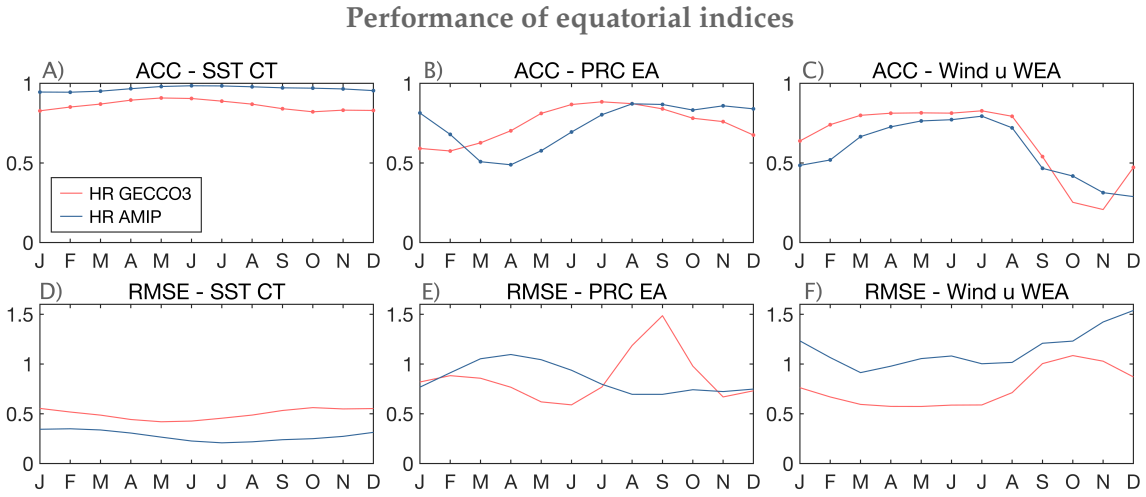

Figure 6.3: Seasonal index performance of interannual anomalies [1982-2014] of AMIP (blue) and HR GECCO3 (red) indicated by the ACC (top) with significant correlation marked by dots, and the RMSE (bottom) normalized by the standard deviation of the observational reference. Indexed variables: A) and D) SST averaged over the Atlantic cold tongue regions [2°N-4°S, 0°-20°W] (reference: OISST), B) and E) precipitation averaged along the equatorial Atlantic [5°N-5°S, 40°W-10°E] (reference: GPCP), and C) and F) zonal wind averaged over the western equatorial Atlantic [5°N-5°S, 40°W-20°W] (reference: ERA-5).

of anomalies are elevated and lead to a larger RMSE. As dynamic atmospheric patterns are shifted southward in the presence of the SST bias, the seasonal increase of equatorial precipitation is delayed by one month. Thus, the seasonal peak of interannual variability in HR GECCO3 is delayed as well and leads to deviations in boreal summer. Linked to the SST bias precipitation is most elevated over the eastern equatorial Atlantic during late boreal summer which leads to a high RMSE, although correlation coefficients stay high (between 0.7 and 0.9). This shows again the large impact of the SST bias on the seasonality and the precipitation signal. However, it does not necessarily reduce the overall performance of simulating the main interannual tropical Atlantic precipitation variability on average.

Zonal surface wind in the Western equatorial Atlantic shows good performance throughout boreal spring and summer, as shown in Figure 6.3 C and F. Both models show a significant decrease in performance from September to January which may be linked to the decreasing variability during boreal fall and rising variability in January with a peak in April/May (not shown). It may also be linked to the biased surface wind pattern during boreal winter over the South Atlantic. After the monsoon season, the ITCZ starts to move south and increasing equatorial precipitation may lead to the sudden change in surface wind performance. With the southward moving ITCZ, the trade wind pattern moves south as well. In the model simulations of AMIP, the southward movement is linked to weakened meridional winds over the eastern tropical South Atlantic and equatorial basin with

an increased zonal component over the western equatorial basin. The southward shifted trade wind pattern during boreal fall and winter may affect the simulated variability as well. The persisting SST bias adds a reduced zonal component of western equatorial winds to the biased wind pattern in boreal fall and winter. The zonal wind variability in the western equatorial Atlantic is important for the simulation of interannual SST anomalies in the South Atlantic. The improved performance in boreal spring compared to boreal winter may explain why SST variability in the ABA peaks later during the year in the coupled model simulation. The surface wind variations showed certain potential for the predictability of SST and linked precipitation anomalies. Simulating realistic equatorial wind variability is thus important for correctly reproducing South Atlantic SST modes which may in turn improve the ability to reproduce precipitation variability.

6.2 West African Monsoon

On average the impact of the SST bias on the variability of the equatorial Atlantic region and performance of interannual precipitation anomalies is small since interannual anomalies can be well represented on a regional average in HR GECCO3 in comparison to AMIP. The analysis of the previous Chapters, however, showed how precipitation patterns are shifted due to the SST bias and led to the assumption of defective precipitation variability simulations along the West African Guinea and Sahel region. For this reason, the performance of precipitation in AMIP and HR GECCO3 regarding the West African Monsoon region is examined in this Section and shows how both models show deficiencies in representing precipitation anomalies affecting the Sahel region (10°N-20°N, 16°W-15°E), where short and heavy rains occur from June to September.

6.2.1 Precipitation performance

Precipitation is indexed over the tropical North Atlantic (Trop NA, 0-18°N, 40°W-16°W), Guinea region (0-10°N, 16°W-15°E), and Sahel region (10°N-20°N, 16°W-15°W) in West Africa, since these regions are directly affected by tropical Atlantic SST variations which modulate monsoon intensity. The precipitation indices are computed for HR GECCO3 and AMIP for the time period of 1982 to 2014 and compared to indices computed from GPCP. Figure 6.4 shows the interannual variations of the three precipitation indices in the first row and their seasonal standard deviation for interannual variations in the second row. The corresponding seasonal performance is shown with the ACC in the third row and the RMSE in the fourth row. As performance is better over the Atlantic ocean areas compared to land areas, the performance of precipitation over the tropical North Atlantic is examined first, to scale the ability of the models to represent the general variability of precipitation during monsoon season. The performance of the indexed tropical North Atlantic precipitation is displayed in Figure 6.4 A.1-A.4. HR GECCO3 shows a good ability to reproduce the variability there with correlation coefficients around 0.7 from May

to September when precipitation is largest over the tropical North Atlantic. However, amplitudes of variations are overestimated, and thus, the RMSE is high. From November to March correlation coefficients are significantly reduced and reach zero during December and January. This is due to the dry precipitation bias north of the equator, especially during December and January as a result of the southward shifted ITCZ by reduced equatorial winds. The effect is enhanced in HR GECCO3 compared to AMIP due to the elevated SST in the Southern tropical Atlantic which intensifies the southward shift. In general, the representation of precipitation variability is weak in AMIP regarding the tropical North Atlantic which may be related to the westward shifted precipitation pattern.

In the Guinea region, the representation of precipitation variability is more difficult which is a result of the shifted position of the ITCZ in both models. The seasonal performance of precipitation over the Guinea region is displayed in Figure 6.4 B.1-B.4. In general the precipitation bias in this area is too dry in AMIP and too wet in HR GECCO3, as shown in Figure 6.4 B.1. The long term variation of decreasing precipitation which could be related to long term SST variability associated with the recent phase of the AMO or global warming, is not shown for either of them. The different seasons showing significant correlation to the reference can be related to the South Atlantic SST anomalies. For instance, the dry anomaly during Benguela Niño events in the Guinea region from April to June can be reproduced by AMIP but not by HR GECCO3. In addition, AZM anomalies produce a large precipitation response in the Guinea region during boreal summer. This response is enhanced by the SST bias over the oceanic part of the region and thus increases the precipitation signal locally. Hence, HR GECCO3 outperforms AMIP during boreal summer for reproducing interannual precipitation anomalies in the Guinea region. Richter et al. (2018) showed a similar result, where the SST bias increased the signal-to-noise ratio in the eastern equatorial Atlantic region. The diverging seasonal performance is also linked to the general seasonality being influenced by the southward shifted precipitation pattern. While precipitation is enhanced during boreal spring in the eastern tropical Atlantic in AMIP, precipitation in HR GECCO3 is enhanced further to the south with a negative bias over the Gulf of Guinea. During boreal summer the ITCZ moves too far to the north over the tropical north Atlantic but stays shifted to the south over the Gulf of Guinea in HR GECCO3 and produces a wet precipitation bias which may enhance the signal during this season.

For the Sahel region precipitation variability can not be represented by either model, as shown in Figure 6.4 C.1-C.4. The magnitude of precipitation is significantly reduced in HR GECCO3 due to the southward shifted precipitation pattern which is intensified by the SST bias. The slight long term increase in precipitation in this region is not represented by either model. The Sahel region experiences precipitation only during the monsoon season and is strongly affected by its interannual variations. The biased atmospheric dynamics in

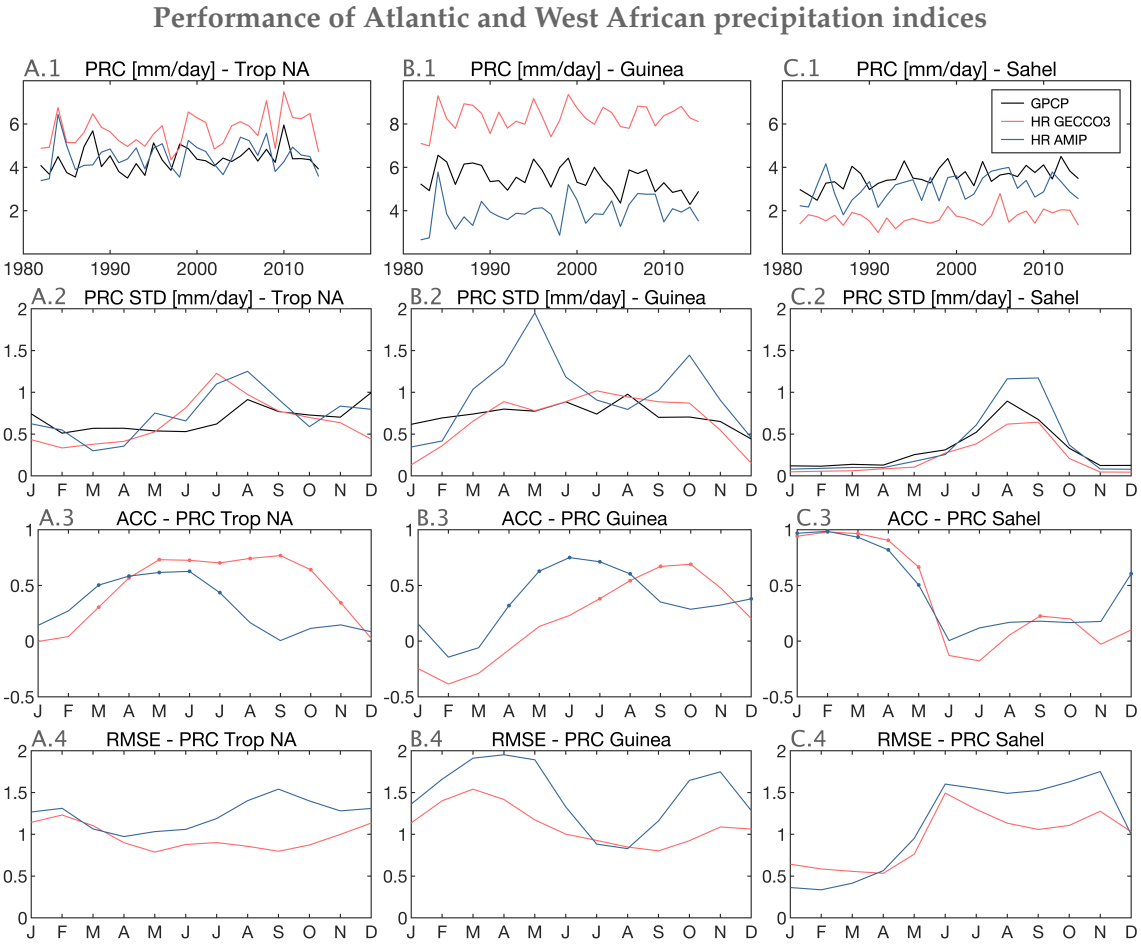

Figure 6.4: Seasonal index performance of interannual precipitation anomalies [1982-2014] over A) the tropical North Atlantic [0-18°N, 40°W-16°W], B) the Guinea region [0-10°N, 16°W-15°E], and C) the Sahel region [10°N-20°N, 16°W-15°W]. First row: historical monsoon precipitation time series annually averaged during JJAS for GPCP (black), AMIP (blue) and HR GECCO3 (red). Second row: seasonal standard deviation of interannual precipitation anomalies in mm/day. Third row: seasonal ACC for AMIP and HR GECCO3 with respect to GPCP and significant coefficients on the 95% confidence level marked by dots. Fourth row: seasonal RMSE normalized by the corresponding standard deviation of GPCP.

the tropics in AMIP reduce the influence of South Atlantic SST on the Sahel precipitation. In HR GECCO3 the Sahel region is strongly affected by a divergent moisture flux bias due to the southward shifted ITCZ, leaving the Sahel area too hot and too dry. As less moisture is transported towards the Sahel region the amount of monsoon rainfall is significantly reduced and as well as the amplitudes of interannual variations.

6.2.2 Coherent Sea Surface Temperature and precipitation modes

Interannual South Atlantic SST variations occur on a broad range of time periods, from year to year variations to decadal long term variations, affecting African precipitation at

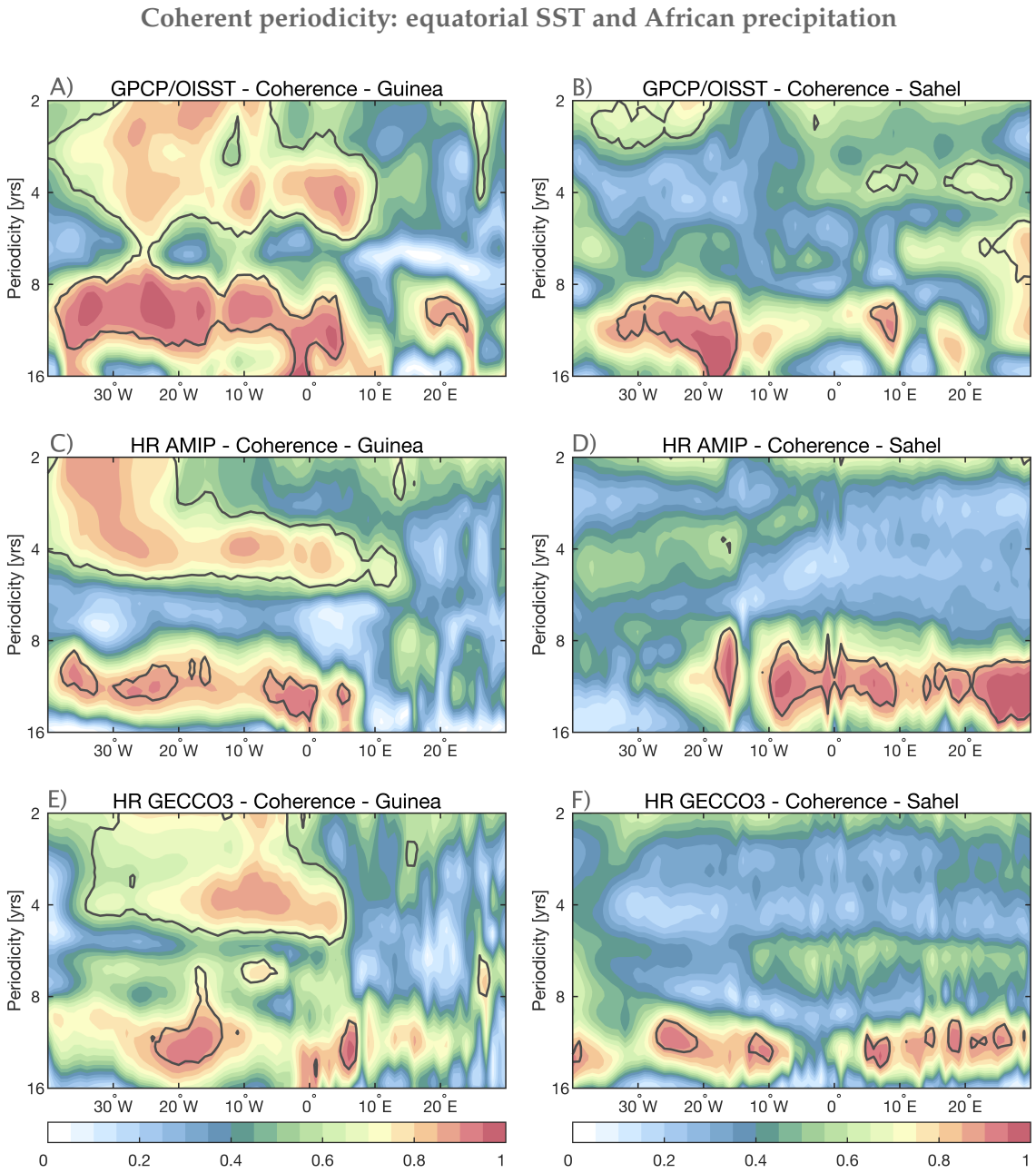

Figure 6.5: Coherent periodic behavior between eastern equatorial SST [2°N-4°S, 0°-20°W] (during April-August) and Atlantic and West African monsoon precipitation (during JJAS) along longitudes averaged over A), C), E) the Guinea zone [0°-10°N] and B), D), F) the Sahel zone [10°-20°N]. Common periods (in years) are estimated by a coherent wavelet analysis for GPCP/OISST (top), AMIP (middle) and HR GECCO3 (bottom) and indicated by dimensionless coefficients between 0 and 1 (shading). Thick gray line outlines significant coefficients on the 95% confidence level computed with the Monte Carlo method.

various locations with different intensities. To get a better understanding of the intensity of the linkage between both variables, the coherence between their periodic behavior indicated by wavelet transforms is computed to highlight the temporal scales on which SST and precipitation vary together. Interannual SST anomalies during April to August

are averaged along the eastern equatorial Atlantic between 20°W and 0° and compared to precipitation anomalies during June to September averaged along longitudes from 40°W to 30°E between 0° and 10°N for the Guinea region, and between 10°N and 20°N for the Sahel region. Figure 6.5 shows the coherent periodicity for the Guinea region (left), and the Sahel region (right) for the observational products OISST and GPCP, the AMIP simulation and the HR GECCO3 simulation from 1982-2014. The observational reference in Figure 6.5 A shows a strong impact of interannual equatorial Atlantic SST anomalies on precipitation variability along the Guinea region with time periods around 4 and 11 years. The influence of SST on precipitation further north is much weaker which becomes evident in Figure 6.5 B. Sahel precipitation is less strongly linked to SST variations, but as well predominantly affected on scales of 3-4 years and around 11 years, with impacts over African land areas further to the east. The model simulations show a similar linkage between both variables for similar time periods. The linkage is however slightly weaker in the model simulations and weighted differently. Common periodic behavior between SST and precipitation in the Guinea region is dominated by higher frequent periods in both model simulations, as precipitation is less dominated by the 11 year period as in the observational reference. Precipitation over the western tropical Atlantic in the AMIP simulation is strongly linked to SST variations, whereas in HR GECCO3 the precipitation response to SST anomalies is more dominant further to the east over the Gulf of Guinea. The precipitation response with periods around 4 years which is likely linked to AZM events, is strongly limited to precipitation anomalies over oceanic regions and does not spread to land areas further to the east. Common periodicity between Sahel precipitation during monsoon season and equatorial SST is most pronounced for lower frequent periods of around 11 years in the model simulations. This linkage is less intense for HR GECCO3. However, the models fail to simulate Sahel precipitation linked to higher frequent SST variations which may reduce interannual precipitation performance. Higher frequent SST modes like the AZM appear to have a reduced impact on Sahel precipitation in the model simulations but are strongly linked to precipitation over the Gulf of Guinea. The SST bias in HR GECCO3 enhances the sensitivity of precipitation over the Gulf of Guinea to SST variations, especially for higher frequent SST variations with periods of 2-4 years. The signal of these variations is presumably elevated by the mean state SST bias and generates a stronger precipitation response over the Gulf of Guinea. The lower frequent periods are less involved in precipitation variability in HR GECCO3 which may affect the reproduced signal. Additionally, the SST bias reduces the moisture flux towards African land areas which causes less intense precipitation signals over Africa.

6.2.3 EOF analysis for West African monsoon precipitation

The influence of South Atlantic SST modes on African precipitation is further investigated using an EOF analysis, illustrating the spatial extent of coherent variability. The multivariate EOF analysis is executed for SST anomalies between March and September in the

South Atlantic (7°N to 35°S and 45°W to 20°E) and West African monsoon precipitation anomalies during June to September in a region including the equatorial Atlantic and West Africa (30°N to 4°S and 40°W to 30°E) within the time period of 1982-2014. In order to highlight spatial features of common modes associated with different time scales, the anomaly fields are separated into interannual and decadal time scales. The results are meant to indicate the influence of the mean state SST bias on precipitation on interannual and longer time scales. A moving average of 8 years is applied to the anomaly time series to account for the decadal variations and a 10 year moving average is removed from the anomaly time series to account for the higher frequent variations before applying the EOF analysis. The PCs of the first and second EOF modes generated for AMIP and HR GECCO3 are correlated to the PCs of the reference data in order to prove the similarity between generated modes. In order to put the modes generated by the EOF analysis into further context, the reference PCs are also correlated to a global mean SST time series as an indication for global warming (GW) and to the Niño3.4 index, available from Smith and Sardeshmukh (2000), to reveal a linkage to Pacific Niño events.

The results of the EOF analysis are shown in Figure 6.6. Rows A, B, and C show the first two EOF modes of lower frequent variability with periods longer than 8 years, whereas rows D, E, and F show the first two EOF modes for interannual variability with periods smaller than 10 years. The first EOF mode of observational low frequent precipitation and SST variability of the South Atlantic is shown in Figure 6.5 A.1 and A.2 respectively. The principal component of the first EOF mode is correlated to global warming SST with a correlation coefficient of 0.93. Thus, the mode shows how long term SST variations, such as the global mean increase of SST, have a large impact on precipitation, as it describes 73.9% of the common variability. Increasing SST can be attributed to global warming or long term variations like the AMO. As the analyzed time series is not long enough for a qualified statement for the origin of the long term variability of SST, this is not further differentiated. However, increasing SST reduces precipitation in the Guinea region and increases precipitation in the Sahel region which could already be seen in the historical graphs of Figure 6.4. A general increase of West African precipitation with rising SST is reproduced by the models, although the explained variability by this mode is significantly reduced compared to the reference. For long term SST variations with periods larger than 8 years the long term variation explains only 53.6% of the variability for AMIP and 59.2% for HR GECCO3. The reduction of Guinea precipitation is not well simulated in AMIP and HR GECCO3 which can be seen in Figure 6.5 B.1 and C.1 respectively. The second EOF mode describes the precipitation response to SST anomalies along the equator and eastern boundary which is well reproduced by the models with a correlation coefficient between PCs of the reference and AMIP of 0.81 and for HR GECCO3 of 0.97. The positive SST anomaly related to periods of approximately 11 years is associated with positive precipitation anomalies along the Sahel region for the reference, as displayed in Figure 6.5

A.3. For HR GECCO3 in Figure 6.5 C.3 the mode is associated with an opposing precipitation response, as the positive SST anomaly is linked to negative precipitation anomalies along the Sahel region. The results suggest the potential to reproduce a more realistic precipitation signal induced by long term SST variations is not yet exhausted in both model simulations, allowing for higher frequent modes to deteriorate the signal.

Higher frequent interannual SST variations affect precipitation patterns on a more diverse range of less intense modes, deteriorating the precipitation signal for these time scales. For the observational reference, the largest part of precipitation variations linked to SST anomalies is described by eastern equatorial AZM like SST variations (Figure 6.5 D.2), explaining 41.2% of the common variability for these time scales. This mode is negatively correlated to the Niño3.4 index which is used to define El Niño and La Niña events in the Pacific ocean. The correlation is moderate with a coefficient of -0.57. The warm SST event in the eastern tropical South Atlantic generates a wet precipitation response in the Guinea region (Figure 6.5 D.1). This mode is well captured by HR GECCO3 (Figure 6.5 F.1 and F.2), with a correlation coefficient of 0.9 between the PCs of the first EOF modes of HR GECCO3 and the reference. The explained variability by this mode is however lower at only 33%. In HR GECCO3 the precipitation response is intense and spatially concentrated, as expected from the AZM analysis in the previous Chapter. The precipitation pattern is shifted to the southeast and does not induce much precipitation over African land areas. The Guinea and Sahel region experience rather a slight reduction of precipitation linked to this mode. The dislocated precipitation pattern is clearly related to the SST bias and even more severe in the second EOF mode, where warm SST anomalies along the eastern boundary of the South Atlantic produce a negative precipitation response over West Africa. For the AMIP simulation AZM like SST anomalies are less dominant and thus shown in the second EOF mode (Figure 6.5 E.4), with a correlation coefficient of 0.81 to the PC of the first mode of the reference. The explained variability by this mode accounts only for 21.5% and shows a positive precipitation response over the Guinea region which is less shifted to the south as seen for the first mode of HR GECCO3 in Figure 6.5 F.1. However, the positive precipitation anomaly is accompanied by a negative anomaly along the Sahel region, highlighting the impact of the poleward shifted convergence zone in the atmospheric model component. This suggests a general deterioration of precipitation variability linked to SST variations which is induced by the double ITCZ pattern and related to the atmospheric wind bias. The affected precipitation anomalies are additionally intensified and shifted further to the south in the presence of the mean state SST bias.

For interannual time scales the AZM like mode generates strong precipitation signals in the model simulations but explains less of the variance generated by the interaction between South Atlantic SST and monsoon precipitation compared to the reference, reaching 41.2% with this mode. In comparison to AMIP, HR GECCO3 generates a stronger

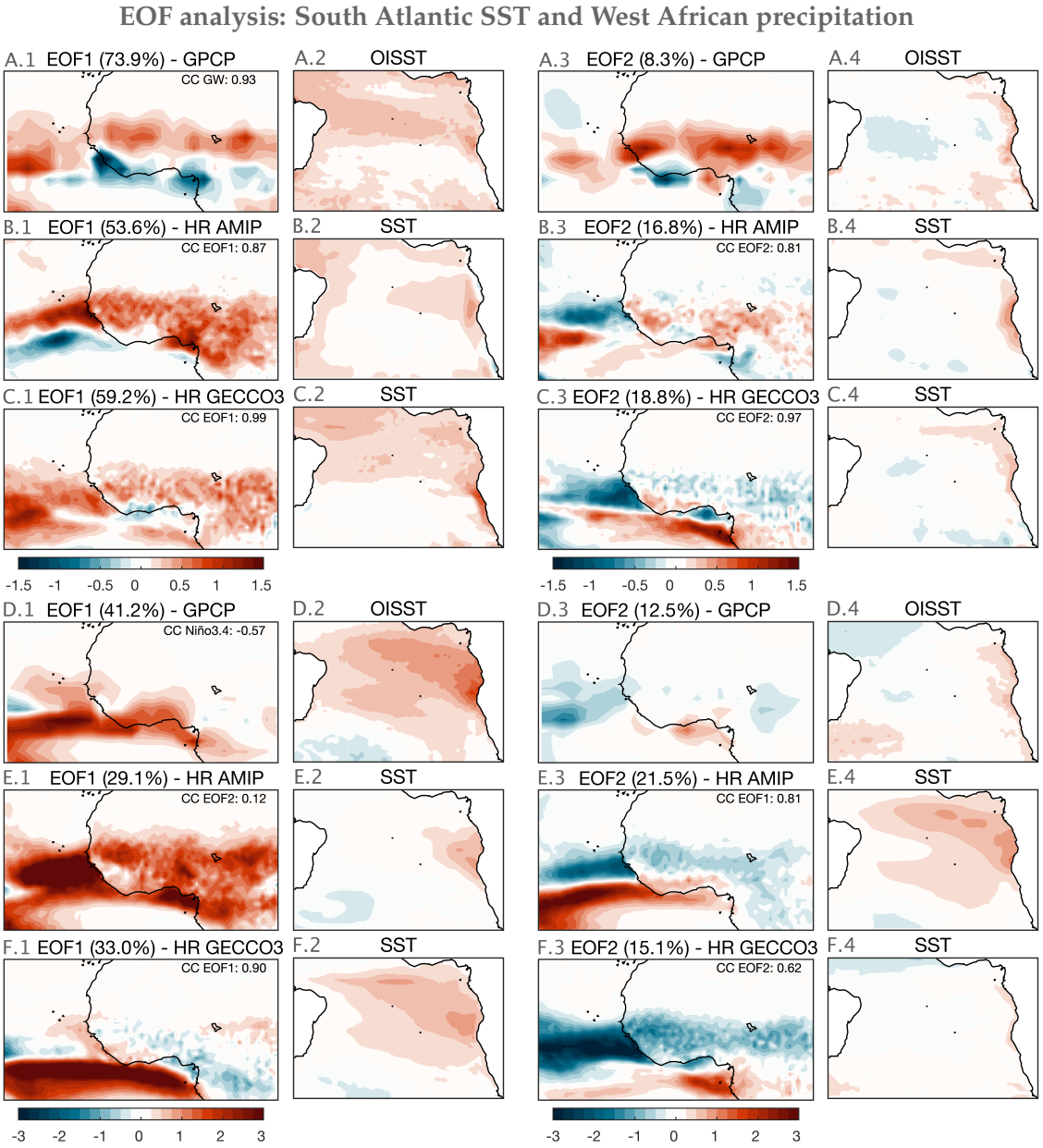

Figure 6.6: First and second EOF modes of covarying West African precipitation and South Atlantic SST [1982-2014] for anomalies with periods longer 8 years (top three rows) and anomalies with periods smaller 10 years (bottom three rows) with corresponding percentage of explained variability shown in parentheses at the top of the panels. The EOFs are normalized by their corresponding PCs maximum value. Correlation coefficients (CC) are given for PCs of the first modes of GPCP/OISST and global mean SST (GW) or Nino3.4 index. CCs for PCs of AMIP and HR GECCO3 give the correlation to the corresponding modes of GPCP/OISST.

precipitations signal related to AZM like SST variations due to the SST bias, and can explain 33% of the variance. This is significantly higher than the explained variability for the same mode in AMIP, explaining only 21.5% of the variance. Thus, other less important SST variations affect precipitation variability in the models, leading to a less

realistic simulation of precipitation with a potential for further deterioration by opposing precipitation anomalies over African land areas for both model simulations.

The EOF analysis shows that the main modes of precipitation variability related to South Atlantic SST variations are disturbed by the shifted dynamics induced by the atmospheric submodel. These disturbances are intensified by the southward shift of precipitation patterns due to the mean state SST bias. The potential for reproducing precipitation variability related to interannual SST modes can thus not be fully utilized. The lack of performance of West African precipitation is a matter of the correct representation of tropical winds which can advect the moisture towards a more realistic position of the convergence zone and enhance the equatorial SST impact on precipitation variability. The increase in atmospheric resolution does not lead to the required improvement regarding the representation of the ITCZ as shown before. Instead of increasing the resolution and exhausting the computational cost of climate models, attention should be directed to the coupling between ocean and atmospheric momentum fluxes and land surface temperatures, that drive atmospheric winds. Elevated SST in the South Atlantic artificially enhances the precipitation signal induced by SST variations. However, the mean state SST bias increases the precipitation signal majorly over oceanic regions, since less moisture is transported toward African land areas. Interannual SST variations have a severely reduced impact on precipitation in the Sahel region in the model simulations, due to the southward shifted pattern. The strong dependency between SST and precipitation highlights the importance to reproduce the linkage between tropical SST and West African precipitation in model simulations to improve model performance for the African continent. Predictability of SST anomalies in the South Atlantic would imply a certain potential for predictable precipitation patterns over Africa in climate simulations as well. This potential induced by the atmospheric teleconnection appears not to be exhausted yet in the model simulations since the dominant SST modes are less pronounced in the precipitation signal of the model simulations. This highlights the importance of an improvement of SST variability representation in climate models along with a more realistic air-sea interaction in terms of surface momentum flux variation as a reaction to SST anomalies.

6.3 Southwest African coastal precipitation

Along the eastern boundary of the South Atlantic interannual SST variations are most pronounced in the ABA between 10°S and 20°S. The area is affected by SST modes like the AZM during boreal spring (March to June) and by less frequent extreme events like Benguela Niños/Niñas during FMA. In comparison to AZM events, Benguela Niño/Niña events generate a less pronounced precipitation response which affects monsoon rainfall over African land areas, as the events occur earlier during the year and are located further south. Thus, the local precipitation response to Benguela Niño/Niña events, affecting

the African land areas along the southwestern coastline, is of greater interest. For this reason, the analysis of the reproduced precipitation variability along Southwest Africa focuses on the linkage to SST variations from February to April in the ABA. The SST anomalies can be a potential source for local precipitation predictability and could add to the performance of coastal precipitation in the models. As the southward shifted model dynamics are suspected to have a less severe impact on precipitation simulation south of the equator, the aim is to examine how the biased mean state SST in HR GECCO3 affects precipitation performance in regions less affected by the representation of the ITCZ and to what extent Bengula Niños can generate predictable precipitation patterns that induce droughts or floods in regions of Southwest Africa which would be highly relevant for the local communities.

6.3.1 Coastal precipitation performance

For the purpose of examining the reproduced precipitation patterns dependent on SST events like Benguela Niños, SST is indexed over the ABA, and precipitation is indexed near the ABA region (ABA2, 10°S-20°S, 11°E-20°E) with coverage of the adjacent land area. In addition, meridional wind along the coast of Angola (ANG, 0°-18°S, 7°E-15°E) is indexed since Benguela Niño/Niña and AZM events are related to local meridional wind fluctuations preceding the events. The indexed time series from 1982 to 2014 are detrended and deseasonalized to examine the performance of the AMIP and HR GECCO3 model simulations to reproduce seasonally phase locked local precipitation responses to

Figure 6.7: Seasonal index performance of interannual anomalies [1982-2014] of A), D) SST averaged over the ABA, B), E) precipitation averaged over the ABA including the adjacent land [10°S-20°S, 11°E-20°E], and C), F) meridional surface wind close to Angola [0°-18°S, 7°E-15°E], for AMIP (blue) and HR GECCO3 (red) with reference to OISST, GPCP and ERA-5 respectively. Top row shows seasonal ACC with significant correlation on the 95% confidence level marked by dots. Bottom row shows the seasonal RMSE normalized by the standard deviation of the reference (OISST/GPCP/ERA-5).

interannual SST events in the ABA.

Figure 6.7 shows the seasonal performance of interannual SST variability in the ABA for AMIP and HR GECCO3, indicated by the ACC and the RMSE. Both model simulations are in good agreement with the observational reference OISST as expected. Correlation coefficients remain between 0.9 and 1 for both models during the relevant season from February to April and hence, serve as a good base to analyze the performance to represent realistic precipitation responses linked to the SST variations. The simulation of precipitation over the adjacent land area performs well in HR GECCO3 during boreal spring, indicated by significant correlation coefficients between February and June. No reasonable performance exists from boreal summer to winter. Interannual variability of precipitation can be best reproduced from March to May when the ACC reaches values of around 0.7. The normalized RMSE during this season reaches its seasonal minimum but is still high with values between 0.7 and 0.8. The result indicates that local precipitation variability during boreal spring can be reproduced dependent on the local SST variations. The coupled model simulation of HR GECCO3 can reproduce these interannual precipitation anomalies better than the AMIP simulation despite the eastern boundary SST bias strongly affecting the ABA. This is true as well for the meridional wind off the coast of Angola which is as well related to interannual SST anomalies along the eastern boundary. Meridional wind anomalies can be reproduced best during boreal spring in HR GECCO3, whereas performance is low for meridional winds in AMIP throughout the year. The SST bias in HR GECCO3 may enhance the local response to SST anomalies and produce a more pronounced atmospheric signal. The high RMSE values during the best performing seasons are within one standard deviation of the reference but indicate in combination with the high ACCs that local variations of SST, surface wind, and precipitation are highly linked during boreal spring but diverge from observations in their intensity.

The performance of precipitation in both model simulations is further examined for land areas along the southwestern coast of Africa between the equator and 34°S. Therefore precipitation is longitudinally averaged between coastal grid points and 7.5° further to the east at every latitudinal grid point, covering a broad band of African land areas along the coast. The ACC of precipitation for AMIP and HR GECCO3 is then computed for moving averages covering precipitation anomalies along the coast within 5° of latitudes to overcome differences between the resolution of the reference and the model simulations. Additionally, seasonal correlation coefficients are computed between the same precipitation anomalies along Southwest Africa and SST anomalies of the ABA during FMA. The resulting correlation coefficients show how precipitation is affected in different locations along the coast by ABA SST anomalies and how the response is lagged in time.

Figure 6.8 shows the monthly lagged correlation between precipitation along the South-

west African coast to SST anomalies in the ABA during FMA. The observational reference in Figure 6.8 A shows the strong linkage between SST anomalies in the ABA and precipitation over Southwest Africa. The anomalous increasing SST values in the ABA are accompanied by enhanced precipitation along the coast between 10°S and 22°S which is as well significantly correlated for the following two months. In addition, wet precipitation anomalies evolve further to the south, lagging in time by two months on average. Wet precipitation anomalies follow as well in coastal areas further north of the ABA with significantly correlated anomalies near the equator lagging by 3 months. Hence, SST anomalies in the ABA can be used to predict Southwest African precipitation. SST anomalies in the ABA are accompanied by local precipitation anomalies, subsequently continuing to affect more remote locations north and south of the ABA. Significantly correlated precipitation anomalies between 10°S and 30°S indicate the existence of natural precipitation predictability dependent on SST variations.

The correlation of SST and precipitation in AMIP in Figure 6.8 B shows a stronger connection of ABA SST anomalies to successive wet precipitation anomalies further north, along the coast of Angola and around 30°S in South Africa. This suggests, a shift of precipitation patterns related to the SST anomalies in the ABA due to atmospheric deficiencies. The composite analysis of Benguela Niños in AMIP shows that precipitation anomalies following the SST event are limited to Southwest Africa between 0° and 15°S. For HR GECCO3 the linkage is only significant for local land areas between 10°S and 22°S, as shown in Figure 6.8 C. The anomaly correlation for precipitation in HR GECCO3 Figure 6.8 E shows as well only good performance for precipitation anomalies located around 10°S during boreal spring, whereas AMIP in Figure 6.8 D shows even less skill in reproducing any precipitation anomalies along the Southwest coast of Africa. Both model simulations show some skill in reproducing precipitation anomalies during June in South Africa which is most likely linked to Benguela Niño/Niña events according to the composite analysis. However, in general, the impact of SST on Southwest African precipitation is not well simulated in the models or superimposed by other variations which reduce performance in reproducing the variability. The mean state SST bias appears not to be the limiting factor for precipitation performance along Southwest Africa, since the performance in the AMIP is even lower than for HR GECCO3.

6.3.2 EOF analysis for Southwest African precipitation

The dependency of African precipitation on SST anomalies in the ABA is further examined by an EOF analysis, in order to understand if the linkage between both variables is affected by the mean state SST bias. For this analysis, the focus is on interannual time periods. Thus, periods longer than 12 years are removed from the anomaly time series to remove long term trends and lower frequent variability which could dominate the signal. The multivariate EOF analysis is executed for SST anomalies in the ABA during FMA and

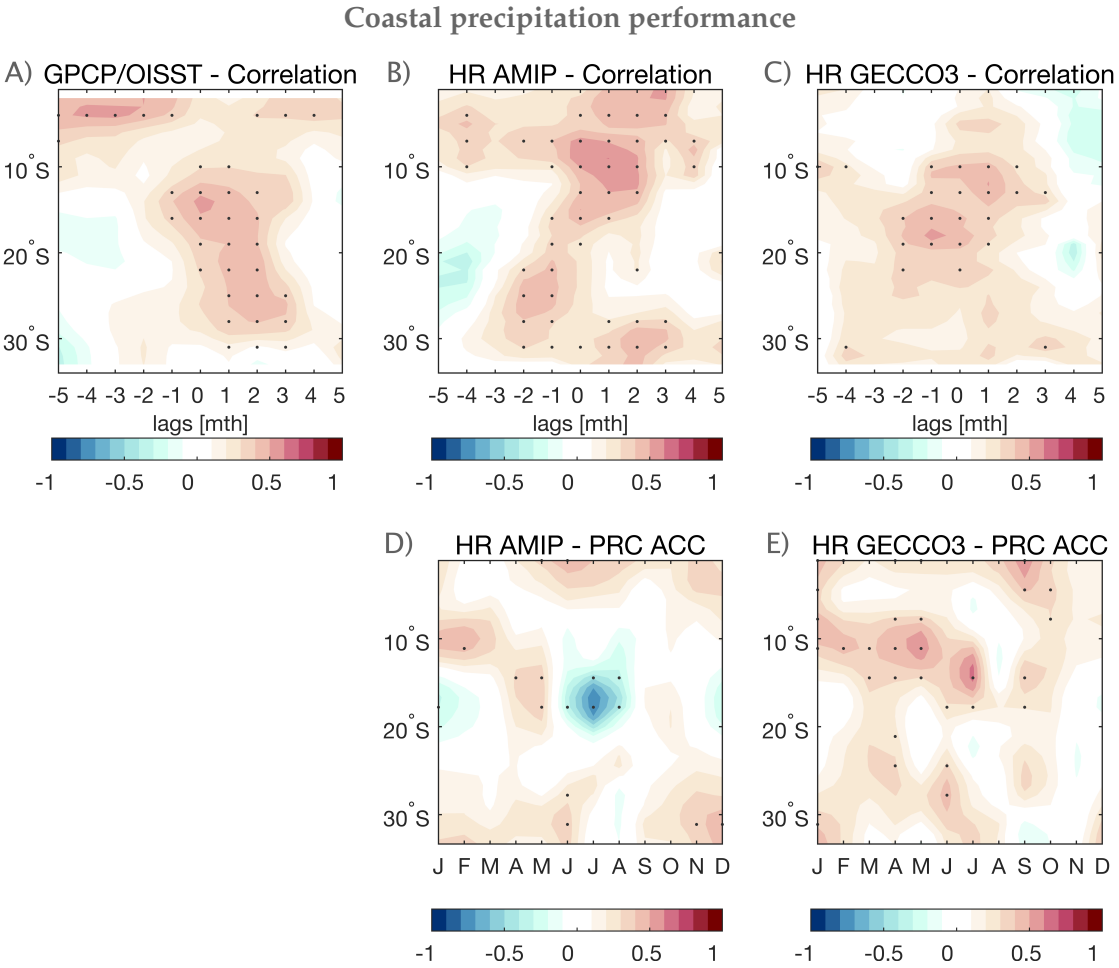

Figure 6.8: Performance of precipitation anomalies [1982-2014] over land areas along the Southwest African coastline. Top row: Monthly lagged correlation coefficients between coastal Southwest African precipitation anomalies along latitudes and interannual SST anomalies during FMA averaged over the ABA for A) GPCP/OISST, B) AMIP, and C) HR GECCO3. Dots indicate significant correlations on the 95% confidence level computed by the Bootstrap method with 2000 repetitions. Bottom row: seasonal ACC for interannual anomalies of Southwest African coastal precipitation along latitudes for D) AMIP and E) HR GECCO3 with reference to GPCP.

precipitation anomalies between March and June from 1982 to 2014.

The resulting first EOF mode is presented in Figure 6.9 for OISST and GPCP (A), AMIP (B), and HR GECCO3 (C) which is normalized by the maximum of the corresponding PCs to make them comparable. The PC of the first mode resembles a quasibiennial oscillation with outstanding peaks during Benguela Niño/Niña events with a periodicity of 2.5 and 5.3 years. For the observational reference, the mode explains 81.1% of precipitation variability during boreal spring induced by SST variations. This demonstrates the dominance of the impact of SST variations on Southwest African precipitation. As the SST variations in the ABA create such a strong signal, the potential to add predictive

skill to the model simulations is high. The precipitation anomalies linked to ABA SST are most intense along the tropical coastline of Angola but show impacts on Namibian and South African precipitation as well. Both simulations of AMIP and HR GECCO3 can reproduce a very similar mode between ABA SST and precipitation. The regions affected by the precipitation response in the model simulations however deviate from the reference. Both models reproduce the strongest precipitation anomaly along the coast of Angola but also affect precipitation over most parts of the southern part of the continent. This is already visible in the Benguela Niño composite in Figure 5.9, where large parts of South Africa experience a severe wet precipitation anomaly during Benguela Niño events in the model simulations. HR GECCO3 shows however more skill in reproducing the linkage between precipitation along the Southwest African coast and the SST anomalies in the ABA in comparison to the AMIP simulation. The EOF modes are less dominant in AMIP and HR GECCO3 though. In HR GECCO3 the mode explains 54.1% of the common variability and explains only 45.6% in AMIP. The lack of dominance of this mode in the model simulations reduces precipitation performance linked to Benguela Niño events as the dependency of precipitation on other minor modes interferes with the signal. The signal induced by SST variations in the ABA is slightly larger for HR GECCO3, which suggests that the coupling between ocean and atmosphere enhances the teleconnection between both variables despite the mean state SST bias, which is largest in the ABA. In the presence of the SST bias in the coupled model simulation, the climatic dependency on SST variations is increased, which suggests that the bias does not necessarily reduce

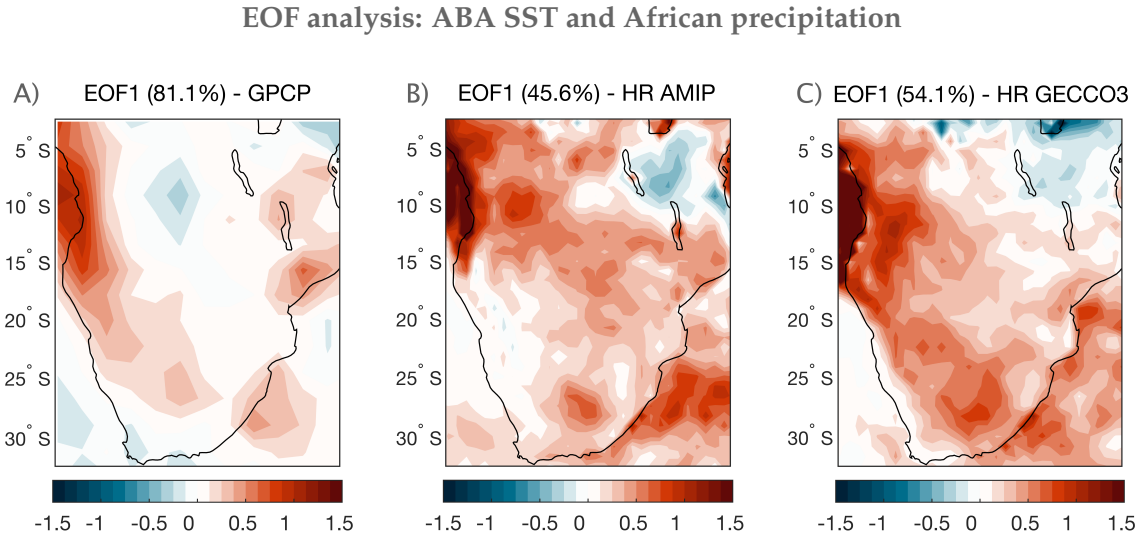

Figure 6.9: First EOF mode of southern African precipitation annually averaged during March-June [1982-2014], covarying with annually averaged SST in the ABA during FMA, for A) GPCP/OISST, B) AMIP, and C) HR GECCO3. Periods larger 12 years are removed from the anomaly time series. The EOFs are normalized by their corresponding PCs maximum value. The percentage of explained variability is shown in parentheses at the top of the panels.

predictability of African precipitation on interannual time scales. The SST bias definitely affects the location of precipitation patterns but most likely also adds to the intensity of the signal, which can potentially increase performance of simulated climate variability.

In summary, the performance of precipitation over Africa is largely affected by biased atmospheric dynamics, that lead to a displacement of tropical moisture convergence and disrupt the moisture transport to the African Sahel region. The shifted precipitation patterns are further affected by the SST bias since elevated SST contributes to the displacement of convective regions as surface winds are largely reduced and northward moisture advection is interrupted. Thus, the SST bias adds to the southward shift of the ITCZ. The result is a reinforced precipitation pattern, which is shifted to the southeast with large implications on African precipitation as less atmospheric moisture reaches African land areas. The SST bias generates a stronger and more localized precipitation response to SST anomalies, which increases the signal and locally increase the performance of reproduced precipitation variability. However, the displacement of moisture convergence and associated precipitation patterns deteriorates the representation of precipitation variability over West Africa, where the positioning of the ITCZ is a crucial factor, which determines whether the SST induced precipitation anomaly is negative or positive. In comparison to the atmosphere-only simulation of AMIP, the performance of precipitation in HR GECCO3 shows no significant decrease induced by the SST bias. An increase in predictability, especially for the African Sahel region, can only be achieved with the improvement of atmospheric dynamics along the tropics which resolves the problem of the poleward shifted moisture convergence.

7 Discussion and conclusion

Coupled climate models are widely used for climate predictions on interannual and decadal time scales in order to provide the opportunity to prepare for possible future climate variations. Despite increased accuracy and computational power over the last decade, it remains challenging to predict interannual variations of African precipitation, especially regarding the Sahel region. As SST variations are a major source for climate predictability, the lack of predictive skill in models had been attributed to the difficulties to simulate realistic mean state SST values along the eastern boundaries of the global oceans. This study analyzed the ability of the coupled model MPI-ESM-HR to reproduce precipitation anomalies in dependency of the represented SST field in the South Atlantic, where the mean state SST bias is usually most elevated. Additional versions of the same model but with a different resolutions of the oceanic or atmospheric components were analyzed to show how the atmospheric representation changes with different magnitudes of the SST bias. The study aims to clarify to what extent the SST bias interferes with the simulation of African precipitation.

Based on remote satellite observations the characteristic behavior of South Atlantic SST on spatial and temporal scales was examined and compared to the SST representation in the coupled climate model to understand the dimension of the SST bias and its influence on the teleconnection between interannual South Atlantic SST anomalies and African precipitation. The resolution of the oceanic and atmospheric model components has major impacts on mean state biases and general model performance. The increased resolution of the ocean component yields a general increase in the performance of atmospheric variables but does not significantly affect the tropical SST biases of global ocean basins but improves mean state SST biases in higher latitudes, especially the Southern Ocean. The study of Gutjahr et al. (2019) attributed the increase of model performance with higher resolution of the ocean component to removed biases in the ocean and atmosphere interior with a high impact on their mean state representation.

In contrast, the increase of resolution for the atmospheric component yields a large reduction of global eastern boundary SST biases, whereas the mean state SST bias averaged over global oceans increases along with the global averaged surface wind bias. With an increased atmospheric resolution the magnitude of the diminished meridional surface winds along the eastern boundaries could be increased and coastal winds presented in higher detail. The improved representation of the near shore WSC along eastern bound-

aries improves the representation of upwelling dynamics and the underlying current system which eliminates a large part of the eastern boundary SST warm bias. Despite this large improvement, the increased atmospheric resolution introduces new biases and difficulties, for example surface wind magnitude decreases generally with impacts on the tropical trade wind representation and a general warming of ocean and air surface temperatures along the tropics. The general performance of precipitation in the tropical Atlantic region can be increased with higher oceanic resolution despite the prevailing eastern boundary SST bias which already indicates a minor role of the eastern boundary SST bias in the precipitation predictability problem.

The SST bias is most elevated where upwelling processes affect SST and interannual SST events reach their maximum amplitudes. The representation of the upwelling dynamics in the climate model also affects the processes that contribute to interannual SST anomalies which are an important driver for precipitation anomalies. The analysis of the representation of upwelling dynamics in the climate model shows how a detailed wind representation on spatial scales is essential for a realistic SST representation in the Benguela upwelling region. Coastal upwelling induced by equatorward alongshore winds that are associated with offshore Ekman transport are well represented even without an increase in atmospheric resolution. In contrast, the representation of offshore Ekman pumping dynamics related to spatial variations in the WSC is highly dependent on the atmospheric resolution and contributes significantly to the SST bias problem. According to Small et al. (2015) a Sverdrup balance prevails at the eastern boundary with the WSC being represented too broad which allows the southward transport of warm tropical water into the Benguela upwelling region and results in a severe warm SST bias. The result of the upwelling analysis shows that the WSC representation is significantly improved when the ocean component of the climate model with a horizontal resolution of 0.4° is combined with an atmospheric component with a horizontal resolution of 0.5°. The improvement leads to the direct removal of a large part of the SST bias along the Benguela upwelling region, as southward intrusions of warm water are significantly reduced during boreal winter and spring when the eastern boundary SST bias was most elevated and upwelling processes are supposed to reach their seasonal maximum. The reduced southward intrusions prevent the dislocation of interannual SST anomalies to the south and reduce the intensity of the mean state bias of the tropical precipitation pattern.

SST along the coast of Angola remains to be biased even with an increased atmospheric model resolution, where upwelling is not driven by the WSC. Ostrowski et al. (2009) and Awo et al. (2022) suggest semiseasonal upwelling is majorly excited by CTWs originating from the equator instead of local alongshore winds. This study shows, that alongshore winds in the model simulations are strongly reduced in the eastern tropical ocean basins where SST is elevated and is not sufficiently improved with increased resolution. The

wind bias is rather related to intrinsic biases of the atmospheric component of the climate model with large implications on tropical moisture convergence. Among other possible contributors, the defective surface wind representation in the eastern tropical ocean basins very likely diminishes oceanic evaporation including erroneous warming. In addition, the absence of alongshore winds in the models could enhance/reduce the consequences of downwelling/upwelling waves via a preconditioned thermocline. Richter et al. (2014b) hypothesize the deepening of the thermocline in the eastern equatorial region, due to equatorial feedback mechanisms, hinders upwelling which would in turn reinforce elevated SST.

The analysis of the intrinsic atmospheric biases of the atmosphere-only simulation in comparison with coupled model simulation including the mean state SST bias showed that tropical moisture convergence is shifted poleward in the simulation of the atmospheric model component. With the coupling of oceanic and atmospheric model components, the southward shifted ITCZ in boreal winter and spring is intensified by elevated SST in the South Atlantic via a reduction of zonal surface winds and the dislocation of convective behavior with resulting excess precipitation over the South Atlantic. The erroneous northward shift of the ITCZ during boreal summer is modified by the SST bias as moisture converges further south over the eastern equatorial Atlantic where SST is most elevated. The double ITCZ already present in the atmosphere-only simulation affects the monsoon dynamics and representation of realistic Sahel precipitation. This bias is further enhanced by the presence of the SST bias. The thermodynamic impact created by elevated temperatures associated with the SST bias is small compared to the large dynamic alterations originating from the atmospheric component and the presence of the SST bias. The improved SST representation of the Benguela upwelling region with increased atmospheric resolution reduces the intensity of the southward shifted part of the convergence zone significantly but can not fully prevent it since the atmospheric momentum flux is still affected by the remaining warm SST bias in the eastern equatorial area.

The biased atmospheric dynamics in the tropics due to intrinsic atmospheric errors and elevated SST in the South Atlantic affect the climatic response to interannual SST anomalies in the model simulations with most severe implications on interannual variations of the West African monsoon. Interannual SST variability of the South Atlantic was found to be dominated by the AZM and related Begnuela Niño/Niña events, explaining the largest part of the interannual SST variability in the South Atlantic. The AZM peaks in May/June with a periodicity of 3-4 years and averaged amplitudes of 1°C along the coast of Angola and the eastern equatorial Atlantic. The lower frequent extreme Benguela Niño/Niña events peak during FMA in the ABA with average amplitudes reaching 2°C. Both types of SST anomalies seem to be two versions of the same mode dependent on the timing of the remote equatorial wind forcing. In contrast to AZM events, Benguela

Niño events are characterized by southward intrusions of tropical warm water into the northern Benguela upwelling region and could thus be linked to periods of 5-6 years with the wavelet analysis. As local forcing conditions vary, not all of the SST anomalies evolve into a full Benguela Niño/Niña extreme event (Lübbecke et al., 2019), therefore fully developed events that meet the criteria for Benguela Niño/Niña events are more rare.

This study shows the strong dependency of both types of SST events on preceding anomalies of the latitudinal position and intensity of the ITCZ, and associated trade wind fluctuations along the equator, inducing lagged temperature anomalies via vertical and horizontal current fluctuations along the eastern boundary, which intensify the locally induced SST anomalies in the ABA. Illig et al. (2020) highlights the importance of local wind forcing for those events and suggests a subsequent expansion of the anomaly via CTWs and reflected Rossby waves. In contrast to Benguela Niño/Niña events, AZM events are excited later during the year and anomalies affect the eastern equatorial Atlantic as well. Thus, their impact on African precipitation is much more pronounced and dominates interannual precipitation variability in the Guinea region with smaller impacts on the Sahel region as well.

The spatial representation of interannual SST variability in the climate model is directly affected by the erroneous southward transport of warm water along the eastern boundary. The two major interannual modes of AZM and Benguela Niño/Niña events can be reproduced by the climate model but travel too far south and affect the Benguela upwelling representation for both types of events. The climate model produces SST variations with a periodicity of approximately 4 to 8 years which are less easy to assign to the corresponding events as for both types of SST events the intrusion into the Benguela upwelling region is large, contributing to the SST bias. This effect vanishes with the improvement of the representation of the Benguela upwelling region via increased atmospheric resolution and WSC representation. With higher atmospheric resolution periodic behavior of SST improves. AZM events are related to periods of 3 years and reach only slightly into the Benguela upwelling region. Benguela Niño/Niña events are likely related to periods of 5-6 years which is more realistic. With increased atmospheric resolution and a consequently reduced SST bias, the periodicity and spatial extent of interannual SST anomalies in the South Atlantic can be significantly improved.

The composite analysis of interannual SST events shows that in addition to periodic behavior and spatial extent of anomalies also the atmospheric response to the events diverges from observations in the coupled model simulation. Characteristic moisture convergence and precipitation patterns linked to the SST events are intensified and shifted southward in the climate model simulation which is affected by the mean state SST bias. The shifted pattern leads to opposing precipitation anomalies over West Africa. The

opposing precipitation variability and altered intensities most likely affect the ability of the climate model to reproduce realistic interannual precipitation anomalies. Comparing the results to the model simulation with increased atmospheric resolution showed that the precipitation response to interannual SST variations becomes more realistic in terms of magnitudes with a decreased eastern boundary SST bias but the dislocation of precipitation anomalies remains similar with an opposing precipitation response along West Africa. The comparison of realistic Benguela Niño events in the atmosphere-only simulation and the coupled model experiment forced with realistic SST anomalies while retaining the mean state SST bias showed a similar result. The precipitation response is largely enhanced in the coupled model version in combination with very sensitive surface wind responses, but the southward shift of the precipitation response, inducing the opposing response over Africa, is very similar in the atmosphere-only simulation. Thus, the mean state SST bias does affect interannual precipitation anomalies, but deterioration of predictive skill of precipitation over Africa, especially in the Sahel region, is in all likelihood rather affected by poleward shifted tropical moisture flux convergence as a result of intrinsic atmospheric momentum flux biases. However, the SST bias intensifies the shift of the dislocated precipitation pattern to the south and to the east. The elevated sensitivity of atmospheric variables to SST variations may contribute to the enhanced but very localized precipitation signals.

The analysis of precipitation performance on interannual time scales in the coupled model supports these results. The analysis shows that interannual variability of precipitation is less reproducible in the tropical Atlantic region than in the tropical Pacific region. This is a matter of natural SST variations being more pronounced along the tropical Pacific Ocean where ENSO drives most of the precipitation variability. The amplitude of comparable AZM events in the tropical Atlantic is comparatively small and the duration of the events is much shorter which would already decrease the potential of interannual climate predictability. However, AZM and Benguela Niño events account for the largest part of SST variations in the South Atlantic and induce variations of tropical precipitation with the largest impact on West African monsoon precipitation. Monsoon rainfall is supplied by moisture fluxes originating from the tropical Atlantic Ocean and thus variate with SST fluctuations. Coherent periodicity between West African precipitation and tropical South Atlantic SST suggests a strong modulation of precipitation in the Guinea region by interannual equatorial SST variability, since coherent periods coincide with those of the AZM. A similar linkage is shown for the atmospheric and coupled model simulation, whereas the South Atlantic mean state SST bias induces a stronger signal over the Gulf of Guinea which is shifted to the southeast. It appears that the SST bias intensifies the atmospheric response locally and increases the precipitation signal over the Gulf of Guinea. The generated signal dominates even over lower frequent variability which modifies the visibility of the long term variability signal. In the model simulations, precipitation over

the Sahel region is only affected by long term SST variations. Interannual SST variability has no significant impact on Sahel precipitation as most of the signal is directed to regions further south. This applies to the atmosphere-only simulation as well and can thus be associated with the defective representation of the state of the atmosphere which is further deteriorated by elevated SST in the South Atlantic.

The EOF analysis confirms the locally enhanced signal induced by the SST bias which affects West African precipitation variability, as already suggested by Richter et al. (2018). Additionally, the coupled model including the mean state SST bias shows higher skill in reproducing precipitation anomalies over Southwest African coastal regions linked to SST variations in the ABA, confirming the assumption of a more pronounced precipitation signal related to the SST bias. Richter et al. (2018) suggest that a more pronounced signal could lead to higher predictive skill. However, coupled feedback mechanisms tend to improve predictive skill for precipitation patterns (Lee et al., 2010; DelSole and Shukla, 2012) in coupled model simulations in comparison to atmospheric simulations. It remains questionable whether the slightly improved performance of precipitation in the coupled model can be actually attributed to the SST bias or to the coupled ocean and atmosphere feedbacks. A theoretically enhanced predictability of the signal related to the warm SST bias stays in contrast to Scaife et al. (2019), who relates the SST bias directly to a reduction of predictive skill. Both statements have their raison d'être, as the elevated SST intensifies the atmospheric response via enhanced and spatially concentrated moisture convergence but also shifts the precipitation pattern to unnatural locations, leaving especially the Sahel region susceptible to large deviations. Shifted moisture convergence and precipitation patterns also dominate the atmospheric model simulation which is forced with realistic SST without any SST bias. The defective representation of the atmospheric state affects the teleconnection between South Atlantic SST and African precipitation and thus might add to the lack of predictability. Additionally, Richter et al. (2018) suggest that West African predictability of precipitation is generally limited for this region. Since the limited predictability is rather related to the defective wind representation and the related double ITCZ problem than to the SST bias, the tropical wind representation needs further attention from the science community. The study of Belmonte Rivas and Stoffelen (2019) associated defective meridional wind representation in ERA reanalysis products to underrepresented SST gradient effects along the tropics and unresolved airflows under moist convection which could also very likely apply to the coupled climate model framework. The defective ITCZ representation shows a higher impact on West African precipitation variability representation on interannual time scales. The EOF analysis shows a less defective representation of long precipitation patterns related to long term SST variations in the Sahel region. Although decreasing precipitation in the Guinea region associated with rising SST is not well represented, the general increase of precipitation over the largest part of African land areas can be well represented. Further analysis using longer

time scales could give a more qualified statement regarding the representation of lower frequent precipitation variations.

In summary, the analysis of the coupled climate model with different resolutions of the oceanic and atmospheric model components led to the result, that an improved representation of upwelling conditions along the eastern boundary with increased atmospheric model resolution eliminates a significant part of the SST bias and reduces the general precipitation bias over the tropical South Atlantic but the representation of African precipitation variability remains deteriorated. The most elevated part of the eastern boundary SST bias can be nearly eliminated with high resolved near shore winds in a simulation with a horizontal resolution of 0.5° for the atmospheric model component. Consequently, the representation of the WSC and related Ekman pumping dynamics improve which prevents the simulation of erroneously large southward intrusions of warm tropical water into the Benguela upwelling region. The representation of interannual SST variability in the South Atlantic significantly benefits from the improvement, as the SST events feature anomalously high southward intrusion via poleward traveling CTWs beyond the climatological position of the Angola Benguela Front. With the reduction of the eastern boundary SST bias the spatial extent and duration of interannual SST events significantly improve. The study showed that this part of the SST bias is related to an intensification of the southward shifted ITCZ and related precipitation in combination with reduced zonal winds along the western tropical South Atlantic due to increased SST gradients. Thereby the thermodynamic impact of the SST bias on tropical moisture fluxes is low in comparison to the severe dynamic alterations. The second part of the SST bias in the eastern tropical South Atlantic remains mostly unchanged due to its relation to intrinsic atmospheric meridional wind representation along tropical eastern boundaries dependent on the land mass distribution which results in a seasonality dependent poleward shift of tropical moisture convergence. The improved SST variability may not necessarily lead to increased skill in reproducing African precipitation variability while the state of the atmosphere is still biased in the model simulation and deteriorates the teleconnection.

In order to determine the impact of the SST bias on the teleconnection between interannual South Atlantic SST and African precipitation anomalies, the characteristics of interannual SST modes were analyzed and their atmospheric response presented with a composite analysis. Interannual SST anomalies in boreal spring cause local precipitation anomalies in Southwest Africa and subsequent anomalies in eastern tropical and equatorial Atlantic modulate the intensity of the African monsoon. The analysis of computed atmospheric moisture fluxes showed that the SST bias is the cause of a dislocation of tropical moisture convergence to the southeast producing a locally condensed and elevated precipitation signal in the region of the Gulf of Guinea. Apart from this the generally southward shifted patterns of characteristic moisture convergence and precipitation anomalies related to

interannual SST anomalies in the South Atlantic remain independent of the presence or magnitude of the SST bias. The poor accuracy of the simulated state of the atmosphere leads to an opposing precipitation response over West African land areas. The elevated sensitivity of atmospheric surface fluxes to SST anomalies in the presence of erroneously elevated SST leads to intensified moisture convergence anomalies which additionally prevent moisture transport to West African regions.

The performance of reproduced African precipitation variability was analyzed generated by an atmosphere-only simulation with prescribed SST fields and by a coupled model simulation with assimilated interannual ocean temperature and salinity anomalies which retained the biased mean state of SST, in order to show the dependency of precipitation variability on the mean state SST pattern. The analysis shows that general precipitation variability can be reproduced over the tropical Atlantic in the presence of the SST bias but reproducible variability is limited by the state of the atmosphere and the SST bias over African land areas. The EOF analysis shows that monsoon variability dependent on the SST pattern is strongly driven by AZM events on interannual scales while the Sahel region is mostly affected by long term SST variations associated with global warming or the AMO. The SST dependent EOF modes of African precipitation can generally be reproduced but the dominant SST modes show a less pronounced impact on precipitation variability in the model simulations with the additional spatial deviations. Coherent variability is affected by the biased state of the atmosphere. The poleward shifted atmospheric pattern prevents an impact of interannual SST variations on Sahel precipitation variability. The impact of long term SST variations is significantly reduced by the SST bias due to an enhanced southward shift of the ITCZ over the eastern tropical Atlantic. The precipitation signal of the Sahel region can however not be reproduced independently of the mean state SST bias due to the missing teleconnection to South Atlantic SST anomalies. As no signal is present, bias correction methods are not expected to provide useful results. In contrast, for precipitation in the Guinea region, the impact of long term SST variability is strongly reduced with further reductions related to the SST bias, as the interannual signal generated by the AZM dominates precipitation variability over the Gulf of Guinea. Related SST anomalies in the ABA linked to Benguela Niños/Niñas are dependent on a seasonally earlier onset of local and remote wind stress fluctuation than for AZM events. The extreme SST events induce a high potential for predictable precipitation anomalies in Southwest Africa with an intensified magnitude and spatial extent by the SST bias but with a high potential for a useful bias correction.

The lack of African precipitation predictability may not only be affected by the mean state South Atlantic SST warm bias. The stochastic characteristics of wind stress variability of the tropical Atlantic most likely add to the low predictability of the dominant interannual SST modes. The lack of predictability may be further enhanced by the severely

reduced zonal wind in the western tropical South Atlantic due to the SST bias. The biased mean state of the atmosphere deteriorates the teleconnection between South Atlantic SST and African precipitation which is further deteriorated by the SST bias. The reduced winds in the tropics may be linked to moist convection patterns. Hence, an improvement in tropical surface winds could lead to an increased SST dependent signal of Sahel precipitation and simultaneously solve the SST bias problem. The lack of reproducible precipitation variability over West Africa and especially the Sahel region does not directly originate from the SST bias. However, the SST bias adds significantly to the defective representation of precipitation patterns which can not be eliminated by improved SST representation along the Benguela upwelling region. Thus, the performance of precipitation variability is to some extent dependent on the SST pattern in the Benguela upwelling region but definitely more important at this point is the representation of tropical convergence in relation to the atmospheric wind representation. As the increase of resolution of the atmospheric component solves a large part of the eastern boundary SST warm bias but also introduces new difficulties, a further increase of model resolution may not lead to the desired improvement of predictive skill and will likely be out of proportion in terms of computational costs.

7.1 Outlook

The purpose of this study is to discuss whether African precipitation variability is negatively affected by the mean state SST bias along the eastern boundary of the South Atlantic. The findings lead to the assumption that the dependency of reproducible precipitation variability on the correct representation of SST is significant but overshadowed by the defective atmospheric wind representation in the tropics. Further research should be directed to the relation between the defective wind representation in the presence of moist convection and its sensitivity to land and sea surface temperature gradients. However, the results of this study should be verified using longer time series which would provide more confident results with regard to interannual SST variability and their climatic response. Longer time series are especially required for the analyzed performance of lower frequent variability which appears to dominate precipitation variability linked to SST. The need for high resolution long term wind observations becomes thereby obvious and could also help to improve model dynamics. The combination of prescribed realistic SST events in a coupled model framework and prescribed realistic wind dynamics along the equatorial Atlantic and eastern tropical North and South Atlantic could give insight into how the precipitation representation over West Africa depends on the dynamics of moisture convergence and how large the actual impact of the SST bias would be without the biased state of the atmosphere and realistic wind stress forcing of interannual SST modes. Furthermore, the moisture convergence analysis in this study shows the importance of the analysis of moisture fluxes in terms of precipitation variability which can provide a

deeper understanding of where the deficiencies originate from. To examine the dynamics of monsoon rainfall and teleconnections the analysis of moisture fluxes is inevitable. However, the accuracy of the computed atmospheric moisture flux estimates computed from atmospheric variables is highly dependent on temporal and spatial resolution of data used for the computation and can largely deviate from fluxes calculated by the climate model itself (Seager et al., 2010). Thus, moisture flux as a standard output variable of the climate models could help to analyze predictive skill of precipitation patterns. Some CMIP6 models already provide moisture flux variables which is largely appreciated (Watterson et al., 2021).

In addition, the predictive skill of precipitation of the coupled climate model could be evaluated with a decadal hindcast experiment in the framework of GECCO3 temperature and salinity anomalies being assimilated into a coupled climate model. A decadal hindcast can provide the possibility to examine predictive skill dependent on lead years and provide more confident statements about predictability being dependent on the mean state SST bias. Furthermore, in-situ observations of upwelling dynamics along the coast of Angola in dependency on local wind fluctuations and CTWs would be very helpful to better understand the local dynamics and their impact on climate model simulations. The need for further investigations regarding the tropical part of the eastern boundaries is highlighted by the severe reinforcement of several intrinsic model biases with an impact on predictions of precipitation. As systematic model biases will continue to exist as long as processes need to be parametrized in coupled model simulations, a good understanding of the actual impacts of the biases on the predictive skill is inevitable for the interpretation of climate predictions.

References

Adler, R., Wang, J., Sapiano, M., Huffman, G., Bolvin, D., Nelkin, E., and Program, N. C. (2017). Global Precipitation Climatology Project (GPCP) Climate Data Record (CDR), version 1.3 (daily). NOAA National Centers for Environmental Information.

Adler, R., Wang, J., Sapiano, M., Huffman, G., Chiu, L., Xie, P., Ferraro, R., Schneider, U., Becker, A., Bolvin, D., et al. (2016). Global Precipitation Climatology Project (GPCP) Climate Data Record (CDR), Version 2.3 (Monthly). *National Centers for Environmental Information*, 10:V56971M6.

Awo, F., Rouault, M., Ostrowski, M., Tomety, F., Da-Allada, C., and Jouanno, J. (2022). Seasonal cycle of Sea Surface Salinity in the Angola upwelling system. *Journal of Geophysical Research: Oceans*, 127(7):e2022JC018518.

Bachèlery, M.-L., Illig, S., and Dadou, I. (2016). Interannual variability in the South-East Atlantic Ocean, focusing on the Benguela Upwelling System: Remote versus local forcing. *Journal of Geophysical Research: Oceans*, 121(1):284–310.

Bachèlery, M.-L., Illig, S., and Rouault, M. (2020). Interannual Coastal Trapped Waves in the Angola-Benguela Upwelling System and Benguela Niño and Niña events. *Journal of Marine Systems*, 203:103262.

Banzon, V., Smith, T. M., Chin, T. M., Liu, C., and Hankins, W. (2016). A long-term record of blended satellite and in situ sea-surface temperature for climate monitoring, modeling and environmental studies. *Earth System Science Data*, 8(1):165–176.

Barnston, A. G., Tippett, M. K., L'Heureux, M. L., Li, S., and DeWitt, D. G. (2012). Skill of Real-Time Seasonal ENSO Model Predictions during 2002–11: Is Our Capability Increasing? *Bulletin of the American Meteorological Society*, 93(5):631 – 651.

Belmonte Rivas, M. and Stoffelen, A. (2019). Characterizing ERA-Interim and ERA5 surface wind biases using ASCAT. *Ocean Science*, 15(3):831–852.

Binet, D., Gobert, B., and Maloueki, L. (2001). El niño-like warm events in the eastern atlantic (6°n, 20°s) and fish availability from congo to angola (1964–1999). *Aquatic Living Resources*, 14(2):99–113.

Bjerkens, J. (1969). ATMOSPHERIC TELECONNECTIONS FROM THE EQUATORIAL PACIFIC. *Monthly Weather Review*, 97(3):163 – 172.

Boyer, D., Cole, J., and Bartholomae, C. (2000). Southwestern Africa: Northern Benguela Current Region. *Marine Pollution Bulletin*, 41(1-6):123–140.

Caniaux, G., Giordani, H., Redelsperger, J.-L., Guichard, F., Key, E., and Wade, M. (2011). Coupling between the Atlantic cold tongue and the West African monsoon in boreal spring and summer. *Journal of Geophysical Research: Oceans*, 116(C4).

Capet, X. J., Marchesiello, P., and McWilliams, J. C. (2004). Upwelling response to coastal wind profiles. *Geophysical Research Letters*, 31(13).

Chavez, F. P. and Messié, M. (2009). A comparison of Eastern Boundary Upwelling Ecosystems. *Progress in Oceanography*, 83(1):80–96. Eastern Boundary Upwelling Ecosystems: Integrative and Comparative Approaches.

Collins, M., Knutti, R., Arblaster, J., Dufresne, J.-L., Fichefet, T., Friedlingstein, P., Gao, X., Gutowski, W., Johns, T., Krinner, G., Shongwe, M., Tebaldi, C., Weaver, A., Wehner, M., Allen, M., Andrews, T., Beyerle, U., Bitz, C., Bony, S., and Booth, B. (2013). *Long-term Climate Change: Projections, Commitments and Irreversibility*, pages 1029–1136. Intergovernmental Panel on Climate Change. Cambridge University Press, United Kingdom.

DelSole, T. and Shukla, J. (2012). Climate models produce skillful predictions of Indian summer monsoon rainfall. *Geophysical Research Letters*, 39(9).

Delworth, T. L., Rosati, A., Anderson, W., Adcroft, A. J., Balaji, V., Benson, R., Dixon, K., Griffies, S. M., Lee, H.-C., Pacanowski, R. C., Vecchi, G. A., Wittenberg, A. T., Zeng, F., and Zhang, R. (2012). Simulated Climate and Climate Change in the GFDL CM2.5 High-Resolution Coupled Climate Model. *Journal of Climate*, 25(8):2755 – 2781.

Desbiolles, F., Blanke, B., and Bentamy, A. (2014). Short-term upwelling events at the western African coast related to synoptic atmospheric structures as derived from satellite observations. *Journal of Geophysical Research: Oceans*, 119(1):461–483.

Diatta, S. and Fink, A. H. (2014). Statistical relationship between remote climate indices and West African monsoon variability. *International Journal of Climatology*, 34(12):3348–3367.

Ding, H., Greatbatch, R. J., Latif, M., and Park, W. (2015). The impact of sea surface temperature bias on equatorial Atlantic interannual variability in partially coupled model experiments. *Geophysical Research Letters*, 42(13):5540–5546.

Dippe, T., Greatbatch, R. J., and Ding, H. (2019). Seasonal prediction of equatorial atlantic sea surface temperature using simple initialization and bias correction techniques. *Atmospheric Science Letters*, 20(5):e898.

Doi, T., Behera, S. K., and Yamagata, T. (2016). Improved seasonal prediction using the SINTEX-F2 coupled model. *Journal of Advances in Modeling Earth Systems*, 8(4):1847–1867.

Exarchou, E., Prodhomme, C., Brodeau, L., Guemas, V., and Doblas-Reyes, F. (2018). Origin of the warm eastern tropical Atlantic SST bias in a climate model. *Climate Dynamics*, 51(5):1819–1840.

Fennel, W., Junker, T., Schmidt, M., and Mohrholz, V. (2012). Response of the Benguela upwelling systems to spatial variations in the wind stress. *Continental Shelf Research*, 45:65–77.

Florenchie, P., Reason, C. J. C., Lutjeharms, J. R. E., Rouault, M., Roy, C., and Masson, S. (2004). Evolution of interannual warm and cold events in the southeast atlantic ocean. *Journal of Climate*, 17(12):2318 – 2334.

Gaetani, M. and Mohino, E. (2013). Decadal Prediction of the Sahelian Precipitation in CMIP5 Simulations. *Journal of Climate*, 26(19):7708 – 7719.

García-Reyes, M., Largier, J. L., and Sydeman, W. J. (2014). Synoptic-scale upwelling indices and predictions of phyto-and zooplankton populations. *Progress in Oceanography*, 120:177–188.

Gent, P. R., Yeager, S. G., Neale, R. B., Levis, S., and Bailey, D. A. (2010). Improvements in a half degree atmosphere/land version of the CCSM. *Climate Dynamics*, 34(6):819–833.

Gimeno, L., Nieto, R., Drumond, A., and Durán-Quesada, A. M. (2013). Ocean Evaporation and Precipitation. In Orcutt, J., editor, *Earth System Monitoring: Selected Entries from the Encyclopedia of Sustainability Science and Technology*, pages 291–318. Springer New York, New York, NY.

Goswami, B. and Ajaya Mohan, R. (2001). Estimate of monthly mean predictability in the tropics form observations. *Current Science*, 80(1):56–63.

Goubanova, K., Sanchez-Gomez, E., Frauen, C., and Voldoire, A. (2019). Respective roles of remote and local wind stress forcings in the development of warm SST errors in the South-Eastern Tropical Atlantic in a coupled high-resolution model. *Climate Dynamics*, 52(3):1359–1382.

Grinsted, A., Moore, J. C., and Jevrejeva, S. (2004). Application of the cross wavelet transform and wavelet coherence to geophysical time series. *Nonlinear processes in geophysics*, 11(5/6):561–566.

Gu, D. and Philander, S. (1995). Secular changes of annual and interannual variability in the tropics during the past century. *Journal of Climate*, 8(4):864–876.

Guo, L., Klingaman, N. P., Demory, M.-E., Vidale, P. L., Turner, A. G., and Stephan, C. C. (2018). The contributions of local and remote atmospheric moisture fluxes to East Asian precipitation and its variability. *Climate Dynamics*, 51(11):4139–4156.

Guo, Y., Cao, J., Li, H., Wang, J., and Ding, Y. (2016). Simulation of the interface between the Indian summer monsoon and the East Asian summer monsoon: Intercomparison between MPI-ESM and ECHAM5/MPI-OM. *Advances in Atmospheric Sciences*, 33(3):294–308.

Gutjahr, O., Putrasahan, D., Lohmann, K., Jungclaus, J. H., von Storch, J.-S., Brüggemann, N., Haak, H., and Stössel, A. (2019). Max planck institute earth system model (MPI-ESM1. 2) for the high-resolution model intercomparison project (HighResMIP). *Geoscientific Model Development*, 12(7):3241–3281.

Hagemann, S. and Gates, L. D. (2003). Improving a subgrid runoff parameterization scheme for climate models by the use of high resolution data derived from satellite observations. *Climate Dynamics*, 21(3):349–359.

Held, I. M. and Soden, B. J. (2006). Robust Responses of the Hydrological Cycle to Global Warming. *Journal of Climate*, 19(21):5686 – 5699.

Hersbach, H., Bell, B., Berrisford, P., Hirahara, S., Horányi, A., Muñoz-Sabater, J., Nicolas, J., Peubey, C., Radu, R., Schepers, D., et al. (2020). The ERA5 global reanalysis. *Quarterly Journal of the Royal Meteorological Society*, 146(730):1999–2049.

Hertwig, E., von Storch, J.-S., Handorf, D., Dethloff, K., Fast, I., and Krismer, T. (2015). Effect of horizontal resolution on ECHAM6-AMIP performance. *Climate Dynamics*, 45(1):185–211.

Hormann, V. and Brandt, P. (2009). Upper equatorial Atlantic variability during 2002 and 2005 associated with equatorial Kelvin waves. *Journal of Geophysical Research: Oceans*, 114(C3).

Hughes, C. W., Fukumori, I., Griffies, S. M., Huthnance, J. M., Minobe, S., Spence, P., Thompson, K. R., and Wise, A. (2019). Sea level and the role of coastal trapped waves in mediating the influence of the open ocean on the coast. *Surveys in Geophysics*, 40(6):1467–1492.

Illig, S., Bachèlery, M.-L., and Lübbecke, J. F. (2020). Why Do Benguela Niños Lead Atlantic Niños? *Journal of Geophysical Research: Oceans*, 125(9):e2019JC016003. e2019JC016003 2019JC016003.

Imbol Koungue, R. A. and Brandt, P. (2021). Impact of Intraseasonal Waves on Angolan Warm and Cold Events. *Journal of Geophysical Research: Oceans*, 126(4):e2020JC017088. e2020JC017088 2020JC017088.

Imbol Koungue, R. A., Illig, S., and Rouault, M. (2017). Role of interannual Kelvin wave propagations in the equatorial Atlantic on the Angola Benguela Current system. *Journal of Geophysical Research: Oceans*, 122(6):4685–4703.

Imbol Koungue, R. A., Rouault, M., Illig, S., Brandt, P., and Jouanno, J. (2019). Benguela Niños and Benguela Niñas in Forced Ocean Simulation From 1958 to 2015. *Journal of Geophysical Research: Oceans*, 124(8):5923–5951.

Jacox, M. G., Edwards, C. A., Hazen, E. L., and Bograd, S. J. (2018). Coastal upwelling revisited: Ekman, Bakun, and improved upwelling indices for the US West Coast. *Journal of Geophysical Research: Oceans*, 123(10):7332–7350.

Jarre, A., Hutchings, L., Kirkman, S. P., Kreiner, A., Tchipalanga, P. C., Kainge, P., Uanivi, U., van der Plas, A. K., Blamey, L. K., Coetzee, J. C., Lamont, T., Samaai, T., Verheye, H. M., Yemane, D. G., Axelsen, B. E., Ostrowski, M., Stenevik, E. K., and Loeng, H. (2015). Synthesis: climate effects on biodiversity, abundance and distribution of marine organisms in the benguela. *Fisheries Oceanography*, 24(S1):122–149.

Jungclaus, J. H., Fischer, N., Haak, H., Lohmann, K., Marotzke, J., Matei, D., Mikolajewicz, U., Notz, D., and Von Storch, J. (2013). Characteristics of the ocean simulations in the Max Planck Institute Ocean Model (MPIOM) the ocean component of the MPI-Earth system model. *Journal of Advances in Modeling Earth Systems*, 5(2):422–446.

Junker, T. (2014). *Response of the Benguela upwelling system to changes in the wind forcing*. PhD thesis, University of Rostock Rostock, Germany.

Keenlyside, N. S. and Latif, M. (2007). Understanding Equatorial Atlantic Interannual Variability. *Journal of Climate*, 20(1):131 – 142.

Kleidon, A. (2019). Energy Balance. In Fath, B., editor, *Encyclopedia of Ecology (Second Edition)*, pages 50–63. Elsevier, Oxford, second edition edition.

Kopte, R., Brandt, P., Dengler, M., Tchipalanga, P. C. M., Macuéria, M., and Ostrowski, M. (2017). The Angola Current: Flow and hydrographic characteristics as observed at 11°S. *Journal of Geophysical Research: Oceans*, 122(2):1177–1189.

Kröger, J., Pohlmann, H., Sienz, F., Marotzke, J., Baehr, J., Köhl, A., Modali, K., Polkova, I., Stammer, D., Vamborg, F. S., et al. (2018). Full-field initialized decadal predictions with the MPI earth system model: An initial shock in the North Atlantic. *Climate dynamics*, 51(7):2593–2608.

Köhl, A. (2015). Evaluation of the GECCO2 ocean synthesis: transports of volume, heat and freshwater in the Atlantic. *Quarterly Journal of the Royal Meteorological Society*, 141(686):166–181.

Köhl, A. (2020). Evaluating the GECCO3 1948–2018 ocean synthesis – a configuration for initializing the MPI-ESM climate model. *Quarterly Journal of the Royal Meteorological Society*, 146(730):2250–2273.

Köhl, A. and Stammer, D. (2008). Variability of the Meridional Overturning in the North Atlantic from the 50-Year GECCO State Estimation. *Journal of Physical Oceanography*, 38(9):1913 – 1930.

Large, W. G. and Danabasoglu, G. (2006). Attribution and Impacts of Upper-Ocean Biases in CCSM3. *Journal of Climate*, 19(11):2325 – 2346.

Large, W. G., McWilliams, J. C., and Doney, S. C. (1994). Oceanic vertical mixing: A review and a model with a nonlocal boundary layer parameterization. *Reviews of geophysics*, 32(4):363–403.

Lee, J.-Y., Wang, B., Kang, I.-S., Shukla, J., Kumar, A., Kug, J.-S., Schemm, J., Luo, J.-J., Yamagata, T., Fu, X., et al. (2010). How are seasonal prediction skills related to models' performance on mean state and annual cycle? *Climate dynamics*, 35(2):267–283.

Lett, C., Veitch, J., Van der Lingen, C. D., and Hutchings, L. (2007). Assessment of an environmental barrier to transport of ichthyoplankton from the southern to the northern Benguela ecosystems. *Marine Ecology Progress Series*, 347:247–259.

Li, G. and Xie, S.-P. (2014). Tropical Biases in CMIP5 Multimodel Ensemble: The Excessive Equatorial Pacific Cold Tongue and Double ITCZ Problems. *Journal of Climate*, 27(4):1765 – 1780.

Li, J. and Ding, R. (2015). Weather Forecasting | Seasonal and Interannual Weather Prediction. In North, G. R., Pyle, J., and Zhang, F., editors, *Encyclopedia of Atmospheric Sciences (Second Edition)*, pages 303–312. Academic Press, Oxford, second edition edition.

Li, T. and Philander, S. G. H. (1997). On the Seasonal Cycle of the Equatorial Atlantic Ocean. *Journal of Climate*, 10(4):813 – 817.

Li, Z., Luo, Y., Arnold, N., and Tziperman, E. (2019). Reductions in Strong Upwelling-Favorable Wind Events in the Pliocene. *Paleoceanography and Paleoclimatology*, 34(12):1931–1944.

Losada, T., Rodríguez-Fonseca, B., Janicot, S., Gervois, S., Chauvin, F., and Ruti, P. (2010). A multi-model approach to the Atlantic Equatorial mode: impact on the West African monsoon. *Climate Dynamics*, 35(1):29–43.

Lübbecke, J. F., Brandt, P., Dengler, M., Kopte, R., Lüdke, J., Richter, I., Sena Martins, M., and Tchipalanga, P. (2019). Causes and evolution of the southeastern tropical Atlantic warm event in early 2016. *Climate Dynamics*, 53(1):261–274.

Lübbecke, J. F., Rodríguez-Fonseca, B., Richter, I., Martín-Rey, M., Losada, T., Polo, I., and Keenlyside, N. S. (2018). Equatorial Atlantic variability—Modes, mechanisms, and global teleconnections. *WIREs Climate Change*, 9(4):e527.

Manganello, J. V. and Huang, B. (2009). The influence of systematic errors in the Southeast Pacific on ENSO variability and prediction in a coupled GCM. *Climate Dynamics*, 32(7):1015–1034.

Mauritsen, T., Bader, J., Becker, T., Behrens, J., Bittner, M., Brokopf, R., Brovkin, V., Claussen, M., Crueger, T., Esch, M., et al. (2019). Developments in the MPI-M Earth System Model version 1.2 (MPI-ESM1. 2) and its response to increasing CO2. *Journal of Advances in Modeling Earth Systems*, 11(4):998–1038.

McClean, J. L., Bader, D. C., Bryan, F. O., Maltrud, M. E., Dennis, J. M., Mirin, A. A., Jones, P. W., Kim, Y. Y., Ivanova, D. P., Vertenstein, M., Boyle, J. S., Jacob, R. L., Norton, N., Craig, A., and Worley, P. H. (2011). A prototype two-decade fully-coupled fine-resolution CCSM simulation. *Ocean Modelling*, 39(1):10–30. Modelling and Understanding the Ocean Mesoscale and Submesoscale.

Mechoso, C., Robertson, A., Barth, N., Davey, M., Delecluse, P., Gent, P., Ineson, S., Kirtman, B., Latif, M., Treut, H. L., Nagai, T., Neelin, J., Philander, S., Polcher, J., Schopf, P., Stockdale, T., Suarez, M., Terray, L., Thual, O., and Tribbia, J. (1995). The Seasonal Cycle over the Tropical Pacific in Coupled Ocean–Atmosphere General Circulation Models. *Monthly Weather Review*, 123(9):2825 – 2838.

Milinski, S., Bader, J., Haak, H., Siongco, A. C., and Jungclaus, J. H. (2016). High atmospheric horizontal resolution eliminates the wind-driven coastal warm bias in the southeastern tropical Atlantic. *Geophysical Research Letters*, 43(19):10–455.

Mitchell, T. P. and Wallace, J. M. (1992). The Annual Cycle in Equatorial Convection and Sea Surface Temperature. *Journal of Climate*, 5(10):1140 – 1156.

Müller, W. A., Jungclaus, J. H., Mauritsen, T., Baehr, J., Bittner, M., Budich, R., Bunzel, F., Esch, M., Ghosh, R., Haak, H., et al. (2018). A higher-resolution version of the max planck institute earth system model (MPI-ESM1. 2-HR). *Journal of Advances in Modeling Earth Systems*, 10(7):1383–1413.

National Research Council (2010). *Assessment of Intraseasonal to Interannual Climate Prediction and Predictability*. The National Academies Press, Washington, DC.

Niang, C., Mancho, A. M., García-Garrido, V. J., Mohino, E., Rodriguez-Fonseca, B., and Curbelo, J. (2020). transport pathways across the West African Monsoon as revealed by Lagrangian coherent Structures. *Scientific reports*, 10(1):1–11.

Oettli, P., Yuan, C., and Richter, I. (2021). 10 - The other coastal Niño/Niña—the Benguela, California, and Dakar Niños/Niñas. In Behera, S. K., editor, *Tropical and Extratropical Air-Sea Interactions*, pages 237–266. Elsevier.

Ostrowski, M., da Silva, J. C. B., and Bazik-Sangolay, B. (2009). The response of sound scatterers to El Niño- and La Niña-like oceanographic regimes in the southeastern Atlantic. *ICES Journal of Marine Science*, 66(6):1063–1072.

Oueslati, B. and Bellon, G. (2015). The double ITCZ bias in CMIP5 models: Interaction between SST, large-scale circulation and precipitation. *Climate dynamics*, 44(3):585–607.

Paeth, H. and Friederichs, P. (2004). Seasonality and time scales in the relationship between global SST and African rainfall. *Climate Dynamics*, 23(7):815–837.

Park, W. and Latif, M. (2020). Resolution dependence of CO2-induced Tropical Atlantic sector climate changes. *npj Climate and Atmospheric Science*, 3(1):1–8.

Peterson, R. G. and Stramma, L. (1991). Upper-level circulation in the South Atlantic Ocean. *Progress in Oceanography*, 26(1):1–73.

Philander, S. G. (1989). El niño, la niña, and the southern oscillation. *International geophysics series*, 46:X–289.

Philander, S. G. H. and Pacanowski, R. C. (1981). The oceanic response to cross-equatorial winds (with application to coastal upwelling in low latitudes). *Tellus*, 33(2):201–210.

Philander, S. G. H. and Yoon, J.-H. (1982). Eastern Boundary Currents and Coastal Upwelling. *Journal of Physical Oceanography*, 12(8):862 – 879.

Pohlmann, H., Müller, W. A., Kulkarni, K., Kameswarrao, M., Matei, D., Vamborg, F. S. E., Kadow, C., Illing, S., and Marotzke, J. (2013). Improved forecast skill in the tropics in the new MiKlip decadal climate predictions. *Geophysical Research Letters*, 40(21):5798–5802.

Polkova, I., Brune, S., Kadow, C., Romanova, V., Gollan, G., Baehr, J., Glowienka-Hense, R., Greatbatch, R. J., Hense, A., Illing, S., Köhl, A., Kröger, J., Müller, W. A., Pankatz, K., and Stammer, D. (2019). Initialization and Ensemble Generation for Decadal Climate Predictions: A Comparison of Different Methods. *Journal of Advances in Modeling Earth Systems*, 11(1):149–172.

Putrasahan, D., Lohmann, K., von Storch, J.-S., Jungclaus, J. H., Gutjahr, O., and Haak, H. (2019). Surface flux drivers for the slowdown of the Atlantic meridional overturning circulation in a high-resolution global coupled climate model. *Journal of Advances in Modeling Earth Systems*, 11(5):1349–1363.

Reick, C., Raddatz, T., Brovkin, V., and Gayler, V. (2013). Representation of natural and anthropogenic land cover change in MPI-ESM. *Journal of Advances in Modeling Earth Systems*, 5(3):459–482.

Renault, L., Dewitte, B., Marchesiello, P., Illig, S., Echevin, V., Cambon, G., Ramos, M., Astudillo, O., Minnis, P., and Ayers, J. K. (2012). Upwelling response to atmospheric

coastal jets off central Chile: A modeling study of the October 2000 event. *Journal of Geophysical Research: Oceans*, 117(C2).

Renault, L., Hall, A., and McWilliams, J. C. (2016). Orographic shaping of US West Coast wind profiles during the upwelling season. *Climate Dynamics*, 46(1):273–289.

Reynolds, R. W., Smith, T. M., Liu, C., Chelton, D. B., Casey, K. S., and Schlax, M. G. (2007). Daily high-resolution-blended analyses for sea surface temperature. *Journal of climate*, 20(22):5473–5496.

Richter, I. (2015). Climate model biases in the eastern tropical oceans: causes, impacts and ways forward. *WIREs Climate Change*, 6(3):345–358.

Richter, I., Behera, S. K., Keenlyside, N., et al. (2018). On the link between mean state biases and prediction skill in the tropics: an atmospheric perspective. *Climate Dynamics*, 50(9):3355–3374.

Richter, I., Behera, S. K., Masumoto, Y., Taguchi, B., Komori, N., and Yamagata, T. (2010). On the triggering of Benguela Niños: Remote equatorial versus local influences. *Geophysical Research Letters*, 37(20).

Richter, I., Behera, S. K., Taguchi, B., Masumoto, Y., Xie, S.-P., et al. (2014a). What controls equatorial atlantic winds in boreal spring? *Climate dynamics*, 43(11):3091–3104.

Richter, I. and Tokinaga, H. (2020). An overview of the performance of CMIP6 models in the tropical Atlantic: mean state, variability, and remote impacts. *Climate Dynamics*, 55(9):2579–2601.

Richter, I. and Xie, S.-P. (2008). On the origin of equatorial Atlantic biases in coupled general circulation models. *Climate Dynamics*, 31(5):587–598.

Richter, I., Xie, S.-P., Behera, S. K., Masumoto, Y., et al. (2014b). Equatorial Atlantic variability and its relation to mean state biases in CMIP5. *Climate dynamics*, 42(1):171–188.

Risien, C. M. and Chelton, D. B. (2008). A global climatology of surface wind and wind stress fields from eight years of QuikSCAT scatterometer data. *Journal of Physical Oceanography*, 38(11):2379–2413.

Roberts, M. J., Jackson, L. C., Roberts, C. D., Meccia, V., Docquier, D., Koenigk, T., Ortega, P., Moreno-Chamarro, E., Bellucci, A., Coward, A., et al. (2020). Sensitivity of the Atlantic meridional overturning circulation to model resolution in CMIP6 HighResMIP simulations and implications for future changes. *Journal of Advances in Modeling Earth Systems*, 12(8):e2019MS002014.

Rouault, M. (2012). Bi-annual intrusion of tropical water in the northern Benguela upwelling. *Geophysical Research Letters*, 39(12).

Rouault, M., Illig, S., Bartholomae, C., Reason, C., and Bentamy, A. (2007). Propagation and origin of warm anomalies in the Angola Benguela upwelling system in 2001. *Journal of Marine Systems*, 68(3):473–488.

Rubio, A., Blanke, B., Speich, S., Grima, N., and Roy, C. (2009). Mesoscale eddy activity in the southern Benguela upwelling system from satellite altimetry and model data. *Progress in Oceanography*, 83(1):288–295. Eastern Boundary Upwelling Ecosystems: Integrative and Comparative Approaches.

Santos, A. M. P., Kazmin, A. S., and Peliz, A. (2005). Decadal changes in the Canary upwelling system as revealed by satellite observations: Their impact on productivity. *Journal of Marine Research*, 63(2):359–379.

Scaife, A. A., Ferranti, L., Alves, O., Athanasiadis, P., Baehr, J., Dequé, M., Dippe, T., Dunstone, N., Fereday, D., Gudgel, R. G., Greatbatch, R. J., Hermanson, L., Imada, Y., Jain, S., Kumar, A., MacLachlan, C., Merryfield, W., Müller, W. A., Ren, H.-L., Smith, D., Takaya, Y., Vecchi, G., and Yang, X. (2019). Tropical rainfall predictions from multiple seasonal forecast systems. *International Journal of Climatology*, 39(2):974–988.

Seager, R., Naik, N., and Vecchi, G. A. (2010). Thermodynamic and Dynamic Mechanisms for Large-Scale Changes in the Hydrological Cycle in Response to Global Warming. *Journal of Climate*, 23(17):4651 – 4668.

Shannon, L. and Nelson, G. (1996). The Benguela: large scale features and processes and system variability. In *The south atlantic*, pages 163–210. Springer.

Sleziak, P., Hlavcova, K., and Szolgay, J. (2015). Advantages of a time series analysis using wavelet transform as compared with a fourier analysis. *Slovak Journal of Civil Engineering*, 23(2):30.

Small, R. J., Curchitser, E., Hedstrom, K., Kauffman, B., and Large, W. G. (2015). The Benguela upwelling system: Quantifying the sensitivity to resolution and coastal wind representation in a global climate model. *Journal of Climate*, 28(23):9409–9432.

Smith, C. A. and Sardeshmukh, P. D. (2000). The effect of ENSO on the intraseasonal variance of surface temperatures in winter. *International Journal of Climatology*, 20(13):1543–1557.

Smith, D. M., Eade, R., and Pohlmann, H. (2013). A comparison of full-field and anomaly initialization for seasonal to decadal climate prediction. *Climate Dynamics*, 41(11):3325–3338.

Song, H., Miller, A. J., Cornuelle, B. D., and Di Lorenzo, E. (2011). Changes in upwelling and its water sources in the California Current System driven by different wind forcing. *Dynamics of Atmospheres and Oceans*, 52(1):170–191. Special issue of Dynamics of Atmospheres and Oceans in honor of Prof. A.R.Robinson.

Stevens, B., Giorgetta, M., Esch, M., Mauritsen, T., Crueger, T., Rast, S., Salzmann, M., Schmidt, H., Bader, J., Block, K., et al. (2013). Atmospheric component of the MPI-M Earth system model: ECHAM6. *Journal of Advances in Modeling Earth Systems*, 5(2):146–172.

Strub, P. T. and James, C. (2022). Evaluation of Nearshore QuikSCAT 4.1 and ERA-5 Wind Stress and Wind Stress Curl Fields over Eastern Boundary Currents. *Remote Sensing*, 14(9):2251.

Stössel, A., Notz, D., Haumann, F. A., Haak, H., Jungclaus, J., and Mikolajewicz, U. (2015). Controlling high-latitude Southern Ocean convection in climate models. *Ocean Modelling*, 86:58–75.

Sun, Y. and Tan, B. (2022). A new subseasonal atmospheric teleconnection bridging tropical deep convection over the western North Pacific and Antarctic weather. *Atmospheric Science Letters*, page e1115.

Szolgayová, E., Blöschl, G., and Bucher, C. (2013). Identifying external influences on discharge time series: Long term variability of the Danube River flow and its relation to precipitation and temperature. In *EGU General Assembly Conference Abstracts*, pages EGU2013–9529.

Taylor, K. E. (2001). Summarizing multiple aspects of model performance in a single diagram. *Journal of Geophysical Research: Atmospheres*, 106(D7):7183–7192.

Tibshirani, R. J. and Efron, B. (1993). An introduction to the bootstrap. *Monographs on statistics and applied probability*, 57:1–436.

Tompkins, A. M. and Feudale, L. (2010). Seasonal Ensemble Predictions of West African Monsoon Precipitation in the ECMWF System 3 with a Focus on the AMMA Special Observing Period in 2006. *Weather and Forecasting*, 25(2):768 – 788.

Torrence, C. and Compo, G. P. (1998). A practical guide to wavelet analysis. *Bulletin of the American Meteorological society*, 79(1):61–78.

Torrence, C. and Webster, P. J. (1998). The annual cycle of persistence in the El Nño/Southern Oscillation. *Quarterly Journal of the Royal Meteorological Society*, 124(550):1985–2004.

Valcke, S. (2013). The OASIS3 coupler: a European climate modelling community software. *Geoscientific Model Development*, 6(2):373–388.

Veiga, S. F., Giarolla, E., Nobre, P., and Nobre, C. A. (2020). Analyzing the Influence of the North Atlantic Ocean Variability on the Atlantic Meridional Mode on Decadal Time Scales. *Atmosphere*, 11(1).

Vizy, E. K. and Cook, K. H. (2002). Development and application of a mesoscale climate model for the tropics: Influence of sea surface temperature anomalies on the West African monsoon. *Journal of Geophysical Research: Atmospheres*, 107(D3):ACL 2–1–ACL 2–22.

Voldoire, A., Exarchou, E., Sanchez-Gomez, E., Demissie, T., Deppenmeier, A.-L., Frauen, C., Goubanova, K., Hazeleger, W., Keenlyside, N., Koseki, S., et al. (2019). Role of wind stress in driving SST biases in the Tropical Atlantic. *Climate Dynamics*, 53(5):3481–3504.

Von Storch, J.-S., Eden, C., Fast, I., Haak, H., Hernández-Deckers, D., Maier-Reimer, E., Marotzke, J., and Stammer, D. (2012). An estimate of the Lorenz energy cycle for the world ocean based on the STORM/NCEP simulation. *Journal of physical oceanography*, 42(12):2185–2205.

von Storch, J.-S., Haak, H., Hertwig, E., and Fast, I. (2016). Vertical heat and salt fluxes due to resolved and parameterized meso-scale eddies. *Ocean Modelling*, 108:1–19.

Wang, B. (1992). The Vertical Structure and Development of the ENSO Anomaly Mode during 1979–1989. *Journal of Atmospheric Sciences*, 49(8):698 – 712.

Wang, B., Ding, Q., Fu, X., Kang, I.-S., Jin, K., Shukla, J., and Doblas-Reyes, F. (2005). Fundamental challenge in simulation and prediction of summer monsoon rainfall. *Geophysical Research Letters*, 32(15).

Wang, D., Gouhier, T. C., Menge, B. A., and Ganguly, A. R. (2015). Intensification and spatial homogenization of coastal upwelling under climate change. *Nature*, 518(7539):390–394.

Wang, L.-C., Jin, F.-F., Wu, C.-R., and Hsu, H.-H. (2017). Dynamics of upwelling annual cycle in the equatorial Atlantic Ocean. *Geophysical Research Letters*, 44(8):3737–3743.

Watterson, I. G., Keane, R. J., Dix, M., Ziehn, T., Andrews, T., and Tang, Y. (2021). Analysis of CMIP6 atmospheric moisture fluxes and the implications for projections of future change in mean and heavy rainfall. *International Journal of Climatology*, 41(S1):E1417–E1434.

Wu, R. and Kirtman, B. P. (2005). Roles of Indian and Pacific Ocean air–sea coupling in tropical atmospheric variability. *Climate dynamics*, 25(2):155–170.

Xiang, B., Zhao, M., Held, I. M., and Golaz, J.-C. (2017). Predicting the severity of spurious "double ITCZ" problem in CMIP5 coupled models from AMIP simulations. *Geophysical Research Letters*, 44(3):1520–1527.

Xie, S.-P. and Okumura, Y. (2004). Interaction of the Atlantic equatorial cold tongue and African monsoon. In *13th Conference on Interactions of the Sea and Atmosphere*.

Ye, C., Zhang, H., Moise, A., and Mo, R. (2020). Atmospheric rivers in the Australia-Asian region: a BoM–CMA collaborative study. *Journal of Southern Hemisphere Earth Systems Science*, 70(1):3–16.

Zebiak, S. E. (1993). Air–Sea Interaction in the Equatorial Atlantic Region. *Journal of Climate*, 6(8):1567 – 1586.

Zhou, W. and Xie, S.-P. (2017). Intermodel spread of the double-ITCZ bias in coupled GCMs tied to land surface temperature in AMIP GCMs. *Geophysical Research Letters*, 44(15):7975–7984.

Eidesstattliche Versicherung | Declaration on Oath

Hiermit erklare ich an Eides statt, dass ich die vorliegende Dissertationsschrift selbst verfasst und keine anderen als die angegebenen Quellen und Hilfsmittel benutzt habe.

|

I hereby declare upon oath that I have written the present dissertation independently and have not used further resources and aids than those stated.

Ort, den | City, date Unterschrift | Signature

Hamburg, den 07.12.2022